

DELFT UNIVERSITY OF TECHNOLOGY

MSC-THESIS REPORT

THOMAS KRIELAART

Deformation of Crane Hardstands

Author:

Thomas Krielaart (4484614)

Commission:

Cor Zwanenburg: *Delft University of Technology*

Sytse Alkema: *BT Geoconsult B.V.*

Ronald Brinkgreve: *Delft University of Technology*

Wouter van den Bos: *Delft University of Technology*

Thursday 5th October, 2023



Contents

Abstract	iii
1 Introduction	1
2 Physical process	4
2.1 Crane Hardstands	4
2.1.1 Design	4
2.1.2 Soil investigation	5
2.1.3 Installation Process	6
2.2 Mitigation measures	7
3 Soil behaviour	8
3.1 Mechanical load influences	8
3.1.1 Flexibility of the foundation	8
3.1.2 Load spreading	8
3.1.3 Load Magnitude	9
3.2 Deformations	10
3.2.1 Elasticity	10
3.2.2 Drained vs. Undrained behaviour	11
3.2.3 Virgin-, un- and reloading	12
3.3 Plasticity	12
3.3.1 Consolidation	13
3.4 Creep	14
3.5 Influence diagram	14
4 Current prediction method	16
4.1 Soil investigation	16
4.2 Plaxis	16
4.3 HSsmall model	16
4.4 Soil model and parameter determination	17
4.5 Mechanical input	18
4.6 Drainage type	19
4.7 Analysis	19
5 Full Scale Monitoring	20
5.1 Monitoring setup	20
5.2 Measuring locations	21
5.2.1 WT2	21
5.2.2 WT4	22
5.3 Results	22
5.3.1 WT2	22
5.3.2 WT4	25
5.4 Analysis	26
6 Full Scale Testing	28
6.1 The test design	28
6.2 Test locations	29
6.3 Results	29
6.3.1 Deformation E3	30
6.3.2 Deformation D1	31
6.3.3 Deformation B3	33

6.3.4	Deformation B1	36
6.4	Analysis	37
7	Sensitivity analysis	39
7.1	Quantifying sensitivity with the influence factor	39
7.2	The soil model choice	40
7.3	The model	40
7.4	Assessed soil types	42
7.5	Parameter range determination	42
7.5.1	Variants	45
7.6	Python code	46
7.7	Results	46
7.8	Analysis	48
8	Soil parameter improvements	49
8.1	Results	49
8.2	Analysis	50
8.2.1	Consolidation time influence	50
8.2.2	Layer thickness influence	53
9	Discussion	56
10	Conclusions	58
11	Evaluation and recommendations	59
	References	60
A	Appendices	62
A.1	Monitoring Plan and Results	62
A.2	Python code and sensitivity analysis input	90
A.3	Uncertainty range results	98

Abstract

Crane hardstands serve as crucial platforms for supporting heavy lifting equipment and ensuring operational efficiency. However, crane hardstands are not infinitely stiff and will deform upon loading. Uneven loading during wind turbine installation will result in differential deformation of the crane hardstand, causing the crane to tilt. A small tilt of 0.3° , which is equivalent to around 30-60mm differential settlement depending on the crane, will create safety hazards, causing construction to be discontinued. As a result accurate deformation predictions are required to design a sufficient crane hardstand.

This research is conducted to investigate the influence factors of the deformation of a crane hardstand, evaluate the current prediction method and to improve the accuracy of future deformation predictions, so the hardstands can be designed more efficiently.

The research begins with a literature study on the above surface influences on the magnitude of the load and the corresponding soil behaviour of the soil profile beneath the hardstand. Furthermore the current prediction method is analyzed to dictate shortcomings. The expected influences found in the literature study are examined with full scale monitoring and testing cases. Finally, a sensitivity analysis is performed on the current prediction model to specify the parameters with the biggest influence on deformation for different variants. These parameters are then assessed on how a more accurate determination might influence the predicted deformations.

The numerical simulations are carried out using advanced finite element analysis software Plaxis, specifically the HS(small strain) model. This model enables the investigation of various factors affecting hardstand deformation, such as varying soil stiffness, load distribution, and foundation characteristics.

The biggest shortcoming of the current prediction method is found to be the exclusion of time dependent behaviour. And the most influential soil parameters of the HS(small strain) model after the addition of a consolidation phase to the model are found to be the stiffness and permeability parameters. The deformation prediction is done for the entire range of uncertainty of these parameters (5-, 25-, 50-, 75-, 95- percentiles) to quantify prediction accuracy improvements were these parameters determined with precise. For both peat and clean clay the permeability coefficient is found to, when determined more accurately, have a 50% chance to result in a predicted deformation reduction of between 40 to 60 %, while a more accurate prediction of the stiffness parameters E_{oed}^{ref} , E_{50}^{ref} , E_{ur}^{ref} has a 50% chance to result in a predicted deformation reduction of between 65 to 75%

The findings of the research can be used by engineers to test the effectiveness of their own hardstand deformation prediction method and provide advice on the benefits extra soil investigation might lead to.

Keywords: Crane hardstands, deformation analysis, differential settlement, cyclic loading, Hardening soil small strain, FEM-modeling, sensitivity analyses.

1 | Introduction

In order to meet the environmental requirements set by the European Union, the Netherlands must invest heavily in green energy. To meet the growing demand, this energy would have to come from varying sources. A combination of solar, hydro, nuclear and the most obvious in the Dutch climate, wind energy, will be required. For wind energy, the Netherlands is looking at both generation on land and generation in the North Sea. Due to the lower investment costs of onshore wind turbines, this option is used where possible. The high loads involved in an onshore turbine installation, in combination with the weak subsoil present in large parts of the country, make the installation of the physical wind turbine a complicated task.

A wind turbine is installed with a crane. Due to the heavy weight of the turbine parts and the great height at which they must be installed, heavy cranes (>700 tons dead weight) are usually used. When these cranes are built on the soft soils typical for the Western part of the Netherlands and perform lifting operations, the subsoil deforms, which can jeopardize the stability of the crane. As a result, a crane hardstand, which is the foundation built for a crane to ensure stability, is designed based on the specific requirements and characteristics of a project. This crane hardstand is often tested for stability and deformations, among other things, to ensure that the hoisting operations can be handled safely.

Because usage of the crane hardstand is limited during its lifetime and the hardstand composes a significant part of the total project costs, it is beneficial to carry out their design as efficiently as possible, while the requirements for stability and deformation remain guaranteed. However, due to the unique combination of high forces and short installation time, there is still a lot of uncertainty in the case of crane hardstands about the best way to design a crane hardstand efficiently yet sound.

A major part of the problem is the strict requirements that the crane hardstand must meet. For example, the maximum rotation of the crane normally required by the crane company is 0.3° , which equates to a difference in settlement between the supports of a common crane between 30-80 mm, depending on the type of crane used. This difference in deformation can be caused by load cases where the forces on the support area's of a crane differ. An important example of this is the hoisting of the boom of the crane. When the boom is hoisted, the full dead weight of the crane, with the center of gravity close to one side of crane's support points, rests almost entirely on one side of the crane. In that situation, a greater vertical deformation will be expected on this side than on the other side of the crane, which will be subjected to less load.

The aim of this research is to provide a better picture of what exactly happens in practice during a wind turbine installation and how this translates into deformations in the subsoil. In addition, it is examined whether the current approach to the design of the crane hardstand can be improved in order to arrive at a more efficient or certain design. The approach is divided into 3 parts.

The first part consists of a detailed literature research to describe what a wind turbine lifting operation consists of and how this results in deformation of the subsoil, using soil mechanics theory.

Subsequently, the common current method for designing a crane hardstand M.P. Rooduijn (2019) will be analyzed and compared on the basis of a full-scale deformation monitoring during the installation of 2 wind turbines located along the A16 in North-Brabant, as well as 7 Full scale tests.

While monitoring the deformations of the outrigger crane that installs the turbines, the duration of the decisive lifting operations, the force changes between and during these operations as well as the associated deformations under each outrigger will be documented. This will be done

with the help of a total station that monitors the vertical deformation of the outriggers with beam points, while cameras focused on the load situation and the position of the crane indicate under which circumstances these deformations occur.

The purpose of monitoring is to clarify to what extent the loads actually differ between certain lifting situations and to compare the duration of these lifting operations. As well as to monitor whether the lifting operations result in time-dependent deformations. Both during specific operations and during the total operation period of one wind turbine installation

With the full-scale tests, the same load case, which simulates the total weight on one crawler track of a crane, in a load case that is normative for differential deformation, is tested on deformation on different crane hardstands with different soil structures. The weight is first built up, after which the full load remains for 6 hours and then reduced again. During the entire period, the entire test setup is monitored every half hour. This shows which part of the deformation is instantaneous and which part is time-dependent. The comparison is also made to how the different soil profiles respond to the same load.

With the help of the tests and monitoring, the shortcomings of the current design method are specified. This gives an indication of which deformation factors can be disregarded in certain situations and which should be included in the model. Specifically time dependent behaviour

The 3rd and last part of the research, that has as a purpose to improve the current design model, is sensitivity analysis. The analysis will be performed on the input parameters of the current design model (HS small strain). The uncertainty of the current model is largely due to the method of parameter determination from available soil data. The sensitivity analysis shows which parameters result in the greatest uncertainty in the deformation prediction and for which it might therefore be beneficial to determine 'more accurately'. An estimation will also be made of how much more precise the prediction might become as a result. For specific soil types and differing layer thicknesses/depths.

The research question to be answered in this thesis is.

What influences the deformation of a crane hardstand and how can this deformation be more accurately predicted to improve the design method

The structure of this research is indicated in the form of a block diagram as shown in Figure 1.1. The report contents are structured as follows aside from this introduction. Chapter 2 describes the physical process that comprises wind turbine lifting operations. It briefly discusses how a crane hardstand is designed to withstand the load cases accessory to turbine installations, what soil survey is performed and how the crane hardstand reduces deformation. Chapter 3 covers the phenomena that are expected to induce soil deformation under a load change. This is coupled to the relevance of these phenomena to the situation of a wind turbine lifting operation as described in chapter 1. The most important influences are designated. Chapter 4 presents the current design method. On the basis of which model the deformations are currently predicted and how the parameters for this model are determined. In addition, it discusses how the normative load cases for which the crane hardstand is tested are specified. Chapter 5 discusses the setup and results of the full scale monitoring performed in this research. Chapter 6 contains the setup and results of the full scale tests performed in this research. Chapter 7 describes the structure of the sensitivity analysis performed and presents the results on what parameters are the cause of the largest uncertainties in the model. Chapter 8 discusses the impact a more precise determination of these parameters might have on the predicted deformation. Chapter 9 discusses and combines the findings and analysis of the research. Chapter 10 covers the conclusions. and provides recommendations for further investigation.

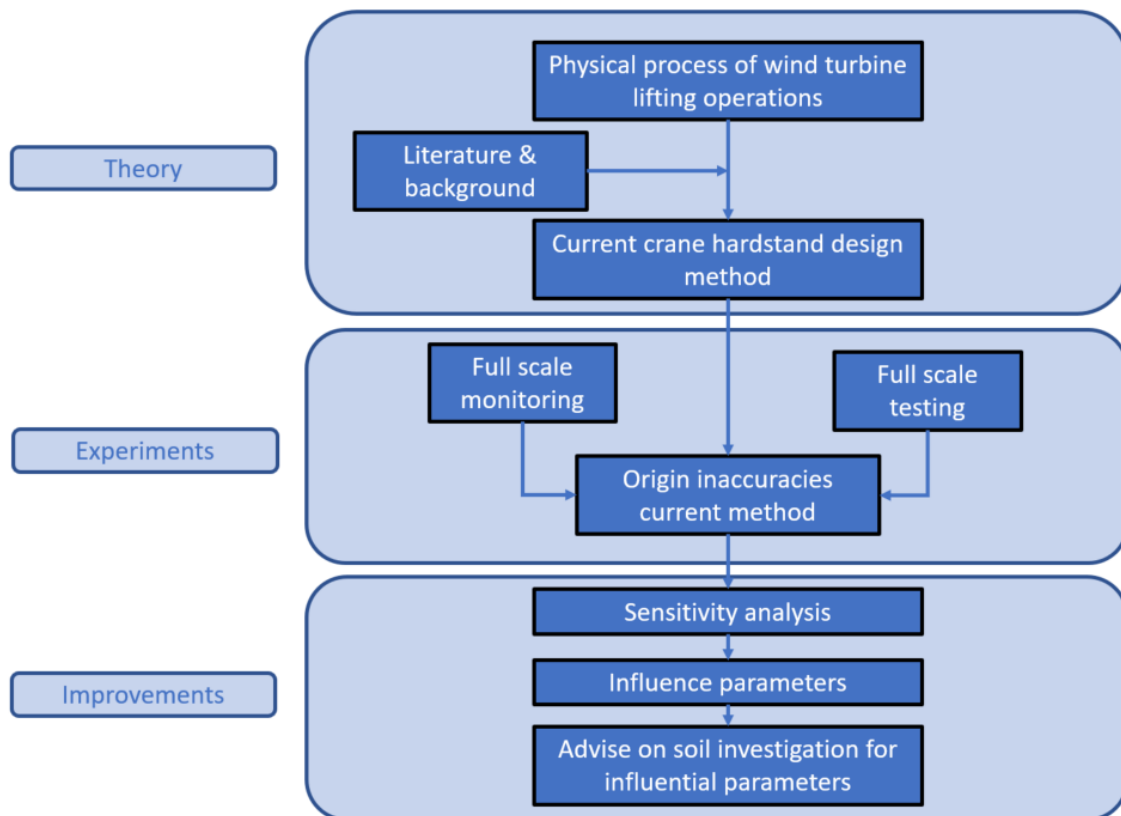


Figure 1.1: Thesis setup

2 | Physical process

Whenever a soil profile undergoes a pressure change a deformation follows. This deformation is influenced by the geometry of the soil profile, the condition of the environment, parameters of the soil and the nature of the load (time, proportion et cetera). The process of hoisting turbine parts into place and the accessory soil deformations are discussed in this chapter.

2.1 Crane Hardstands

In this section the installation process of an on-shore wind turbine is discussed. An in depth analysis concerning crane hardstands is summarized in the handbook: Crane Hardstands For Installation Of Wind Turbines M.P. Rooduijn (2019).

2.1.1 Design

For the design of the crane hardstand it is important to take into account the type of turbine, type of crane, supply routes, storage space and of course the subsurface.

Turbines come in varying sizes with hub heights of on-shore turbines ranging from 60-165m accompanied by rotor diameters of the same magnitude. Since a larger rotor diameter increases the area of influence to the power of two an increase in height of the wind turbine greatly improves the power output. Because of this wind turbines are only expected to get larger.

This increase in length however, has as a result that larger cranes are needed for installation. This crane needs a horizontal surface to preserve stability and guarantee safety during installation. The cranes types that are primarily used for the installation of on shore wind turbines are crawler cranes, as seen in Figure 5.1b, where the load is transferred to the surface by the crawler, and outrigger cranes, as seen in Figure 5.1c, where the crane lifts itself by 4 outriggers through which the load is carried to the surface. Both will be considered in this report.

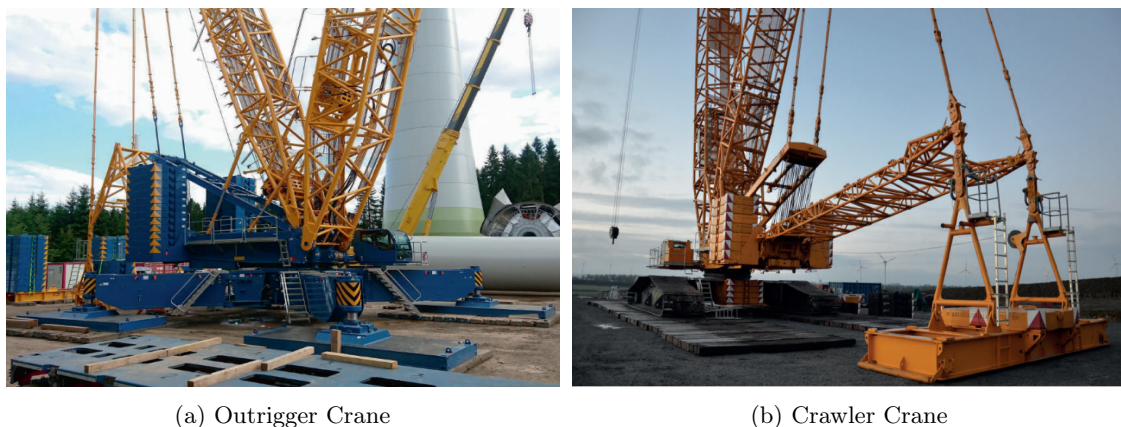


Figure 2.1: Different crane types

The load exerted on the crane hardstand consists primarily of the weight of the crane, the weight of the turbine part, the superlift and a wind load. During the installation process many different load cases should be considered as discussed in Section 2.1.3. These loads might cause the crane hardstand to deform or even fail. Due to the load not being uniform over the area underneath the crane and because of heterogeneity in the soil profile the crane foundation may undergo differential deformations. These deformations cause the crane to tilt. A small tilt can already lead to a positional difference at the top of the crane of multiple meters, resulting in

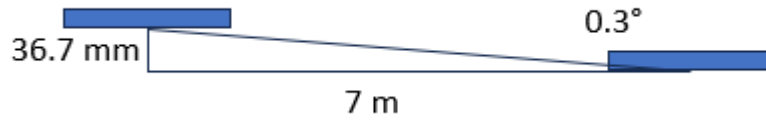


Figure 2.2: Max allowable deformation for 7m wide crane

very different load cases. Therefore only 0.3° tilt is allowed, which comes down to ± 30 mm differential settlement between crane boundaries, depending on the width of the crane used. For this reason the crane hardstand needs to be checked for bearing capacity as well as maximum tolerated settlement. An example for the differential deformation that results in a 0.3° is provided in Figure 2.2.

2.1.2 Soil investigation

The intention of the crane hardstand is to provide a stable base for the crane during the installation of the wind turbine. After the turbine is installed the crane hardstand might be used again for maintenance or eventual disassembly. Due to the limited time the crane hardstand is being used and the limited budget available, the emphasis of the design is to be cost effective.

Because of the small budget it is not always possible to execute extensive soil investigation. The soil investigation on which the crane hardstand design is based, consists mostly of cone penetration tests (CPT's). A CPT is relatively easy to perform in-situ and cheap. It records the tip resistance, sleeve friction and sometimes porewater pressure over a soil profile, as can be seen in Figure 2.3 Geoservices (2023). An extensive description of the use of a CPT in geotechnical engineering is provided by (Lunne et al., 1997). With the output of the CPT specific soil layers can be classified according to Robertson (2009).

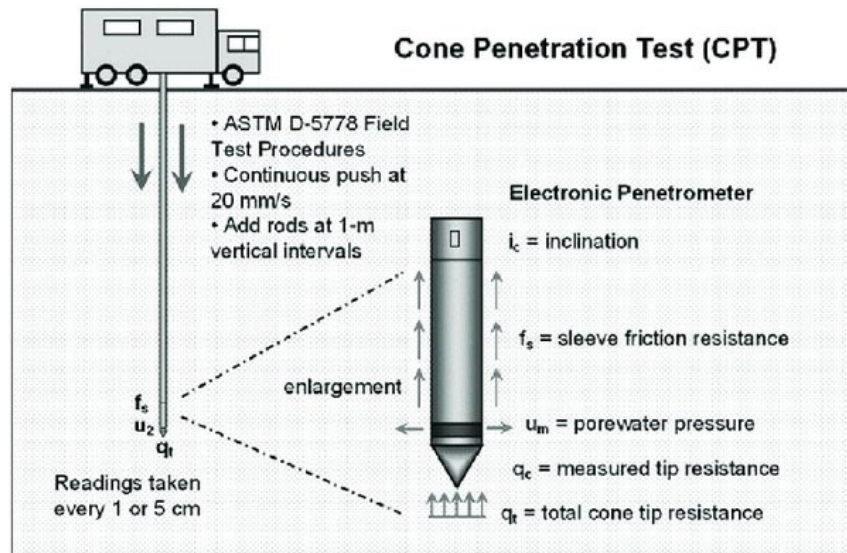


Figure 2.3: CPT overview

To get an idea of the subsurface, the first step is to see which information is already available through open source databases such as Dinoloket TNO (2022). Aside from this, a combination of boreholes and CPT's near the desired hardstand location are used to create a profile from where the stability and deformation are assumed to be the largest. The crane hardstand design will be

based upon this specific profile to make sure the deformations will stay within the requirements of a specific project. This is elaborated on in Chapter 4

2.1.3 Installation Process

The installation process of an onshore wind turbine consists of multiple phases. During each phase a different load is exerted on the pressure points of the crane. The lifting stages where the difference of the load on different outriggers or crawler tracks is largest are the most critical for differential settlement. This is not necessarily the stage where the highest load is occurring. In this project the installation of 2 turbines and the corresponding deformations are closely monitored. This will be discussed in more detail in Chapter 5. 2.4 gives an overview of the tower parts that need to be lifted.

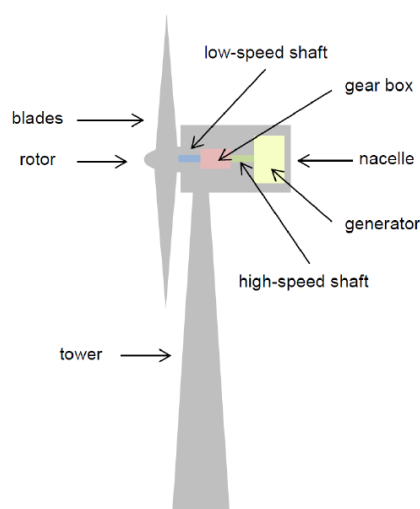


Figure 2.4: Wind turbine parts

Turbine construction Phase	Description
1. Build up of the crane	The base of the crane is driven onto the crane hardstand and the boom is assembled laying down step by step
2. Adding the counter weight	The counter weight used to keep the crane balance while rigging the boom
3. Rigging of the boom	During boom rigging the moment on the pressures points of the crane becomes large. To counteract this the counterweight is lifted resulting to a large force on a specific crawler track / set of outriggers
4. Installation of the tower elements	as the tower is to large to lift as a whole it is constructed in different parts. The lower parts are the heaviest because they need to carry the most weight
5. Installation of nacelle	The nacelle is the box around the parts needed for the energy conversion
6. Installation of the rotor blades	the rotor blades are installed one by one.
7. Letting down the boom	After construction of the wind turbine the crane boom is let down. This once again leads to the heaviest loads exerted on the pressure points

Table 2.1: Wind turbine construction phases

During installation, the load of the crane is continuously changing. This results in multiple un/reloading cycles. The effect this can have on the soil is discussed in Section 3.2.

The time it takes to install a wind turbine is highly variable. This is partly due to logistical issues and differences between turbines. However, the variability is caused for a large part by the wind conditions. Hoisting operations are halted when the expected wind speed at the top of the crane is higher than 10m/s and if the wind speeds get above 20 m/s the boom of the crane has to be hoisted down. Therefore, construction time of a single turbine can vary between 2 days and multiple weeks

2.2 Mitigation measures

To ensure stability for the crane during installation, different kinds of mitigation measures can be taken to ensure the deformations stay within the requirements. Deformations in the subsoil below the water-level occur primarily due to a change of soil pressure. The mitigation measures used for a crane hardstand can be divided into two categories: mitigation measures that decrease the magnitude of pressure change or mitigation measures that reduce the effect the pressure change will have on the soil deformation.

The 'simplest' way to reduce the pressure change in the subsoil is by decreasing the loads. Different cranes have different weights. However, specific height and lifting strength requirements combined with crane availability often don't leave a choice on which crane can be used.

Another way to limit the pressure change in the deformable subsoil layers is by distributing the load over a larger surface area. This can be done with wooden or steel beams, a stratum layer (a geogrid filled with gravel) , an enviromat a soil spreading measure designed by HeavyLiftNews (2021) or even constructing the crane hardstand on a piled foundation

Pre-loading is a commonly used technique in geotechnical engineering to minimize the deformation of a foundation constructed on soft soils. The idea behind pre-loading is to apply a temporary load to the foundation before the permanent load is applied. The purpose of this temporary load is to cause the soil to undergo some deformation, which will help to consolidate the soil and improve its strength and stiffness. This process can take several months, depending on the soil type. The duration of the pre-loading will be determined by how much consolidation is required to achieve the desired level of settlement.

Vertical drains are another technique that can be used to reduce the amount of deformation that will occur in a crane hardstand. Vertical drains are typically installed in the soft soil layer, and they allow water to flow out of the soil more quickly, which in turn reduces the amount of time it takes for the soil to consolidate. This can significantly reduce the amount of time required for pre-loading, as the soil will consolidate more quickly.

The combination of pre-loading and vertical drains can be an effective way to minimize the deformation of a crane hardstand on soft soils. By using pre-loading to consolidate the soil and vertical drains to accelerate the consolidation process, the amount of deformation that will occur when the crane is placed on the foundation can be significantly reduced.

3 | Soil behaviour

This chapter discusses the behaviour of a soil when it is exposed to a pressure change. The goal of the chapter is to summarize what influences the expected deformation as a result of the crane activities during the hoisting of the turbine parts. This is used to evaluate the current deformation prediction method used in practice.

3.1 Mechanical load influences

3.1.1 Flexibility of the foundation

The flexibility of the foundation has a big influence on how the load is transferred to the surface. While the crawler tracks or outriggers of the crane are commonly perceived as rigid components, the crane mats used to distribute the load can vary greatly. Where wooden beams are usually more flexible than steel beams. The response of the soil on the footing depends on the characteristics of the footing, the superstructure, connections, soil type and loads. Since it is not possible to analytically determine the soil response, assumptions have to be made. The effect of footing flexibility on structural response is researched by (Tabsh & Al-Shawa, n.d.). For rigid footings, the soil pressure distribution can be assumed to be linear. For flexible footings, Bowles designed a method to subdivide the footing into discrete elements on elastic supports where the soil pressure distribution is governed by the modulus of sub-grade reaction Bowles (1996). A footing is considered to be rigid when the relative stiffness factor of the footing $K_r \geq 0.5$. Tabsh & Al-Shawa (n.d.) validated the relative stiffness factor to be Equation (3.1).

$$K_r = \frac{Et^3}{k(1 - \mu_z^2)(B - b)^2(L - l)^2} \quad (3.1)$$

Where:

E = modulus of elasticity of the structure

t = uniform structure of the footing

k = relationship between the modulus of elasticity and the subgrade reaction Equation (3.2)

b = column dimension along footing dimension B

L = footing dimension perpendicular to B

l = column dimension along the footing dimension L

κ = Equation (3.2)

$$k = \frac{E_s}{B(1 - \mu^2)} \quad (3.2)$$

Where E_s = modulus of elasticity of the soil.

Tabsh found that a stiffness factor K_r of 1.0 or higher can safely be assumed to be rigid while for values of K_r lower than 1.0 assuming the foundation to be rigid is assumed to be conservative.

3.1.2 Load spreading

A pressure change on the surface does not result in the exact same pressure change throughout the soil profile. Over depth the load is carried by an increasingly large area decreasing the pressure change over depth. Many different methods to determine the propagation of the load through the soil column have been. Most commonly used for calculation purposes are the Boussinesq method Boussinesq (1883), the Westergaard equation (Westergaard, 1938) and the 2:1 method. Das (2017) describes the Boussinesq method as 'a relationship for stress increase due to a point load Q acting

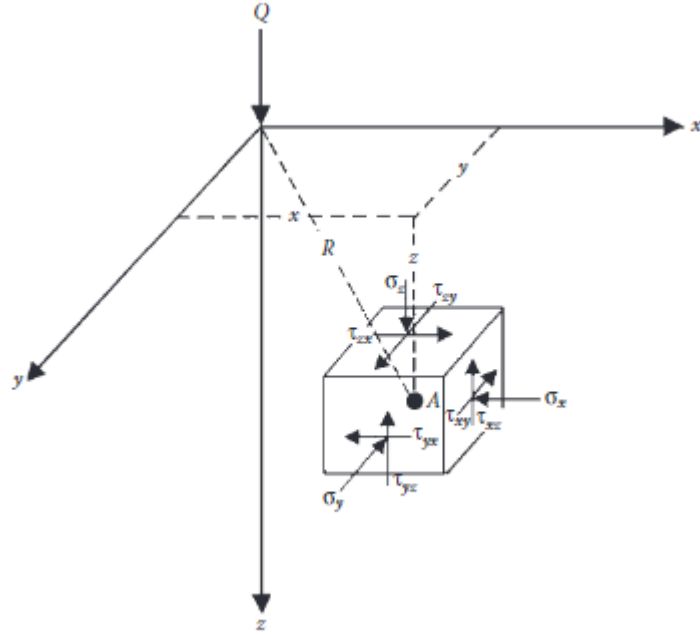


Figure 3.1: Boussinesq's problem

on the surface of a semi infinite mass' Das (2017). The Boussinesq equations for the Cartesian coordinate system are depicted in Equation (3.3)-Equation (3.5)

$$\sigma_z = \frac{3Qz^3}{2\pi R^5} \quad (3.3)$$

$$\sigma_x = \frac{3Qz}{2\pi} \left[\frac{x^2 z}{R^5} + \frac{1-2\nu}{3} \left[\frac{1}{R(R+z)} - \frac{(2R+z)x^2}{R^3(R+z)^2} - \frac{z}{R^2} \right] \right] \quad (3.4)$$

$$\sigma_y = \frac{3Qz}{2\pi} \left[\frac{y^2 z}{R^5} + \frac{1-2\nu}{3} \left[\frac{1}{R(R+z)} - \frac{(2R+z)y^2}{R^3(R+z)^2} - \frac{z}{R^2} \right] \right] \quad (3.5)$$

Since a point load is not applicable in most loading cases, a lot of research is done to describe the influence of a loaded area on the stress increase in the subsurface.

Ahlvén describes how the Boussinesq equations can be translated to a rectangular surface pressure Ahlvén & Ulery (1962)

The load distribution determines the magnitude of pressure change at a certain depth. A larger distribution results in smaller pressure changes in a soil layer which in turn results in smaller deformations

3.1.3 Load Magnitude

The load of the crane and turbine parts and therefore the pressure exerted on the soil surface is highly variable. This un- and reloading can lead to deformations as described in 3.2.3

3.2 Deformations

Deformations of the soil as result of a load change can either be elastic (reversible) or plastic (irreversible). This section discusses both types of deformation.

3.2.1 Elasticity

The reversible strains occurring as a result of a stress increment are described in the theory of elasticity (Timoshenko & Goodier, 1951). Elastic deformations are expected when the pressure increment stays within the elastic zone and does not exceed the pre-consolidation pressure. The most important soil parameters to describe the elastic behaviour are the Poisson's ratio ν and the modulus of elasticity E_s . The Poisson's ratio describes how a strain in the vertical direction translates to a strain in horizontal direction. The modulus of elasticity indicates the stiffness of a soil.

Trautmann and Kulhawy (Trautmann & Kulhawy, 1987) proposed a relationship to determine Poisson's ratio based on the relative friction angle, which in turn can be determined from laboratory tests. In an undrained situation the Poisson's ratio of a saturated clay is 0.5. This is explained in Section 3.2.2.

Empirical correlations between cone resistance q_c and the modulus of elasticity were proposed by (Schmertmann & Brown, 1978) (R. P. Terzaghi K. & Mesri, 1995). Whenever limited soil information is available ballpark values for both parameters are suggested per soil type for an initial calculation of the elastic deformation.

The elastic relations between stress and strain components in tension are described by Hookes law (Timoshenko & Goodier, 1951) as shown in Equation (3.6)

$$\begin{aligned}\epsilon_x &= \frac{1}{E}[\sigma_x - \nu(\sigma_y + \sigma_z)] \\ \epsilon_y &= \frac{1}{E}[\sigma_y - \nu(\sigma_x + \sigma_z)] \\ \epsilon_z &= \frac{1}{E}[\sigma_z - \nu(\sigma_x + \sigma_y)]\end{aligned}\tag{3.6}$$

ϵ = strain

E = stiffness modulus

σ = soil pressure

This method to determine strain is only valid when deformations are small enough so that the effect of the deformations on the external forces can be neglected.

To account for shear stresses on the element the shear modulus G is used to express the relation of shear strain γ and shearing stress τ as shown in Equation (3.7)

$$\gamma = \frac{\tau}{G}\tag{3.7}$$

Where G = Shear modulus Equation (3.8), γ = shear strain and τ = shear stress

$$G = \frac{E}{2(1 + \nu)}\tag{3.8}$$

Furthermore, the bulk modulus K can be defined as the ratio of the mean stress increment and the volumetric strain increment Equation (3.9). This bulk modulus is based on isotropic compression.

$$K = \frac{E}{2(1 - 2\nu)}\tag{3.9}$$

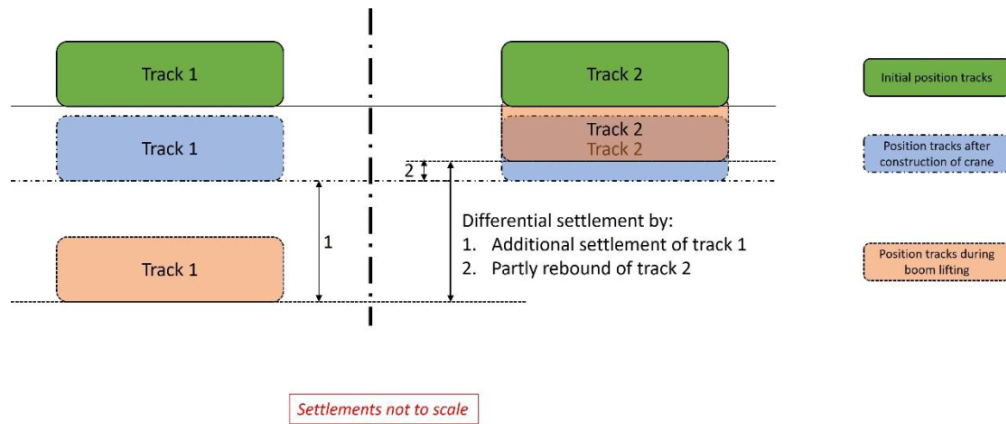


Figure 3.2: Causes differential deformation

Elastic deformations are important concerning crane hardstand due to rebounding of the soil. Whenever a load increase during a lifting operation is modeled compared to the load of the dead-weight of the crane, it should be noted that the load on another pressure point might decrease compared to the dead-weight. The rebound of the soil will add to the differential displacement of the pressure points as shown by 3.2

3.2.2 Drained vs. Undrained behaviour

Whenever external loading is applied over a small time period and water cannot flow easily through the pores the water will carry the isotropic part of the stress change. This results in excess pore pressure. When considering the effective stress principle from Terzaghi K. Terzaghi et al. (1996) this excess pore pressure causes a decrease in effective stress, which in turn lowers the strength of the soil profile.

Whether a soil acts drained or undrained on external loading can be determined on the hydrodynamic period of the soil. The Hydrodynamic period is determined as in Equation (3.10)

$$T = \frac{kE_{oed}t}{\gamma_w L^2} \quad (3.10)$$

Where:

- T = hydrodynamic period
- k = permeability
- E_{oed} = oedometer stiffness
- t = consolidation period
- γ_w = unit weight of water
- L = drainage length.

Vermeer and Meier determined the behaviour to be undrained if $T < 10^{-4}$ and drained if $T > 2$. (Vermeer & Meier, 1998)

From this formulation it can be concluded that under the short term loading to which the crane hardstands are exposed fine soil types with a low permeability are likely to behave undrained (dependent of the layer thickness) while coarser soils will behave drained.

Due to the very low compressibility of water an undrained soil is assumed not to show any volumetric shear. Resulting in a poisson ratio of $\nu = 0.5$.

To implement undrained behaviour in Hooke's law the elastic parameter E and ν become undrained elastic parameters E_u and ν_u . Brinkgreve (2022) The bulk modulus of the water in the pores is a combination of the bulk modulus of water K_w , the bulk modulus of pore air K_{air} and

the degree of saturation of the soil S as described by Equation (3.11)

$$K_w = \frac{K_w^0 K_{air}}{S K_{air} + (1 - S) K_w^0} \quad (3.11)$$

From this equation can be concluded that a small change of degree of saturation has a large influence on the bulk modulus of the pore water.

3.2.3 Virgin-, un- and reloading

Whenever a soil element has previously experienced a pressure higher than the current pressure the soil is over consolidated. If the pressure in the soil is increased until the pre-consolidation pressure (the maximum experienced pressure) the load increment is classified as 'reloading'. In a perfect elastic model the reloading follows the same trend on the stress strain curve as the unloading that occurred after the release of the pre-consolidation pressure. In reality plastic deformations occur slightly changing the strain path as further discussed in Section 3.3. The unloading-reloading is important concerning the crane loads due to the dynamic nature of the turbine installation process, constantly un- and reloading the different pressure points. This cyclic loading can result in plastic deformation as a result of hysteresis, energy dissipation, damping Toyota & Takada (2021) or strain/pore pressure accumulation Sanin & Wijewickreme (2006). Whenever the pressure increment is large enough such that the total pressure is higher than a previously experienced pressure the load type is virgin loading.

3.3 Plasticity

Plastic deformations are irreversible. This means that upon unloading the soil stays deformed.

Although in an undrained situation the isotropic load is carried mostly by the 'in-compressible' water the soil can still undergo plastic deformation without the excess pore pressure leaving the pores.

This can occur for instance by means of a change in the micro-structure of the undrained layer. Zang et al. performed loading and unloading tests combined with field emission scanning electron microscope (FESEM) tests on undisturbed clays to study the influence the loading-unloading process has on the pore evolution of the clay structure (Zhang et al., 2020). The paper distinguishes pores between small pores $< 0.2\mu m$ and large pores $> 0.6\mu m$. The small pores are shown to have intrinsic characteristics and do not change significantly in the fragmentation fractal dimension. The large pores, however, were influenced greatly by (un)loading. Therefore, the change in pore size distribution can be contributed for the most parts to the changes of the larger pores. The change in pore size distribution caused a change of the swelling index C_s (increased as the total area of the large pores decreased) as well as a change in the compression index C_c . C_c is proved to change non-linearly with the pore evolution under loading and unloading. The paper differentiates 3 stages of the evolution of pore fractal characteristics under the un(load)ing process, namely: the natural structural stage, the structural adjustment stage and the new equilibrium stage.

More research on un- and reloading oedometer test on natural stiff clays, namely Ypresian clays, was performed by Cui et al. (Cui et al., 2013). When examining the un- and reloading curves they found that the paths of these curves can be considered to be bi-linear. The curves can be distinguished by a small and large slope separated by a threshold stress. This stress is identified as 'the swelling pressure corresponding to the void ratio just before the unloading or reloading'. Upon unloading, if the stress is higher than this threshold swelling pressure the mechanical restructuring effects dominate resulting only in small microstructure changes and therefore a small rebound of the soil. Whenever the threshold pressure is surpassed the physico-chemical resulting in a larger microstructure change and more swelling occurs. Upon reloading the physico-chemical repulsive

force prevents the soil from deforming at first but when the pressure passes the threshold pressure the mechanical effects dominate resulting in larger microstructure changes.

Another form of significant plastic deformations is by accumulation of smaller plastic strains under unloading and reloading. Oedometer tests under repeated unloading-reloading on reconstituted Ariake clay samples for the Saga Plain, Japan, were performed by Suddeepong et al. (Suddeepong et al., 2015). The article states that even in the over-consolidated stress range un- and reloading does not occur purely elastic. Repeated un- and reloading results in plastic strain accumulation. The paper provides a modification of the elasto-plastic soil model proposed by Butterfield Butterfield (2011) by not assuming the 'intermediate' un- and reloading in the overconsolidated range to be fully elastic.

On (un)loading situations with small frequency the aforementioned deformations will not induce extreme deformations. Whenever the amount of cycles of the un- and reloading or the amplitude of the cyclic load is high, as is the case with for example an earthquake or underneath a busy road, the resulting plastic deformations might be significant. Lin Gua et al. Have researched the impact of long term cyclic loading (50.000 cycles) on the deformation of undisturbed soft clay from Wenzhou, China Guo et al. (2013). They came to the conclusion that the stress-strain hysteric loop, resilient modulus and permanent strain are significantly dependant on the cyclic stress ratio and the confining pressure.

3.3.1 Consolidation

In a soil layer with limited permeability such that water can not flow freely, a change in pressure conditions will result in excess pore pressures. Over time, if the load is kept constant, the excess pore pressures will dissipate over time, resulting in a soil deformation. This process is called consolidation.

Whether a soil layer can be assumed to behave drained or undrained depends on the hydrodynamic period of the soil as discussed in Section 3.2.2. This section discusses the dissipation of excess pore pressure over time, resulting in deformations.

Whenever a fully or partially saturated soil is subjected to a partial pressure the deformation is dependent mostly on the stiffness of the porous material as well as the characteristics of the fluid in the pores. The deformation of the soil as well as the flow of the pore water is described by the theory of consolidation. A publication by Verruijt covers the general consensus of the basic equations considering the theory of consolidation Verruijt (2016). The consolidation theory was at first developed by Terzaghi. The theory was only valid for the one-dimensional case. Terzaghi considered the deformations to be caused primarily by reorganization of the soil particles and assumed the pore volume to be incompressible. This assumption often simulates real soil behaviour for compressible soils such as clay. Biot elaborated on the theory by expanding the theory to 3 dimensions and to by taking the compression of the pore fluid into account.

For the case of crane hardstands it is relevant to know the degree of consolidation after a, for settlement cases, small time period of 2-6 hours. 3.3 . displays the degree of consolidation after a specific time factor T .

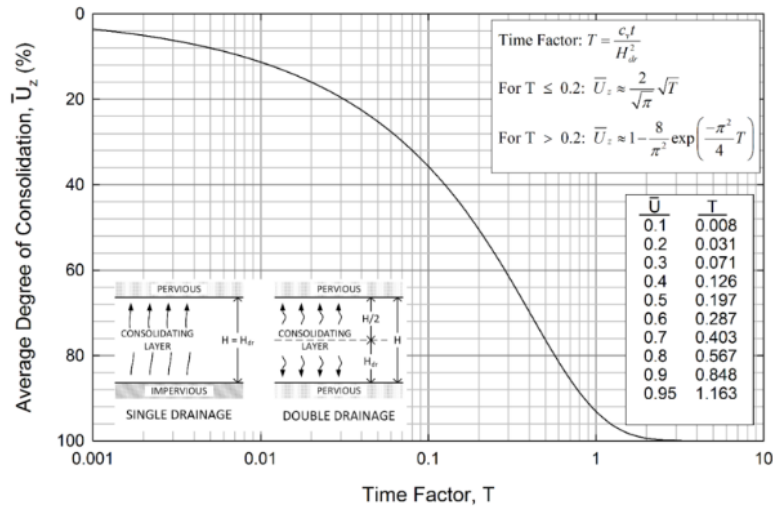


Figure 3.3: Degree of consolidation

c_v = consolidation coefficient $\frac{k}{m_v \gamma_w}$
 t = time
 H = soil layer thickness
 k = permeability coefficient
 m_v = coefficient of volume change
 γ_w = water weight

This indicates that the degree of consolidation is mostly dependent on the permeability and layer thickness.

3.4 Creep

Creep is the development of time-dependent shear and/or volumetric strains at a state of constant effective stress Khoshghalb (2013). Creep usually only results in significant deformations after long time periods and is therefor not considered in this research.

3.5 Influence diagram

Figure 3.4 provides an overview of the expected influences of the deformation of the crane hardstand based on literature and how they are connected. The parts that are the most relevant for this research are highlighted in red:

Virgin, un- and reloading: The un/reloading nature of the turbine parts lifting and its possible resulting deformations are researched in Chapter5

Distribution of the soil profile: The influence of the depth of a soil layer on the models accuracy is researched in Chapter7

Primary compression strains: The rigging of the boom will likely exceed the pre-consolidation pressure, resulting in primary compression strains

Consolidation: Whether consolidation should be included in the deformation prediction model is assessed in Chapter6

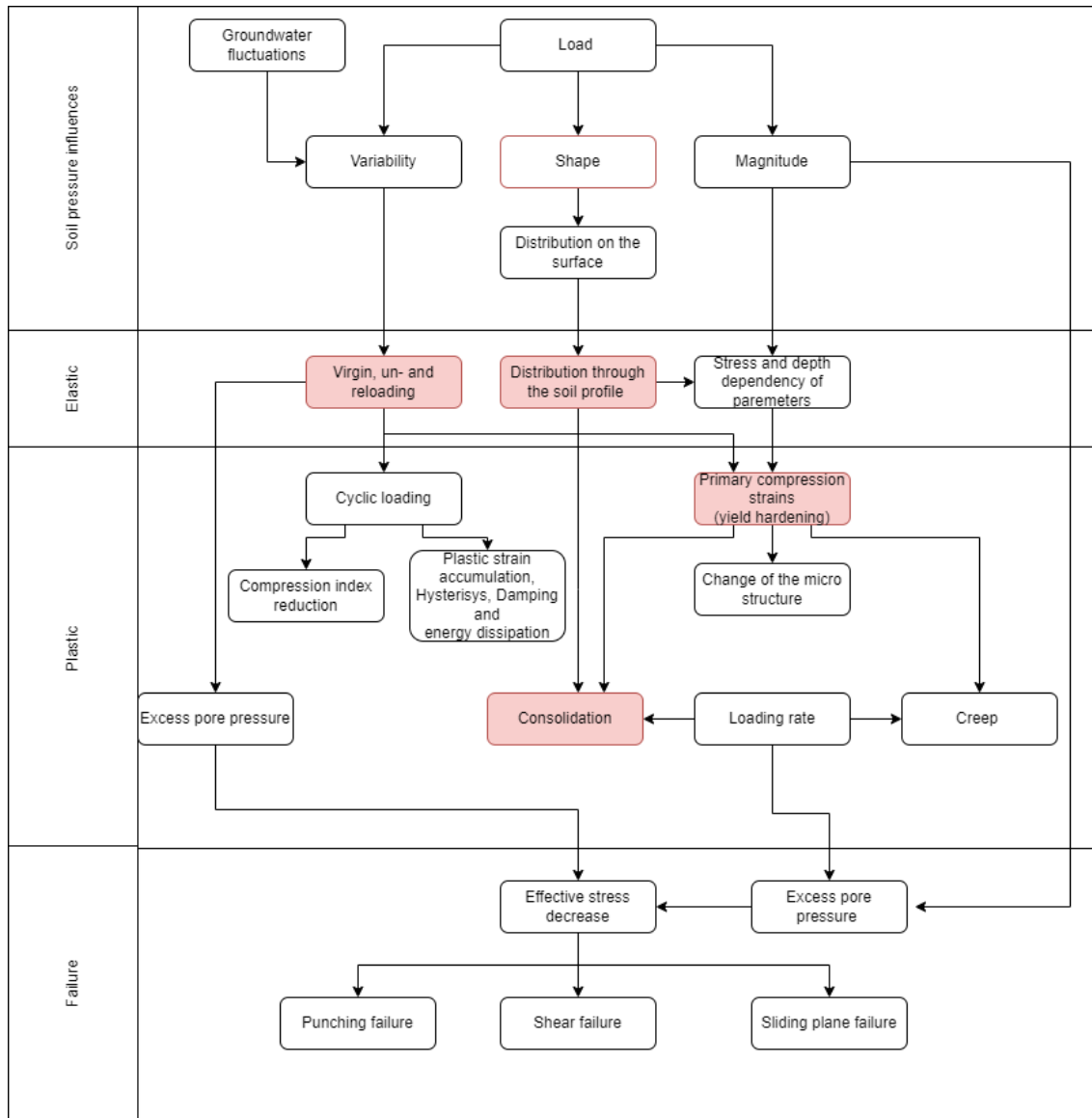


Figure 3.4: Influence Diagram

4 | Current prediction method

This chapter discusses the current method used to predict the deformations of a crane hardstand and analyzes the shortcomings of this method.

4.1 Soil investigation

The soil investigation is performed during multiple stages of the design process. At first during the feasibility study of the project. A lot of information about the subsoil in the Netherlands is collected on the open source website dinoloket TNO (2022) and other databases. Previously documented CPT's and boreholes are stored here. These can be used to give an indication of the strength and deformation susceptibility of the subsoil and whether or not a location is suitable for a specific project.

Whenever the project is past the feasibility stage more extensive soil investigation is performed to determine the best possible locations of the wind turbines. This extra soil investigation mostly consists of CPT's as well as boreholes due to the relatively low costs of these methods, while still providing sufficient information for the design stage. Other factors influencing the final locations are the possibilities for access roads, possible harm to the environment and local residents and of course yearly wind speed averages in the area.

After the locations are determined additional CPT's and boreholes might be used to give an more precise view of the subsoil at the locations of the Main Crane HardStand (MCHS) as well as the Auxillary Crane HardStands (ACHS's). The most critical CPT (the one that is expected to result in the largest deformation) is then used to determine the model specific soil parameters.

4.2 Plaxis

PLAXIS is a finite element program that is commonly used in geotechnical engineering to analyze the behavior of soil and rock structures. The finite element method is a numerical technique that is used to solve complex engineering problems by dividing the structure into small and simpler elements and then solving the mathematical equations considering forces and displacements for each element and well as the effect it has on other elements. The method can be used to analyze stress, strain, and deformation of the structure under various loading conditions.

In the case of PLAXIS, the finite element method is used to simulate and analyze the behavior of soil and rock structures. The program allows the user to model the geometry of the structure, define the material properties of the soil or rock, and apply various types of loading conditions. The program has different built in soil behaviour models which can be used for problems of different levels of complexity and expected behaviour. These models and how they simulate soil behaviour are elaborated on in the Plaxis Material Models Manual Bentley (2023).

4.3 HSsmall model

The model currently used in practice to assess the deformation of a crane hardstand as a result of hoisting activities is the HSsmall model. Extensive research is done on the correlations between the HSsmall model parameters and the cone resistance that results from a CPT. Therefore, the input parameters of the model are determined relatively easily and accurately with minimal soil investigation. Limiting the need for additional laboratory tests.

the Hardening Soil Small Strain (HS) model is a constitutive model that is implemented in PLAXIS to simulate the behavior of soil and it excels in assessing the behaviour under small

strain conditions. The model makes distinction between primary loading and un- / reloading and remembers pre-consolidation stress. Therefore, it includes compaction hardening. Another feature of the model is that it includes friction hardening which decreases the stiffness in deviatoric loading.

Limitations of the model are that it does not consider softening and it is not able to model time-dependent behaviour. It is possible however, to add a consolidation phase to your model. As creep is not expected to be significant for the crane hardstand case, the limitation is acceptable.

4.4 Soil model and parameter determination

The Hardstands are often designed based on the most representative CPT or of a combination of multiple CPT's and boreholes. The representative CPT(s) is/are used to divide the subsoil in specific layers. This is done based on changes of the cone resistance q_c [Mpa] as well as friction ratio R_f [%]. A specific soil type is described to each layer based on Robertson Robertson (2009). Table 2b of NEN9997-1+C2 Normcommissie "Geotechniek" (2017) uses the layer type in combination with the normalized cone resistance to assign the strength and stiffness parameters to each layer.

The deformation of the MCHS as a result of the installation process is determined with the FEM program Plaxis. Current practices use the Hardening Soil Small Strain as described in Section 7.2. Since the parameters used in this model are not directly obtainable from a CPT empirical correlations are used to arrive to a sufficient model.

The layer description, thickness and type are derived directly from the CPT according to Robertson Robertson (2009) as previously described.

Once a layer is distinguished and classified parameters are assigned to this layer. Some of these parameters are determined solely by the type of soil and other are also influenced by state and pressure at the location. For the hardening soil small strain model the parameters are determined based on CPT's as follows.

Strength parameters The volumetric weight, saturated and unsaturated, the internal friction angle and the cohesion are determined with table 2b as discussed above Normcommissie "Geotechniek" (2017).

Stiffness parameters The oedometer stiffness is determined from the CPT with the correlation as shown in Equation (4.1).

$$E_{oed} = \alpha * q \quad (4.1)$$

α = Empirical cone factor
 q = Cone resistance from CPT

The Empirical cone factor is dependent on the soil type classification as presented by Sanglerat (1972)

With the volumetric weight of the soil and additional information on the thickness of the soil layers and the water level, the average effective stress of a layer can be predicted. This stress is used to transform the E_{oed} to E_{oed}^{ref} , which would be the oedometer stiffness of the same soil layer at a reference pressure (often taken as 100kPa). The correlation between E_{oed} to E_{oed}^{ref} is given by 4.2

$$E_{oed} = E_{oed}^{ref} (\sigma / p^{ref})^m \quad (4.2)$$

σ = average effective stress
 p^{ref} = reference pressure [100kPa]
 m = stress dependency parameter

The E_{50}^{ref} and E_{ur}^{ref} are determined as factors of the E_{oed} based on soil type as presented in table 4.1 CUR2003-7.

Soil type	E_{50}	E_{ur}
Sand	1xEoed	4xEoed
Silt	1xEoed	5xEoed
Clay, very sandy	1xEoed	5xEoed
Clay	2xEoed	10xEoed
Clay, organic	2xEoed	12xEoed
Peat	2xEoed	12xEoed

Table 4.1: Relation between Eoed, E50 and Eur

The small strain parameters G_0^{ref} and $\gamma_{0,7}$ are determined by 4.3 and 4.4

$$G_0^{ref} = (2.5 \times 10^4) G_{ur}^{ref} \approx 4 \times \frac{E_{ur}^{ref}}{2(1 + \nu_{ur})} \quad (4.3)$$

$$\gamma_{0,7} \approx \frac{1}{9G_0} \left[2c'(1 + \cos(2\phi')) - \sigma'_1(1 + K_0) \sin(2\phi') \right] \quad (4.4)$$

4.5 Mechanical input

The loads that need to be taken into account when designing the Main and Auxiliary Crane Hard Stands are dependent on the type of crane to be used. During the preliminary design stage certain starting points/boundary conditions are defined. What safety class is appropriate, whether or not the water level will be lowered under the hardstand level during operation etc. These will vary for each situation and should be accounted for appropriately.

The critical load cases that the hardstand will be exposed to will be provided by the company delivering the crane. These loads depend on the self weight of the crane and the foundation, the weight of the turbine parts to be lifted and the distance of the weight from the center of mass. The total load consists of a permanent and a variable load, which when designing the hardstand for the ultimate limit state (ULS) results in different partial factor used in calculations. Often a rate of 50/50% is used to divide the load in a permanent and variable part.

Aside from the vertical load as described above a horizontal load caused by wind and acceleration of the crane is exerted on the hardstand. For simplicity the maximum horizontal load a hardstand should be able to with-stand is taken to be 10% of the total vertical load.

Since the type of crane that will be used for the project is often only known weeks before start of the project due to availability of the cranes, the hardstand should be designed for different type of cranes. A mobile crane transfers the load as a point load through 4 outriggers. The outriggers have a sufficiently stiff foundation such that the load can be assumed to be distributed evenly over the area of the foundation. A crawler crane transfers the load through it's crawler tracks. The load on the crawler tracks depends on the positioning of the crane. As mentioned different the different load situations are provided by the crane company. An example for both a crawler and an outrigger crane is shown in Figure 4.1. These critical loading situations are used to design the crane hardstand. They can however differ based on the type of calculation that is to be done. For bearing capacity checks for example the highest exerted load is often most critical while for differential deformations the loading situation with the biggest difference of loads between two outriggers/crawler tracks might be critical. The choice of the right load case to be used in the design calculations is made with engineering judgement.

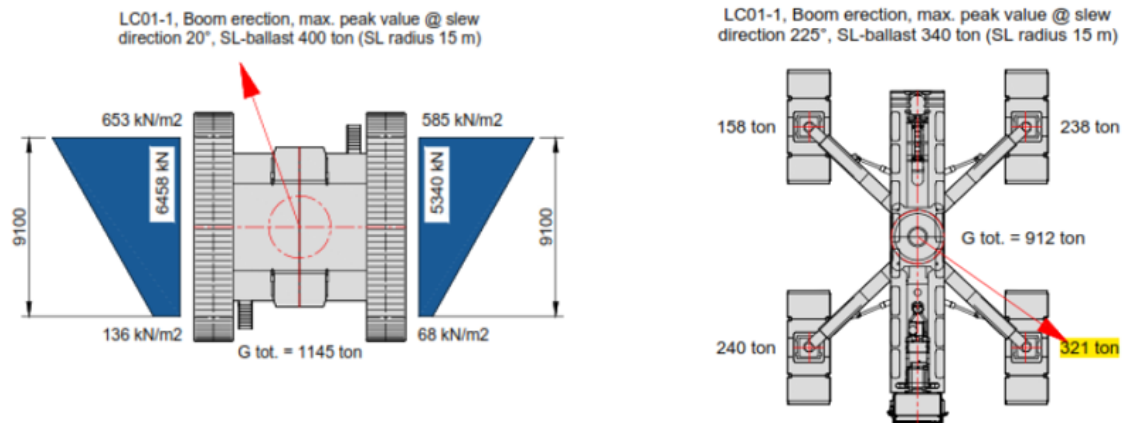


Figure 4.1: Lifting Plans from

4.6 Drainage type

In the current prediction method coarse layers (Gravel, Sand, Silt) are modeled to show drained behaviour while the finer layers (Clay, Peat) are modeled to behave undrained in the deformation analysis. Furthermore, due to the small time assumed needed for lifting specific lifting operations time dependent behaviour (consolidation and creep) are not taken into consideration. The load caused by the self-weight of the crane inbetween lifting operations is distributed evenly over the pressure points. Therefore, it is not expected to result in differential settlement.

This approach however, is very questionable. As the full scale tests, discussed in chapter Chapter 6, indicate, time dependent behaviour might indeed result in significant deformation for specific soft soil layers with a significantly large permeability.

4.7 Analysis

The current prediction method is simplified due to cost considerations. This simplification results in large possible ranges of model parameters. To ensure the design is safe the eurocode prescribes the parameter used for calculation to be the 5-percentile of this range. This causes the deformations to be overestimated in the design. While this overestimation is safe, a more accurate determination of the soil properties might result in a more favorable deformation resulting in a more cost efficient crane hardstand design to stay within the deformation requirements. The influence of smaller parameter ranges on the deformation is investigated further in this research Chapter 7.

Furthermore, the assumption to not include time dependent behaviour such as consolidation and creep is questionable. This research also investigates the time needed for specific lifting operation, chapter 5, and the part of that is instantaneous and which part occurs over time, chapter 6.

5 | Full Scale Monitoring

To provide an overview of the deformation phenomena occurring during the installation of a wind turbine and the accessory deformations a full scale monitoring project was conducted. The deformations of each outrigger of an outrigger crane are monitored carefully during critical operation moments with the use of a total station. The total station measures the deformation of a predetermined point manually during the lifting operations.

The goal of the monitoring is to document the deformations occurring during the most critical hoisting operations of a wind turbine installations. To register the position of the crane, the lifting stage, the corresponding loads and the deformation of the outriggers. With this information the aim is to justify or refute certain choices made in the design stage of the hardstand . Such as whether time dependent behaviour influences the deformation and for what time periods load cases are occurring.

5.1 Monitoring setup

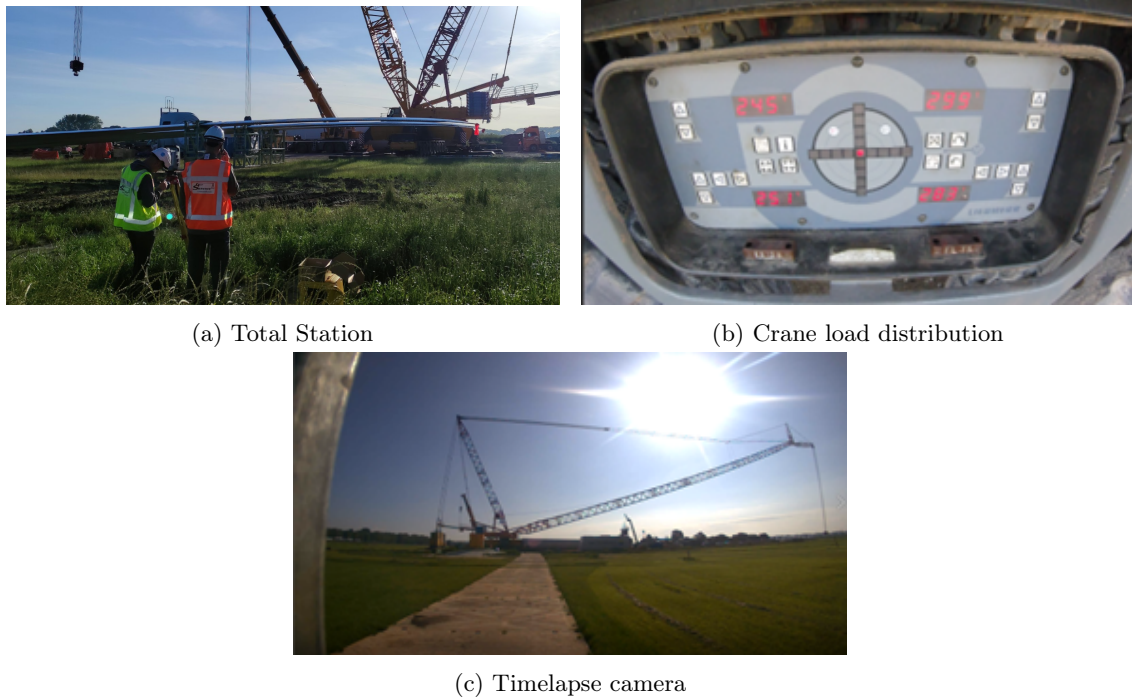
The entire monitoring plan is attached in Appendix A.1 Full scale monitoring plan. The setup of the monitoring consisted of tree different parts:

1. The total station: The total station is used to measure the deformation of specific points in time. The specific measuring locations will be discussed in detail in Section 5.2.1. At a specific point in time the total station will measure the position of the measurement point compared to a checkpoint at a fixed location. Whenever the crane will perform a movement the time stamp is documented in combination with the description of the movement. At this time the total station will start to measure the locations of the measurement points. This way the lifting actions can be assigned to its corresponding deformations.

2. The timelapse camera: During the entire monitoring phase a timelapse camera was positioned to film the crane during lifting operations. This can be used as additional information of the position of the crane at a certain time stamp.

3. The GoPro: The GoPro is fixated on a monitor located at the base of the crane. This monitor shows the pressures exerted through each outrigger at that moment.

All parts of the setup are displayed in Figure 5.1



(a) Total Station

(b) Crane load distribution

(c) Timelapse camera

Figure 5.1: Monitoring setup

5.2 Measuring locations

5.2.1 WT2

For the monitoring of the differential settlements 4 measurement points are considered, 1 in the middle of each outrigger. A depiction of the 4 measurement points for WT2 is given in Figure 4.2: Number 1=A, 2=B, 3=C and 4=B.

Aside from the differential settlement measurements the corners of the wooden dragline mats underneath the most critical outrigger C are also measured (5, 6, 7 en 8) to give an indication of the spreading of the mats on the Tensar geogrid surface. Whenever time implication is a factor (during a loading phase or rigging of the boom) the measurement points in the middle of the outriggers (1-4) have priority. They should be measured before points (5-8). For WTG-4 the same points are measured as indicated in Figure 4.3. The most critical outrigger is outrigger C so for that outrigger again the corners of the wooden dragline mats are measured with priority for points 1-4.

The main crane hardstand consisted of a 1m thick stratum layer for both cases. As described in the Appendix A1.

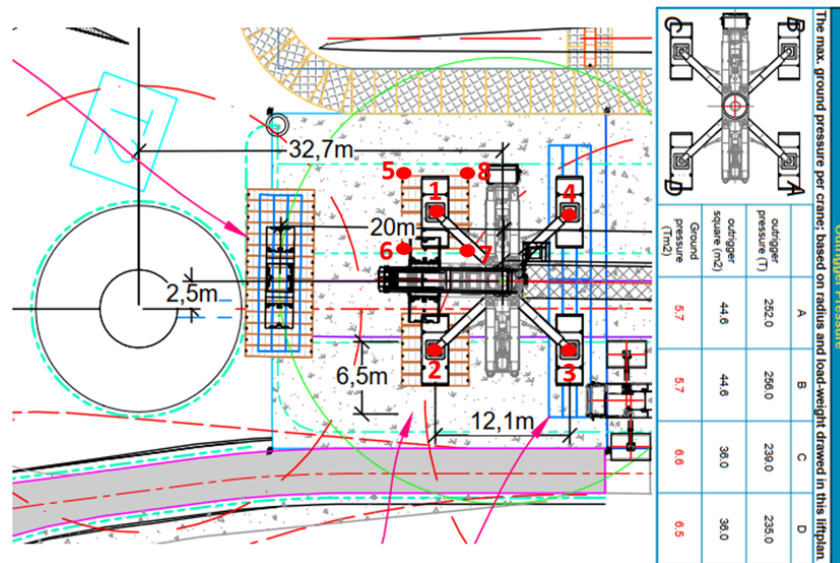


Figure 5.2: Measuring points WT2

5.2.2 WT4

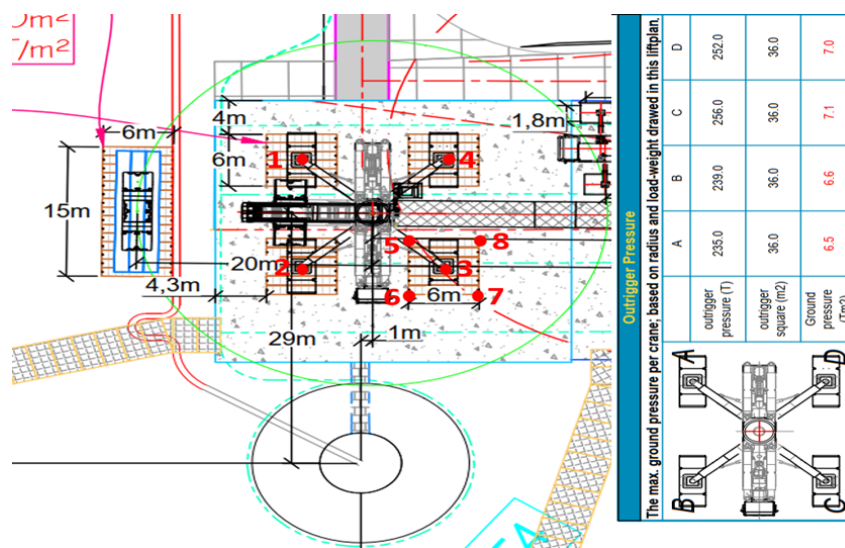


Figure 5.3: Measuring points WT4

5.3 Results

The results of the full scale monitoring are shown in this section. The two measurement opportunities of WT2 are described in detail. While the measurements of WT4 are analyzed as a whole. The extended results are attached in Appendix A.1 Full scale monitoring results.

5.3.1 WT2

At the location of WT2, two lifting phases were monitored, namely the rigging of the boom and the lifting of tower element Mid 2. The intention was to keep the measurement checkpoints in

the same place so the deformation between these loading phases could be assessed. However, the measuring points were moved in between the phases and therefore these stages are only analysed as separate measurement phases.

Boom Rigging The first wind turbine selected for monitoring is wind turbine location 2. The first measurement performed was during the rigging of the boom. The camera providing the pressures on each outrigger was not situated correctly and therefore the loads are not documented during this loading stage. The measured deformations are depicted in 5.4 and the description and time stamps of the measurements are documented in 5.1

From the measurements it becomes evident that the load is increased on all four outriggers at the start of the boom rigging. The weight of the boom is lifted of the extra support points it was resting on, increasing the load exerted on the outriggers. After initial liftoff the loads stay more or less the same for a time. During this time no significant deformation occurs. As the boom moves up the loads on the outriggers decrease and the deformation decreases, the surface bounces back up. The maximum differential settlement occurring during the lifting of the boom is 8 mm between outrigger 2 and 4. Once the boom rigging is complete the crane settles in a stable position in where the pressure on each outrigger is more or less the same. The deformations at the final measurement are positive. This is probably due to the load during the zero measurement was larger than the load caused by the dead weight of the crane. However due to the missing pressure data of the outriggers this cannot be verified.

The data shows an unexpected deformation during measuring moment 10. At this moment the super lift was lifted again, increasing the total weight and thus the load, and the crane was lifted back down slightly. This was due to a stray plank still lying on top of the boom that needed to be brought down safely. After the plank was retrieved safely the super lift was touched back down and the hoisting continued.

The rebounding of the soil surface, suggests the deformations are largely elastic. However, because the data of the exact pressures is not available during this stage it is difficult to draw conclusions on the plastic part of the deformations as the load between the start and end of the measurements could differ. The total active time of the boom rigging phase is 63 minutes and they largest loads are occurring for 36 minutes (measuring moment 2-6).

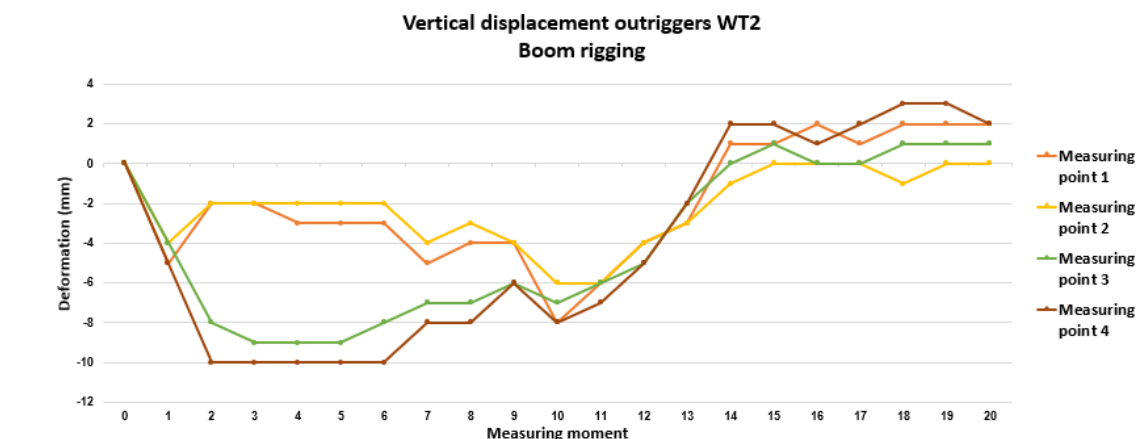


Figure 5.4: Vertical displacement during boom rigging WT2

Nr.	Description	Time
0	Zero measurement before boom rigging	8:30:00
1	Start boom rigging	8:40:00
2	Boom rigging 2m high superlift is floating	8:44:50
3	Boom rigging 10m high superlift is floating	8:47:40
4	Boom rigging 20m high	8:49:40
5	Boom rigging 30m high	8:51:50
6	Boom rigging 40m high	8:53:50
7	Boom rigging 50m high superlift is touched down	8:55:50
8	Boom rigging 70m high superlift is picked back up	8:57:50
9	Boom rigging 80m high superlift is touched down	9:00:00
10	Boom is lifted back down a little and superlift is lifted again	9:03:00
11	Boom is lifted back to 80 m and superlift is touched back down	9:06:00
12	Boom rigging 90 m and the effect of the superlift is gradually decreased	9:10:00
13	Boom rigging 100m	9:13:00
14	Boom rigging ready	9:16:00
15	Ballast weight above point 1 during turning	9:25:00
16	Ballast weight between point 1 and 4	9:26:00
17	End turning weight between 1 and 4	9:28:00
18	Weight above point 4	9:40:00
19	Weight between point 1 and 3	9:41:00
20	Last measurement, weight between 1 and 2	9:43:00

Table 5.1: Measuring moments boom rigging WT2

Lifting tower mid 2 The other action measured at this turbine location is the lift of the heaviest tower element, namely mid 2. The results are depicted in 5.5 and the outrigger pressures and measuring moment descriptions are presented in 5.2 . During measuring moment 8 the line of sight with measuring point 2 was disturbed and therefore no result was available.

During this stage the tower element was placed carefully next to the crane. The crane, with the superlifted hoisted makes a 360° turn fluctuating the loads exerted on the outriggers causing them to deform. These types of movements and load fluctuations (-un and reloading) might result in plastic deformations as discussed in the chapter Virgin-, un- and reloading. After the test run the tower part was slowly lifted. Once lifted the crane rotated placing the tower element above the already placed turbine base. The tower part was carefully fitted on top of the base and secured with bolts.

By comparing the deformations between points in time where the outrigger pressure on the same outrigger is the same, such as measuring moment 4 and 15 for outrigger 1, it becomes evident that the deformation in both cases is 4mm. The time between these measuring moments is 28 minutes. During this specific loading stage the deformations as a results of un-/ reloading and time dependent behaviour appears to be insignificant.

The largest measured differential deformation during the lifting of tower mid 2 is 10mm and the total allotted time of this stage is 3:06 hours.

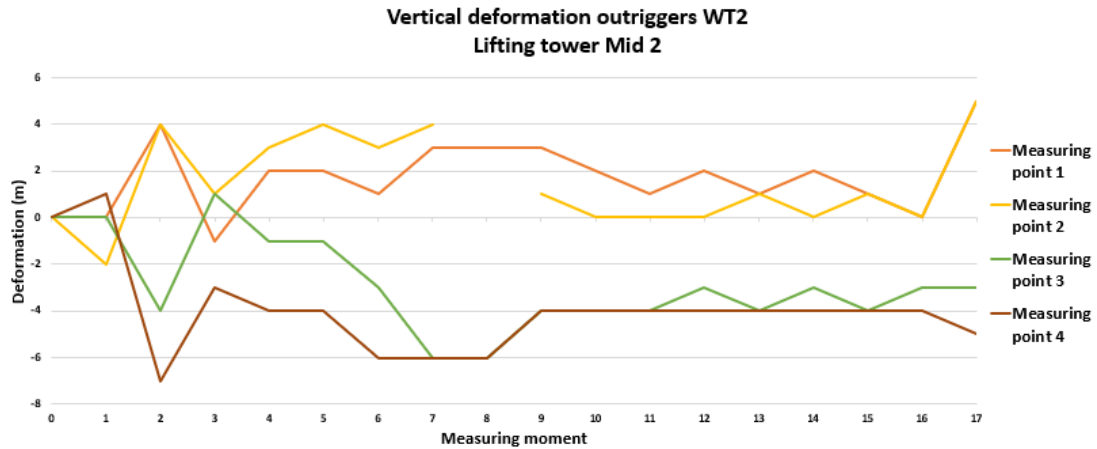


Figure 5.5: Vertical displacement during lifting of tower mid 2 WT2

Nr	Description	Time	Outrigger pressure			
			1	2	3	4
0	Zero measurement	07:16	225	235	148	154
1	Only own weight of crane and superlift	07:34	223	251	154	142
2	Superlift between 3 and 4, no extra load	07:43	158	141	223	252
3	Superlift above 1, no extra load	08:49	251	208	127	186
4	Start with tension on the tower	09:26	222	206	181	205
5	The tower is lifted	09:36	218	208	186	206
6	The load is fully above 3	09:38	227	207	178	208
7	Aux crane is not under tension	09:39	241	209	168	208
8	Aux crane is loose	09:41	190	205	238	228
9	Tower above 3	09:47	186	204	245	230
10	Tower between 3 and 2	09:48	186	199	245	236
11	Tower above 2	09:49	185	220	247	221
12	Tower above 2	09:50	192	237	237	208
13	Tower between 1 and 2	09:51	213	241	213	205
14	Tower next to the foundation between 1 and 2	09:52	212	244	214	201
15	Tower right above foundation	09:54	221	244	207	201
16	Tower is partially carried by the foundation	10:02	227	246	202	201
17	Tower is fully loose	10:22	163	164	186	198

Table 5.2: Measuring moments and outrigger pressure mid 2

5.3.2 WT4

For the second wind turbine it was not possible to locate the total station safely at a location from where all 4 outriggers were visible. For this reason only 3 outriggers were measured. During the installment of this turbine the deformations were measured at 4 separate occasions. Namely: Lifting of the boom, the installment of the bottom tower, the installment of the drive train and hub and lastly during the boom letdown. Because the measurement locations remained in place in-between these measurements it was possible to add the measurements in one single graph analyze the displacements occurring over time.

Rigging of the boom During the crane build-up it was discovered that the location the super-lift would rest on was unstable if the full load of the super-lift resting on the platform. To prevent

the platform from failing it was decided to have the load of the super lift partially carried by the crane overnight. This caused the pressures of the crane to be unevenly distributed during the zero measurement. For convenience of the assessment of the differential deformations the resting position of the crane after the boom lifting was complete was set as 0 mm displacement. Aside from this the deformations follow a similar trajectory as the deformations of WT2 during boom rigging. With the pressures and deformations increasing as the boom is lifted and decreasing. The maximum load exerted on the outrigger pressure during the boom hoisting is 307 Ton. This is 51 Ton higher than the max expected load of 256 Ton where the hardstand was designed for. The maximum differential settlement occurring was 8mm between point 2 and 3. The load difference at this time was 57 Ton. The total hoisting time was 1:10 hour between measuring point 2-23.

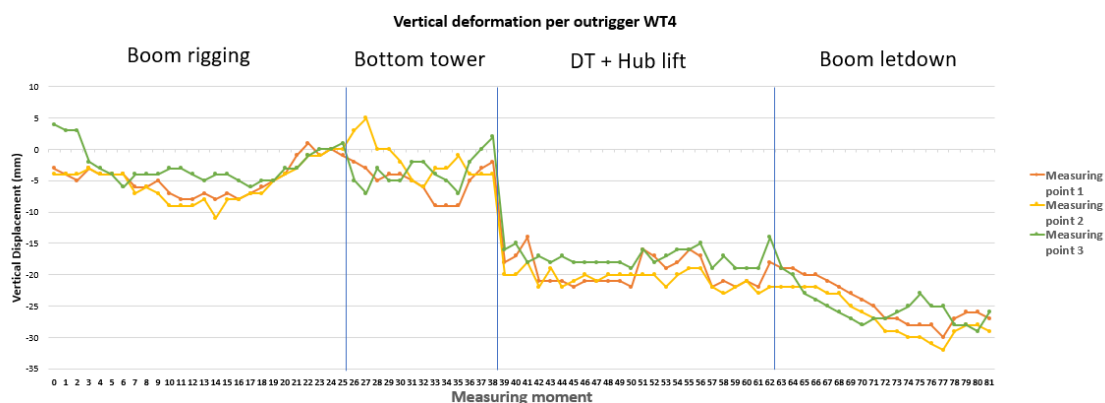


Figure 5.6: Vertical deformation WT4

5.4 Analysis

The results of the full scale monitoring indicate that due to movements of the crane un- and reloading does happen on the soil surface as seen in Section 5.3.1. This is however not directly linked to plastic deformations as the soil rebounds after the soil profile is unloaded again. It is assumed the soil profile behaves elastically during these load increments due to the initial stress falling in the elastic area and the loads not exceeding previously experienced stress as described in Section 3.2.

Time dependent behaviour such as consolidation and creep can be assessed by comparing two moments spread over time where the outrigger pressure is equal. With this method it is not possible to distinguish between consolidation and creep. However because of the short elapsed time period, the deformations are assumed to be primarily due to consolidation. For these monitoring results a distinction is made between deformations over time during a single monitoring session as well as the time dependent deformations over the time period the crane is located at a single location Figure 5.6 no specific deformations caused by un- and reloading

The deformation during a single monitoring session can be analyzed by comparing for example measuring moment 0 and 16 of the hoisting of tower mid 2 WT2 Section 5.3.1. The elapsed time between these measuring moments is 2:46 hour and the outrigger weights are 225 and 227 Ton respectively. The vertical displacement is both 0mm indicating no significant time dependent deformations.

When assessing the boom rigging of WT4 however plastic deformations are observed 5.6. Comparing the vertical displacement of outrigger 3 at measuring moment 2 and 22 indicates a 198 and 196 Ton respectively while the measured vertical displacement is +3mm and -1mm compared to the 0 measurement. This indicates a plastic deformation of 4mm over a 1:03 hour

time period. This deformation however, cannot be directly classified as time dependent behavior as the measurements are during the rigging of the boom. This means the soil pressure likely exceeded the pre-consolidation pressure causing the soil to deform.

Comparing outrigger 3 during boom letdown of WT4 5.6 between measuring moment 67 and 81 the outrigger weights are 243 and 234 Tons respectively. The vertical displacements compared to the zero measurement are -6 and -7mm indicating 1 mm of displacement on 7 Ton less weight over a 0:36 hour time period. As the pressures in between these measurements do not exceed the pre-consolidation pressure this deformation is assumed to be caused by time dependent behaviour.

Due to high wind speeds, the crane could not be operated over periods of time. The time past between the hoisting of the bottom tower and drivetrain/hub of WT4 is 6 days. Time dependent deformation is apparent between these phases. However, because the crane, when in resting position, distributes the load equally over the outriggers these deformations are equal on all outriggers. For this reason these deformations are irrelevant for differential deformations and tilting of the crane

Notable events during the monitoring were the surface load spreading measures underneath outrigger 3 and 4 of WT4 were changed from wooden planks to larger steel beams because they were available at the time. As well as the maximum occurring weight on the outrigger being 313 Ton during the boom letdown of WT4 while the maximum load described by the liftplan was 256 Ton. These events highlight the importance of sufficient safety margins being included in the design

6 | Full Scale Testing

At 2 locations of a large wind farm project next to the highway A16 in the Netherlands the contractor suggested to use a new mitigation measure to distribute the load at the crane hardstands. The new enviromat from Mammoet was suggested HeavyLiftNews (2021). This mat should be a quick, more cost effective and sustainable alternative to other mitigation measures such as a stratum layer. In addition the weight of the enviromat is quite low, decreasing expected deformations.

However, from B.T. Geoconsult B.V. there were questions about the strength of the enviromat and the load distribution effect of the mat. Because of these question it was agreed upon with the contractor to carry out 2 full scale test on the crane hardstand for which the deformation requirements where critical. The full scale tests would simulate the maximum expected load during lifting operations. If deformations of the hardstand would stay below the required 30 mm, the enviromat would be deemed sufficient.

Due to the first test failing it was decided to perform the full scale test at additional locations as shown in 6.2.

The goal of the full scale testing for this research is to compare how different soil profiles behave under the same loading conditions. To assess the significance of time dependent behaviour during a 6 hour time period and to evaluate the effectivity of different load spreading measures

6.1 The test design

The test is the same at every location: the draglines, gantry beams and measurement stickers are placed on the first day, after which a zero measurement is performed. Then road plates are stacked until a weight of 43% of the total load (330,3 tons) is applied. This weight is a simulation of the crane's own weight in rest position. After this, a settlement measurement of the measuring points is performed. This load remains overnight.

On day 2, the settlement of each measuring point is measured first. Then the remaining 57% of the total load, 437.8 tons, is added in 4 steps, as shown in Figure 1. After completing each step, the settlements are measured again. After step 5 has been carried out and the full load is present, the test set-up remains in place for another 6 hours and is measured every half hour. After 6 hours, the load is removed again and the settlement is measured for the last time the following day. The test setup is displayed in 6.1

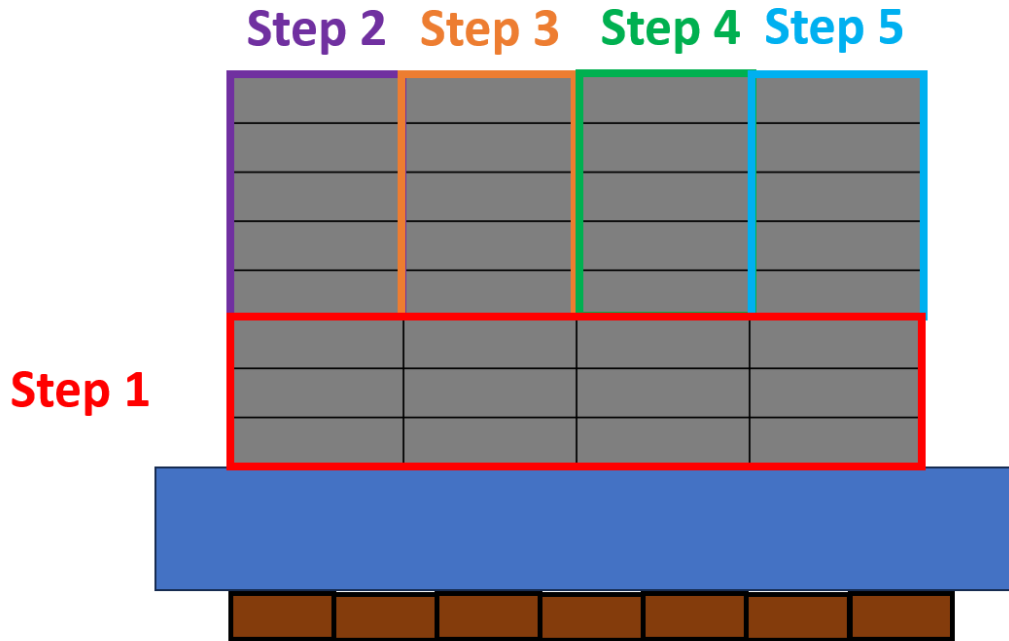


Figure 6.1: Test Setup

6.2 Test locations

The different testing locations are described in 6.1.

Test nr.	Location	Foundation	Subsoil	Surface spreading
1	B-6	0,55 m Enviromat	3,0 à 3,5 m clay/peat	6x9 m2 wooden beams
2	E-3	0,55 m Enviromat	ca. 1,5 m clay, medium	6x9 m2 steel beams
3	D-1	0,25 m granulate	Zand	6x9 m2 wooden beams
4	B-3	1,0 m Stratum	3,0 à 3,5 m clay/peat	6x9 m2 steel beams
5	B-1	1,3 m Stratum	ca. 1,0 m clay/peat	8x9 m2 steel beams
6	B-3	1,0 m Stratum	3,0 à 3,5 m clay/peat	10x13,6 m2 steel beams
7	B-6	1,0 m Stratum	3,0 à 3,5 m clay/peat	10x13,6 m2 steel beams

Table 6.1: Test locations overview

6.3 Results

The Full Scale Tests as described in Chapter 6 were performed 7 times. The results are depicted in this section. The results are shown in 3 ways.

Firstly an overview of the measurements points of the location is presented in a deformation figure. This figure also shows the vertical deformation of these measurement locations where the area between the points is interpolated. The deformations are shown for the test day only, so from the start of step 2 as described in Chapter 6 until after the 6 hour waiting period. The figure presents the deformation during loading step 2-5, the deformations during the 6 hours and the total deformation.

Secondly the deformation averages of the two measurement points at the same location over the width of the gantry at each outrigger are depicted in a table indicating the deformation over time. The points used are specified for each location but they are always located on the gantry.

The third way is the deformation of these same points are depicted in a graph to provide an visual overview of the deformation over time.

6.3.1 Deformation E3

The foundation used for location E3 was an Enviromat with a thickness of 0.55m. The deform-able layer in the subsoil was ca. 1.5 m clay, medium. An overview of the measurements points of the location is presented in Figure 6.11. The maximum deformation during the test was 16mm of which 5mm was during the 6 hour resting period. The soil rebounds up to 14 mm upon unloading.

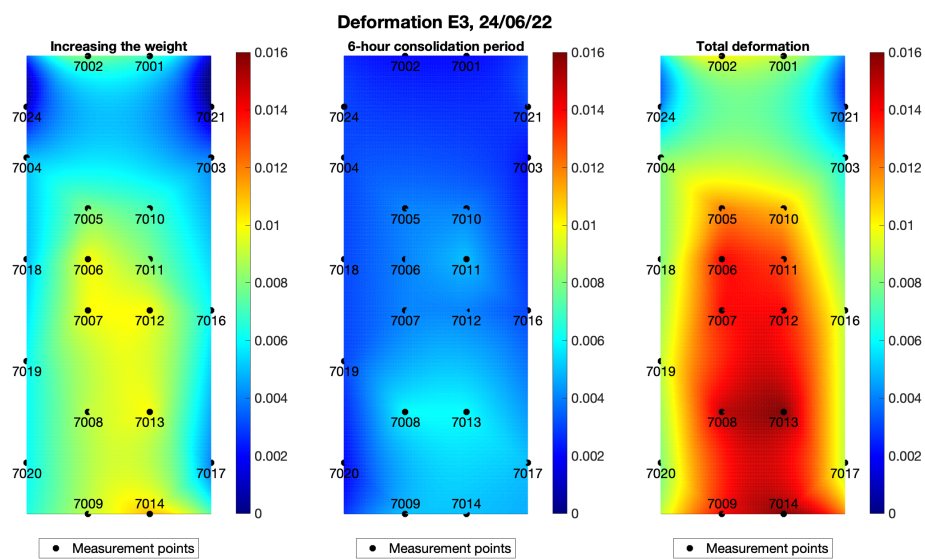


Figure 6.2: From left to right: deformation during increasing the weight, deformation during the 6-hour test and the total deformation.



Figure 6.3: From left to right: deformation during increasing the weight, deformation during the 6-hour test and the total deformation.

Time [hh:mm]	Measurement points				Description
	7005/7010	7006/7011	7007/7012	7008/7013	
17:30	-0.009	-0.011	-0.012	-0.011	Deformation day 1
6:30	0.000	0.000	0.001	-0.001	Deformation over night
12:30	-0.008	-0.010	-0.011	-0.011	Deformation during loading
18:30	-0.004	-0.004	-0.004	-0.005	Deformation 6 hours
Totaal	-0.021	-0.024	-0.025	-0.027	Total Deformation
08:40	0.011	0.013	0.014	0.013	Rebound

6.3.2 Deformation D1

The foundation used for location D1 was 0.25 m of granulate. The subsoil consists mostly of sand and therefore the expected deformations were low. An overview of the measurements points of the location is presented in Figure 6.4. The maximum deformation during the test was 15mm of which 2 mm was during the 6 hour test. The soil rebounds up to 8 mm upon unloading.

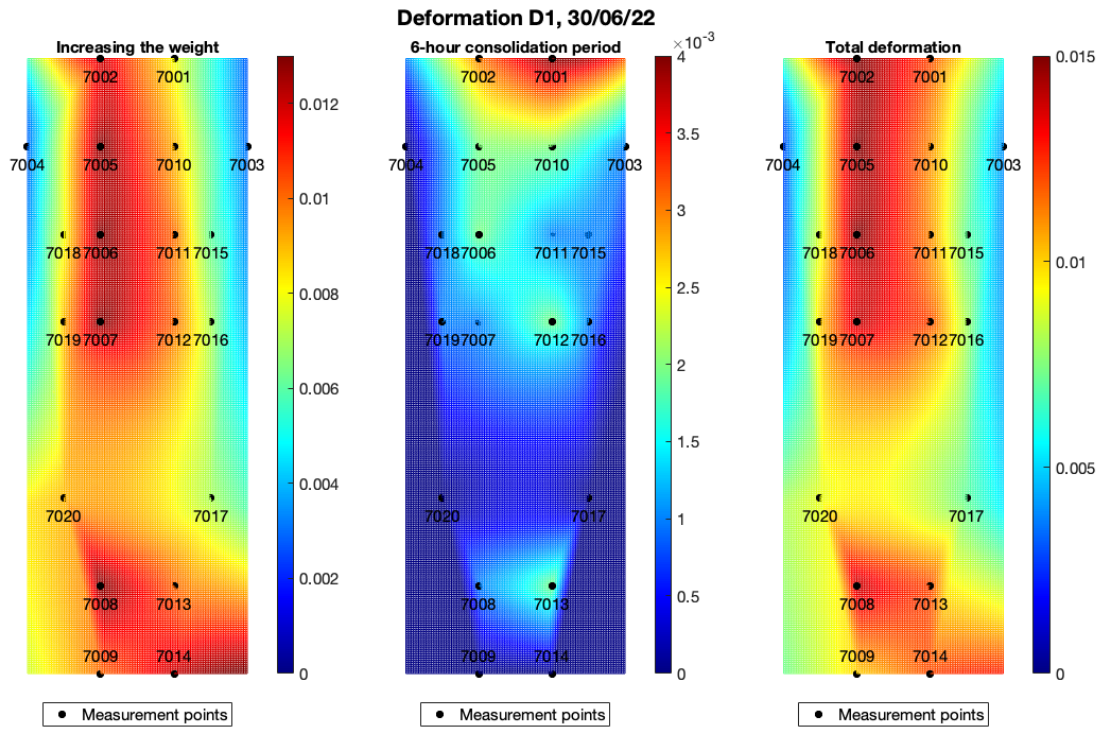


Figure 6.4: From left to right: deformation during increasing the weight, deformation during the 6-hour test and the total deformation.

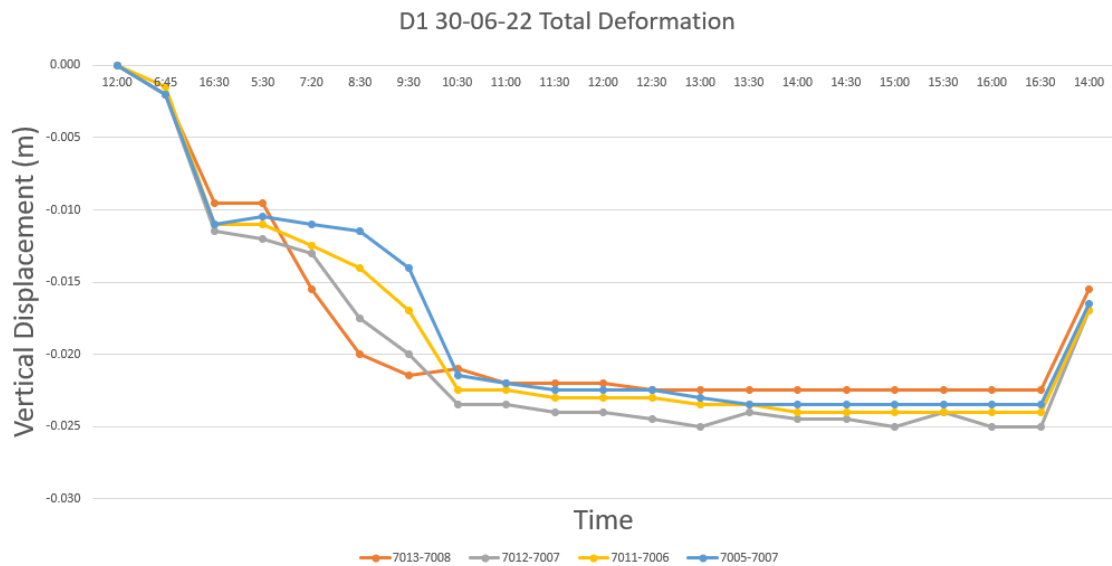


Figure 6.5: From left to right: deformation during increasing the weight, deformation during the 6-hour test and the total deformation.

Time [hh:mm]	Measurement points				Description
	7013-7008	7012-7007	7011-7006	7005-7007	
16:30	-0.010	-0.012	-0.011	-0.011	Deformation day 1
5:30	0.000	-0.001	0.000	0.001	Deformation over night
10:30	-0.012	-0.012	-0.012	-0.011	Deformation during loading
16:30	-0.002	-0.002	-0.002	-0.002	Deformation 6 hours
Totaal	-0.023	-0.025	-0.024	-0.024	Total Deformation
14:00	0.007	0.008	0.007	0.007	Rebound

6.3.3 Deformation B3

04/08/22

The foundation used for location B3 at first was 1m sffratum. The subsoil consists 3.5 m highly deformable layers of 3.5m clay and peat. An overview of the measurements points of the location is presented in Figure 6.10. It should be noted however that during loading the gantry was hanging to much over the wooden planks. Therfor the deformation at locations 8003 and 8005 is higher then expected. The maximum deformation during the test was 96mm of which 25 mm was during the 6 hour test. The soil rebounds up to 5 mm upon unloading.

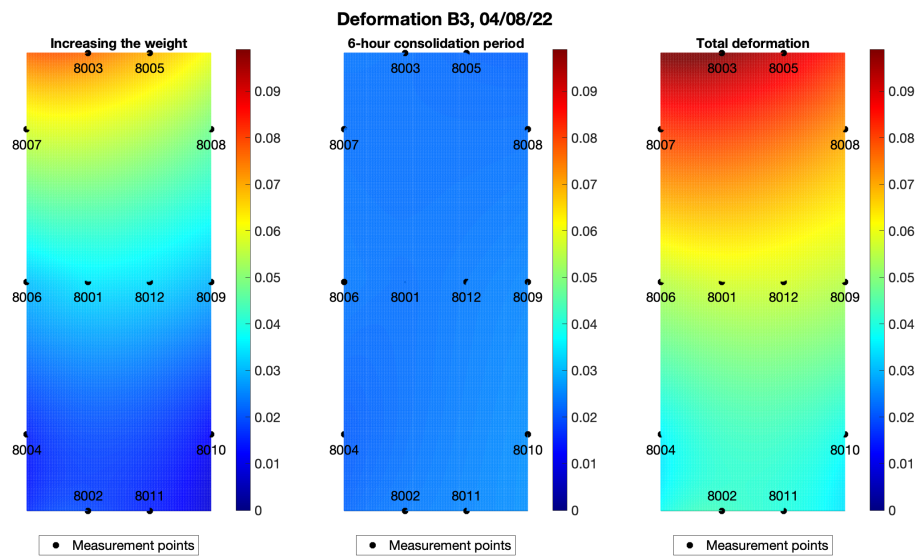


Figure 6.6: From left to right: deformation during increasing the weight, deformation during the 6-hour test and the total deformation.

Time [hh:mm]	Measurement points			Description
	8002/8011	8001/8012	8003/8005	
16:00	-0.025	-0.026	-0.028	Deformation day 1
06:00	-0.011	-0.012	-0.010	Deformation over night
10:15	-0.017	-0.035	-0.073	Deformation during loading
16:15	-0.025	-0.024	-0.023	Deformation 6 hours
Total	-0.077	-0.096	-0.133	Total Deformation
07:30	-0.001	0.005	0.019	Rebound

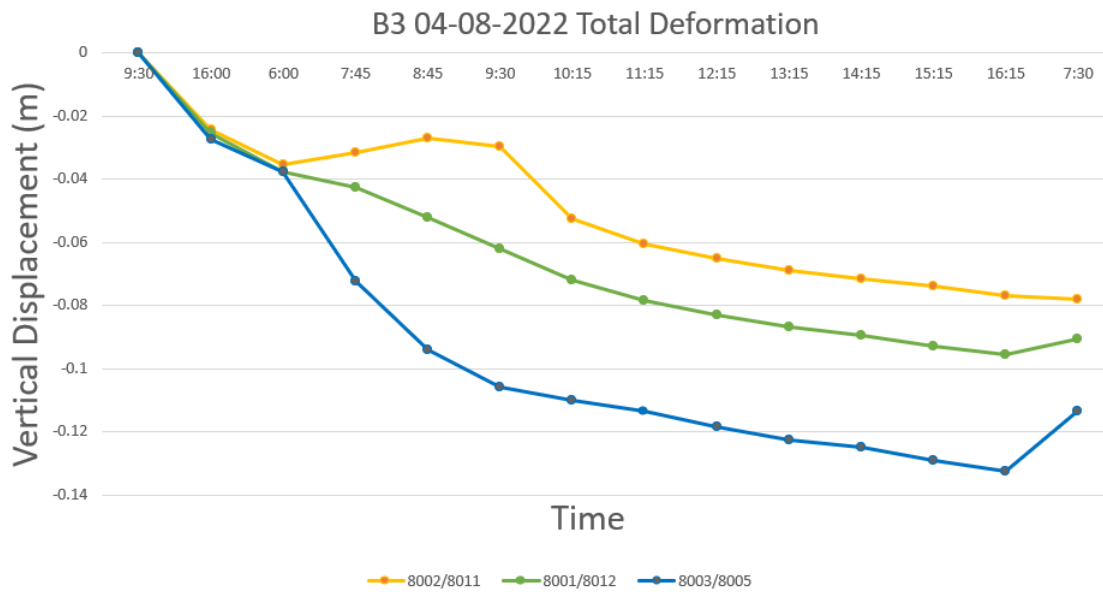


Figure 6.7: From left to right: deformation during increasing the weight, deformation during the 6-hour test and the total deformation.

25/08/22

For the second measurement at location B3 the foundation was upgraded to steel with a larger area. The foundation used for location B3 at first was 1m stratum. The subsoil consists 3.5 m highly deformable layers of 3.5m clay and peat. An overview of the measurements points of the location is presented in Figure 6.10. It should be noted however that during loading the gantry was hanging too much over the wooden planks. Therefore the deformation at locations 8003 and 8005 is higher than expected. The maximum deformation during the test was 96mm of which 25 mm was during the 6 hour test. The soil rebounds up to 5 mm upon unloading.

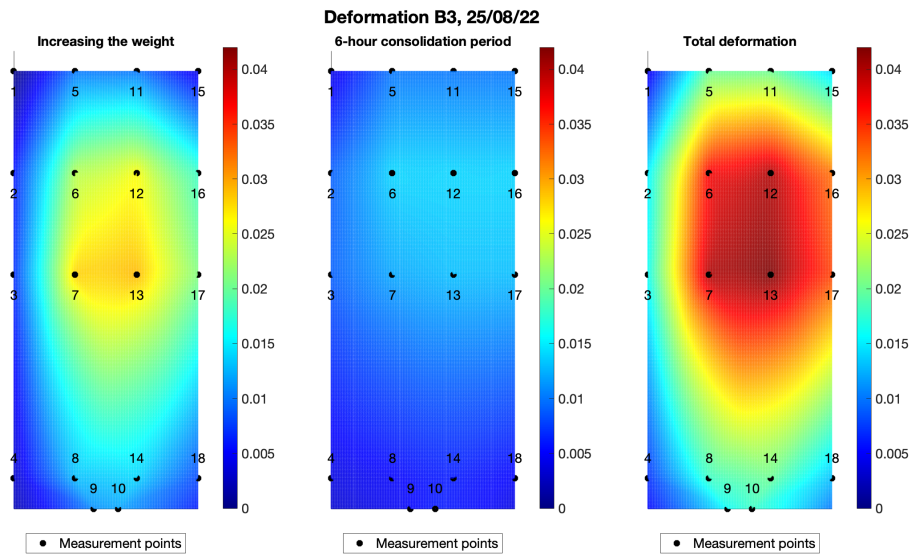


Figure 6.8: From left to right: deformation during increasing the weight, deformation during the 6-hour test and the total deformation.

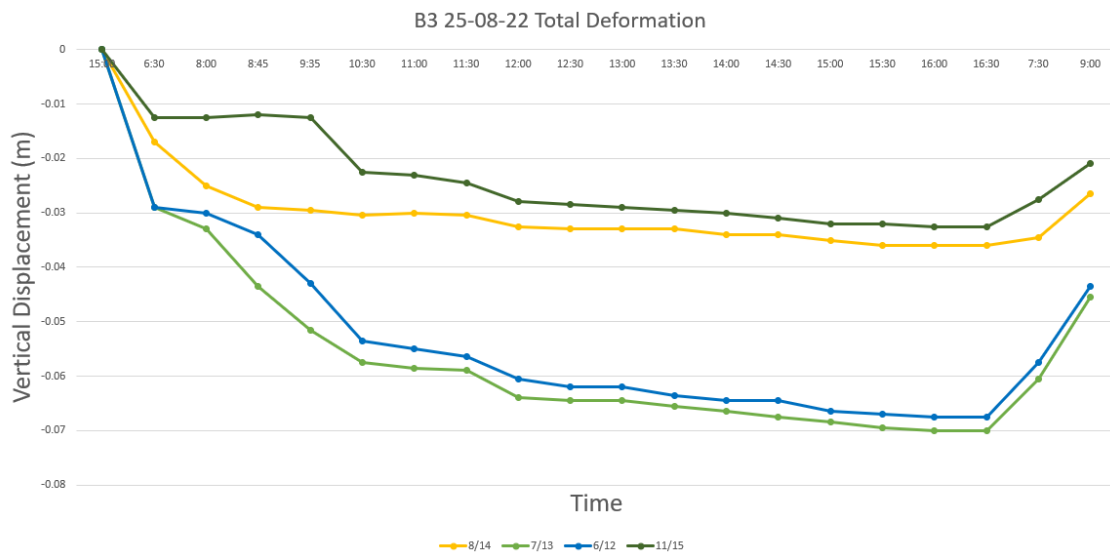


Figure 6.9: From left to right: deformation during increasing the weight, deformation during the 6-hour test and the total deformation.

Time [hh:mm]	Measurement points				Description
	8/14	7/13	6/12	11/15	
15:00	N.B.	N.B.	N.B.	N.B.	Deformation day 1
6:30	-0.017	-0.029	-0.029	-0.013	Deformation over night
10:30	-0.014	-0.013	-0.025	-0.010	Deformation during loading
16:30	-0.006	-0.041	-0.014	-0.010	Deformation 6 hours
Totaal	-0.036	-0.070	-0.068	-0.033	Total Deformation
7:30	0.002	0.010	0.010	0.005	Rebound 42% load
9:30	0.010	0.025	0.024	0.012	Rebound 0% load

6.3.4 Deformation B1

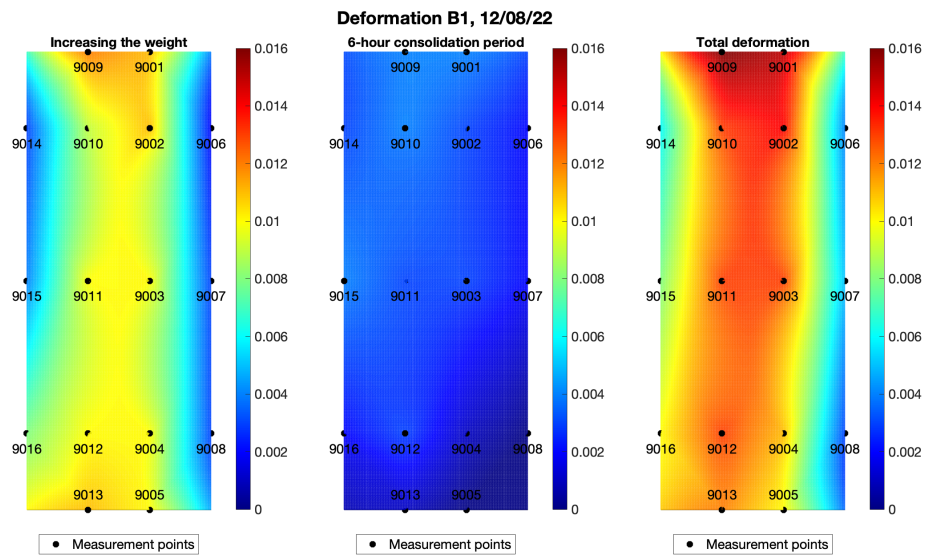


Figure 6.10: From left to right: deformation during increasing the weight, deformation during the 6-hour test and the total deformation.

Time [hh:mm]	Measurement points			Description
	9004-9012	9003-9011	9002-9010	
15:30	-0.008	-0.011	-0.013	Deformation day 1
6:00	-0.003	-0.004	-0.004	Deformation over night
10:30	-0.010	-0.010	-0.010	Deformation during loading
16:30	-0.002	-0.003	-0.004	Deformation 6 hours
Total	-0.023	-0.027	-0.030	Total Deformation
6:30	0.004	0.004	0.004	Rebound

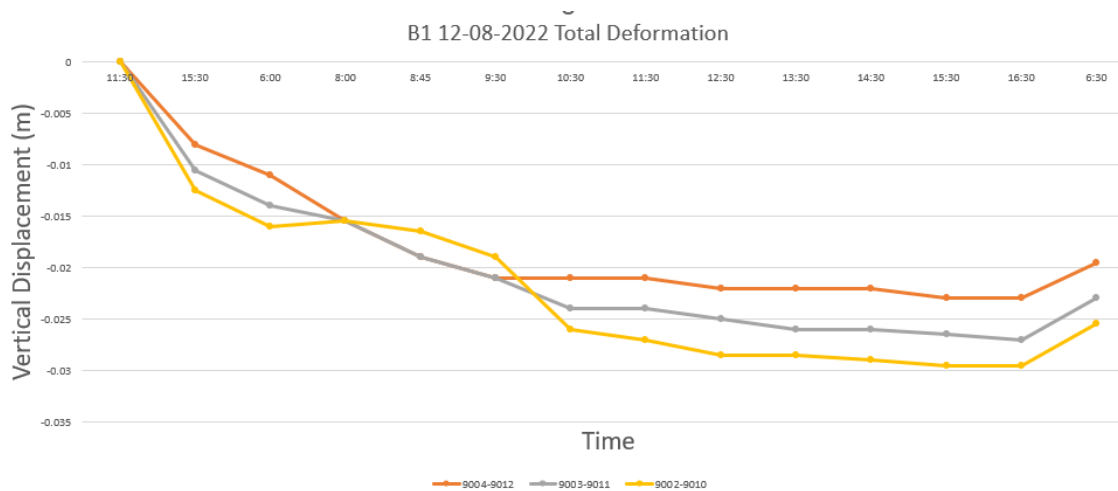


Figure 6.11: From left to right: deformation during increasing the weight, deformation during the 6-hour test and the total deformation.

6.4 Analysis

The full scale tests provide an overview of how different soil profiles behave under the maximum crane load. Figure 6.12 gives an overview of the behaviour of the crane hardstands underneath the simulated crane load. The figure makes distinction between deformation during the loading phase of the test, and deformation as a result of the 6 hour waiting period. It should be noted that buildup of the load took 2 hours, and thus the deformations over time are larger than measured during the 6 hour period.

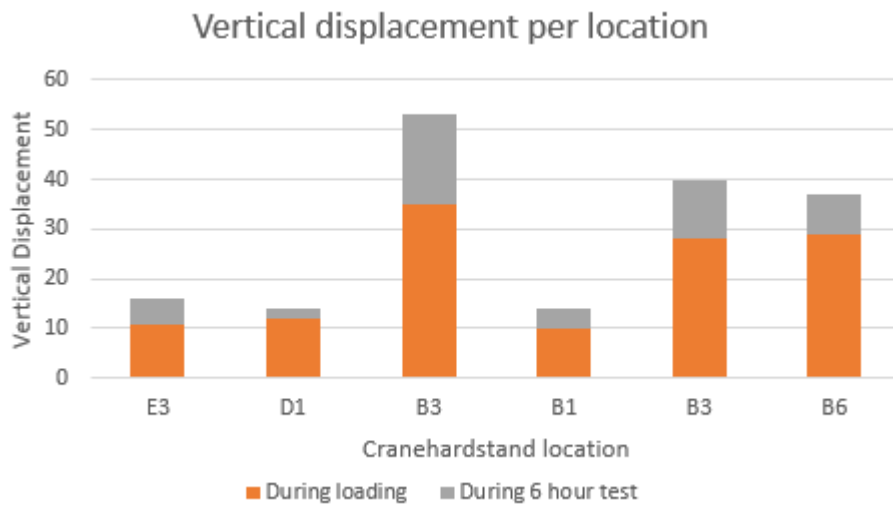


Figure 6.12: Full scale test comparison

Test phase	During loading [mm]	During 6 hour test [mm]	Percentage 6 hours [%]
E3	11	5	31
D1	12	2	14
B3	35	18	34
B1	10	4	29
B3	28	12	30
B6	29	8	22

Table 6.2: Deformation distribution full scale tests

From the results in Table 6.2 it becomes evident as expected that the total deformations depend heavily on the soil type and thickness of the deformable layers. The crane hardstands on top of the soil profiles with the thickest deformable layers B3 and B6 show the most deformation.

The Full scale tests show the significance of time dependent behaviour on the total deformation. Even at location D1, where the soil profile consisted of sand, 14% of the total deformation occurred during the 6 hour waiting part of the test. While at layers consisting of 3,5m clay and peat (B3) the part of the deformation during the 6 hour tests was even 34% at 18mm. Which compared to the maximum allowed deformation of 30 mm is a significant amount. Because of these results, the sensitivity analysis performed in the final part of this thesis includes a consolidation phase.

7 | Sensitivity analysis

To improve on the current design method it is important to evaluate the different influences on the outcome of the used model. This is done by performing a sensitivity analysis on the used model. Plaxis has a built in sensitivity analysis tool which can be used to assess the influence of the parameters on the outcome of the prediction model. With this function in Plaxis however, only 1 parameter at the time can be varied. This causes problems with the hardening soil small strain model due to parameters that are dependent on one another. To assess for example the sensitivity of the model to stiffness parameters the E_{oed} has to be varied, while the E_{ur} would stay the same. This will result in unrealistic ratio's between the stiffness parameters making the assessment invalid. By performing the analyse manually the E_{ur} can be varied along with the E_{oed} to assess the sensitivity of the model to the stiffness parameters.

7.1 Quantifying sensitivity with the influence factor

Prediction models always contain a certain degree of uncertainty. Soil models assign specific soil parameters to soil layers. For simplicity of the calculation specific soil layers are determined and classified. This classification is done by assigning parameters representing the strength of the soil, the stiffness, permeability etc. Each soil model uses specific parameters.

For crane hardstands specifically as mentioned in Chapter 4 the soil is classified based on solely a cone penetration test. The layer specific parameters are determined based on correlations with high uncertainty. To ensure a safe design safety standards such as for example Eurocode 7 for geotechnical engineering in the EU are created. This specific standard mandates that a characteristic value of a soil parameter used for deformation predictions should be used. The characteristic value of a parameter is defined as the 95% certainty interval of the uncertainty range. A larger uncertainty range due to limited soil investigation will result in a larger predicted deformation. This results in more expensive mitigation measures. Extensive soil investigation in the form of laboratory tests provides a more accurate estimation of the model parameters. This will result in more accurate predictions.

A sensitivity analysis is a method to determine the sensitivity of a model to a change of a specific parameter. When a relatively small parameter fluctuation results in a significant change of deformation prediction, the model is sensitive to changes of that specific parameter. This emphasizes the importance of the accuracy of the parameter. Whenever the model is sensitive to a change of a parameter it might be beneficial to perform additional soil investigation and so get a more accurate prediction of the parameters range.

The available soil investigation for the design of a crane hardstand often consists of only cone penetration tests. When converting the CPT's to soil parameters correlations are used which result in large possible ranges. This project performs a sensitivity analysis for specific soil profile's as discussed in Table 7.6 to give an indication for which situations extended soil investigation might be beneficial.

The sensitivity score of specific parameters is determined by first determining the range of the parameters by using a minimum, reference and maximum value of each parameter. The Plaxis calculation is then performed with each of these parameter values as an input. The rest of the parameters is kept constant at the reference value. This results in a minimum and maximum deformation at a specified node. The global sensitivity score for the parameter is the difference in deformation between the maximum and minimum input. This is done for each model parameter which is expected to have an influence.

The sensitivity of the parameters compared to one another is determined with the use of an influence factor. The parameter score presents the difference in vertical deformation between when the min and max values of a specific parameter is used in the calculation Equation (7.1). The influence factor, x_i , indicates the influence of a parameter on the calculated deformation compared to other assessed parameters and provides an idea for which parameters it might be

beneficial to be determined more accurately Equation (7.2).

$$\eta_{SS,i} = |f(x_{i,max}) - f(x_{i,min})| \quad (7.1)$$

$$x_{i,score} = \frac{100\eta_{SS,i}}{\sum_{j=1}^n \eta_{SS,j}} \quad (7.2)$$

$\eta_{SS,i}$	= Parameter score
$f(x_{i,min}), f(x_{i,max})$	= vertical deformation for max and min value of parameter x
$x_{i,score}$	= influence factor if n parameters are varied
n	= amount of parameters used in analysis

7.2 The soil model choice

The model currently used in practice to assess the deformation of a crane hardstand as a result of hoisting activities is the HSsmall model. Extensive research is done on the correlations between the HSsmall model parameters and the cone resistance that results from a CPT. Therefore, the input parameters of the model are possible to be determined relatively accurately with minimal soil investigation. In some cases limiting the need for additional laboratory tests.

The Hardening Soil Small Strain (HS) model is a constitutive model that is implemented in PLAXIS to simulate the behavior of soil and it excels in assessing the behaviour under small strain conditions. The model makes distinction between primary loading and un- / reloading and remembers pre-consolidation stress. Therefore it includes compaction hardening. Another feature of the model is that it includes friction hardening which decreases the stiffness in deviatoric loading.

Limitations of the model are that it does not consider softening and it is not able to model time-dependent behaviour. It is possible however, to add a consolidation phase to your model. As creep is not expected to be significant for the crane hardstand case, the limitation is acceptable.

Another constitutive model which might be able to accurately predict crane hardstand deformations is the Soft Soil Creep model, which as the name suggests does take time dependent behaviour into account. A limitation is however that it is not suitable for sand, which would create the need for different constitutive models and parameter determination methods within one soil profile. Another limitation is that the over consolidation ratio is not accounted for as detailed as with the HS small model.

While different constitutive models might improve the accuracy of the crane hardstand deformation prediction, it is not analyzed within the scope of this research due to time considerations. Rather the focus lays on improving the accuracy of the current HSsmall model most often used in practice.

7.3 The model

The geometry and structures used to assess the deformation of the soil are depicted in figure 7.1.

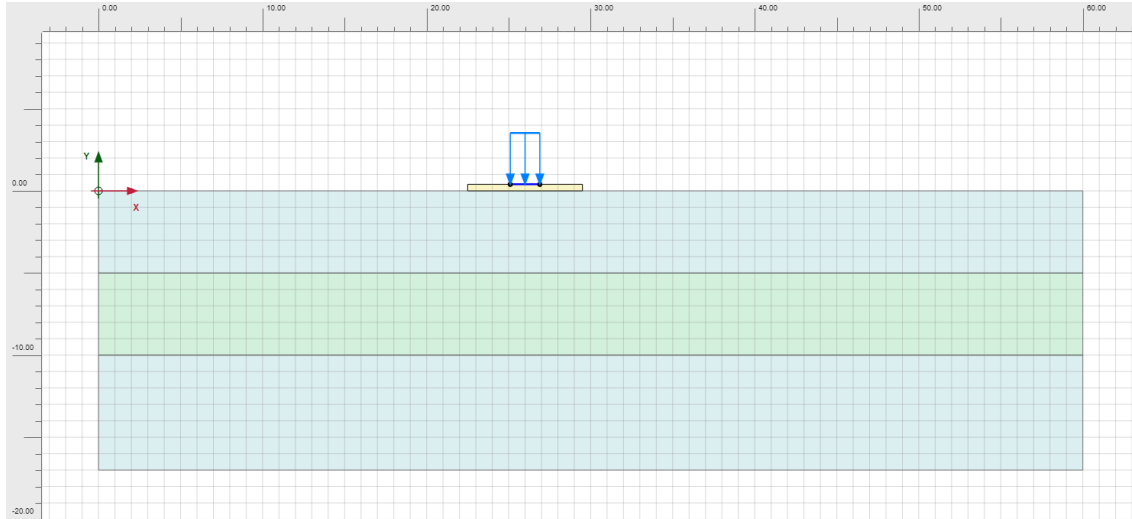


Figure 7.1: Model geometry

The width of the model is taken from 0 to 60 meters. This width is chosen such that the load change effects do not reach the boundary of the model and the border does not influence the results. Symmetry is not often used in practice for crane hardstands the modeled load exerted by the crane is not always uniform. Therefore symmetry is not used in this model

The load case used for the sensitivity analysis is the same as the load used during the full scale testing. This is a distributed load of 460 kN/m^2 of 1.8m wide running from 25.1m to 26.9m in the geometry. This load simulates a crawler track as used in Chapter 6. To analyze the influence of load magnitude there are also variants where a load of 200 kN/m^2 is used.

7 meter wide steel beams are used to spread the load along the surface to as would be the case during wind turbine lifting operations. The beams are modelled as a linear elastic layer with a stiffness of 210 MN/m^2 and a Poisson ratio of 0.1.

For the sensitivity analysis the model always consists of 3 soil layers. Namely 2 layers of stiff sand with high permeability enclosing a deform-able layer representing a soft soil present in the Netherlands. The sand layer is modeled as a drained layer with properties as presented in Table 7.1. This layer is used in each variant to allow free flow of water while ensuring equal circumstances for each calculation.

	Drainage type	γ_{sat}	γ_{unsat}	Eoed	E50	Eur	ϕ	c'	κ
Sand	Drained	20	18	1.5E6	1.5E6	6.0E6	37.5	5	0.2624

Table 7.1: Sand layer properties

The model is constructed in 3 stages. At first the initial phase is activated. The initial phase simulates the initial situation before any construction has taken place. The initial pressures are a result of the soil weight and the water level, which is at surface level. After the initial stage the max crane load is added in stage 2: Crane Load. This stage includes the crane load (which can be 460 kN/m^2 or 200 kN/m^2) as well as the previously described steel beam. A plastic calculation is performed with a staged construction loading type. Lasty a consolidation stage is added to the model with a time period between 2 and 6 hours, depending on the variant. The full calculation stage settings are displayed in Figure A.1 and Figure A.2.

7.4 Assessed soil types

The full scale tests at location D1 showed that a soil profile containing only sand does not show significant deformations. For this reason the sensitivity analysis focuses on soft soils, clay and peat.

Table 2b. of NEN-9997 Normcommissie"Geotechniek" (2017) is composed by averaging the characteristic properties of assessed soil profiles with a specific cone resistance and friction ratio of different samples throughout the Netherlands. The properties assigned to the fictional soils types used in this thesis are based on the table 2b.

The saturated volumetric weight and and friction angle for the soil types are derived from previously mentioned table 2b. The cohesion is taken significantly larger then the advised value from the same table. When the soft soil layer is modeled as Undrained (A) the strength is underestimated for soil layers close to the surface where stresses as a result of soil weight are low. To simulate the undrained shear strength of the clay and peat layers the cohesion is increased to ensure the variant where the soft layer is 1m below the surface does not fail, making it unable to create the calculation.

The E_{oed}^{ref} is determined by multiplying the average stress in the specific layer with the proposed empirical cone factor Sanglerat (1972). And determining the reference stiffness for a reference pressure of 100kPa according to Equation (7.5). The small strain parameters are determined by eq. 4.3 and 4.4, the K_0 is taken as $1 - \sin \phi$ and κ as taken from StructX (2023). The assessed soil types with the corresponding soil parameters are displayed in Table 7.2

Parameter	γ_{sat} [kN/m ³]	ϕ [o]	c [kPa]	E_{oed} [MPa]	E_{50} [MPa]	E_{ur} [MPa]	m	G0 [MPa]	$\gamma_{0,7}$ -
Clay, weak sandy	18	22.5	60	8.76	17.52	87.6	0.9	146	1.02E-04
Clay, very sandy	18	27.5	40	14.74	14.74	73.71	0.9	122	1.17E-04
Clay, clean	17	17.5	45.65	12.46	24.92	124.62	0.9	207	6.26E-05
Clay, organic	15	15	30	4.55	9.11	54.65	1	91	1.09E-04
Peat	12	15	40	0.67	1.35	8.09	0.9	13	7.99E-04

Parameter	OCR	POP	K_0	κ
	-	[kN]	-	[m/day]
Clay, weak sandy	1	10	0.61	4.75E-01
Clay, very sandy	1	10	0.54	4.75E-01
Clay, clean	1	10	0.70	4.06E-04
Clay, organic	1	10	0.74	8.64E-03
Peat	1	10	0.74	8.64E-03

Table 7.2: Parameters per assessed soil type

7.5 Parameter range determination

The uncertainty range of the parameters is based on the correlations used to determine the soil parameters from a cone penetration test. The parameters determined from table 2b of NEN9997-1 Normcommissie"Geotechniek" (2017) are characteristic values with a variation indicated in the same table. This concerns the cohesion (c), the internal friction angle (ϕ) and the volumetric weight (γ). With this variation the maximum and minimum value for the parameters can be estimated as follows. Multiplication factor $Z_{n,v}$ is given as a function of the amount of samples n and the variation coefficient v . And this factor can be used to back calculate the average and

maximum value as shown in your rig Equation (7.3).

$$X_{avg;c} = Z_{n;v} * X_{avg} \quad (7.3)$$

$X_{avg;c}$ = characteristic parameter value
 $Z_{n;v}$ = multiplication factor
 X_{avg} = the average (50- percentile) of the parameter uncertainty range

The characteristic value of table 2b. is determined by multiplying this factor with the mean value. The characteristic value is defined as the value where there is 95 % probability that the real value is equal or higher than the characteristic value. By backwards calculation the mean and value where there is a 95% probability that the value is lower than the maximum value can be determined. This is the case for the saturated and unsaturated volumetric weight (γ_{unsat} and γ_{sat}), the cohesion (c), the internal friction angle (ϕ).

The small strain parameters specific to the Hardening Soil Small strain model are described in Section 4.4. G_0 is dependent on the E_{ur} and μ_{ur} as indicated by Equation (4.3). $\gamma_{0.7}$ is depicted in Equation (4.4). Their ranges are determined by using the minimum and maximum parameters used to calculate the paramters.

Permeability parameters

The range of the permeability parameters is taken as the minimum and maximum as described by StructX (2023). The values for peat are taken to be the same as organic clay.

Stiffness parameters

To determine the stiffness parameters from the CPT data the correlation suggested by Sanglerat (1972) is used.

$$E_{oed} = \alpha q_c \quad (7.4)$$

Where α is the emperical cone factor. Sanglerat proposed values of the cone factor based on the type of soil as shown in table 7.3

The way to transform E_{oed}^{ref} to E_{oed} and is provided in 7.5

$$E_{oed} = E_{oed}^{ref} \left(\frac{c \cos(\phi) - \sigma'_3 \sin(\phi)}{c \cos(\phi) + p^{ref} \sin(\phi)} \right)^m \quad (7.5)$$

c = Cohesion
 ϕ = Internal friction angle
 σ'_3 = average effective soil pressure in corresponding soil layer
 p^{ref} = reference pressure [100kPa]
 m = power m

Table 7.3: Emperical cone factor

	Sanglerat param α	
	min	max
Clay, Medium sandy	2	5
Clay, Very Sandy	1	3
Clay, clean	2	6
Clay, organic	1.5	4
Peat	1	1.5

The empirical cone factor proposed by Sanglerat is dependent on soil type, which is determined by the cone resistance of the CPT, as well as moisture content. This factor ranges between a maximum and minimum possible value per condition. These maximum and minimum values are used to determine the range for E_{oed}

In turn E_{50} and E_{ur} are determined based on a correlation with E_{oed} . This correlation is once again dependent on the soil type. Since the stiffness parameters are heavily correlated with each other they can not be evaluated separately in the sensitivity analysis.

The pre overburden pressure range difficult to assess based on literature and was taken to be between 10 and 30 kPa. This is done to see the sensitivity of the model to the P.O.P.

The parameter ranges for each parameter and the sanglerat factor α for the stiffness parameters for each soil type is shown in Table 7.4

Soil type		γ_{unsat}	γ_{sat}	ϕ'	c'	α	E_{oed}^{ref}	E_{50}^{ref}	E_{ur}^{ref}
		[kN/m ³]	[kN/m ³]	[o]	[kPa]	[-]	[MPa]	[MPa]	[MPa]
Clay, weak Sandy	min	18.0	18.0	22.5	60.0	2.0	5.84	11.68	58.40
	max	21.43	21.4	29.9	93.8	5.0	14.60	29.20	146.00
Clay, very Sandy	min	18.0	18.0	27.5	40.0	1.0	7.37	7.37	36.85
	max	21.4	21.4	35.8	62.5	3.0	22.11	22.11	110.57
Clay, clean	min	17.0	17.0	17.5	45.6	2.0	5.53	11.08	55.38
	max	20.2	20.2	23.6	71.3	6.0	16.61	33.23	166.16
Clay, organic	min	15.0	15.0	15.0	30.0	1.5	3.41	6.83	40.98
	max	17.8	17.8	20.4	46.8	5.0	9.10	18.21	109.29
Peat	min	12.0	12.0	15.0	40.0	1.0	0.67	1.34	8.09
	max	14.3	14.3	20.4	62.5	1.5	1.01	2.02	12.132

Table 7.4: Parameter ranges per soil type

Soil type		G_{0ref}	OCR	$P.O.P.$	$K0$	κ
		[MPa]	[-]	[-]	[kN]	[-]
Clay, weak Sandy	min	97.33	1.0	10	0.62	4.75E-01
	max	243.33	1.0	30	0.50	4.75E-04
Clay, very Sandy	min	61.42	1.0	10	0.54	4.75E-01
	max	184.28	1.0	30	0.41	4.75E-04
Clay, clean	min	92.31	1.0	10	0.70	4.06E-04
	max	276.93	1.0	30	0.60	8.64E-07
Clay, organic	min	40.98	1.0	10	0.74	8.64E-03
	max	109.29	1.0	30	0.65	4.32E-05
Peat	min	8.09	1.0	10	0.74	8.64E-03
	max	12.13	1.0	30	0.65	4.32E-05

7.5.1 Variants

There are three variants used to describe the behaviour of specific soil types under the high temporary loads. The soft soil layers are varied in thickness and in depth. This is done to assess the effect layer thickness and depth have on the importance of accurate model parameter determination.

To ensure the only layer influencing the difference in deformation the layer on top and bottom of the deformable layer is always taken as the same stiff and permeable sand.

The variants are shown in Figure 7.2 and they are a layers with 1m thickness and 5m thickness. The depth is differentiated with the top of the layer laying at 1 m below surface and 5m below surface. The load simulates the load of a single crawler track as in Chapter 6. The load is varied for different variants. The soil types used are described in Table 7.2. The colors of the layers indicate the soil type, where the top and bottom layers are the same sand layer as indicated in Table 7.1

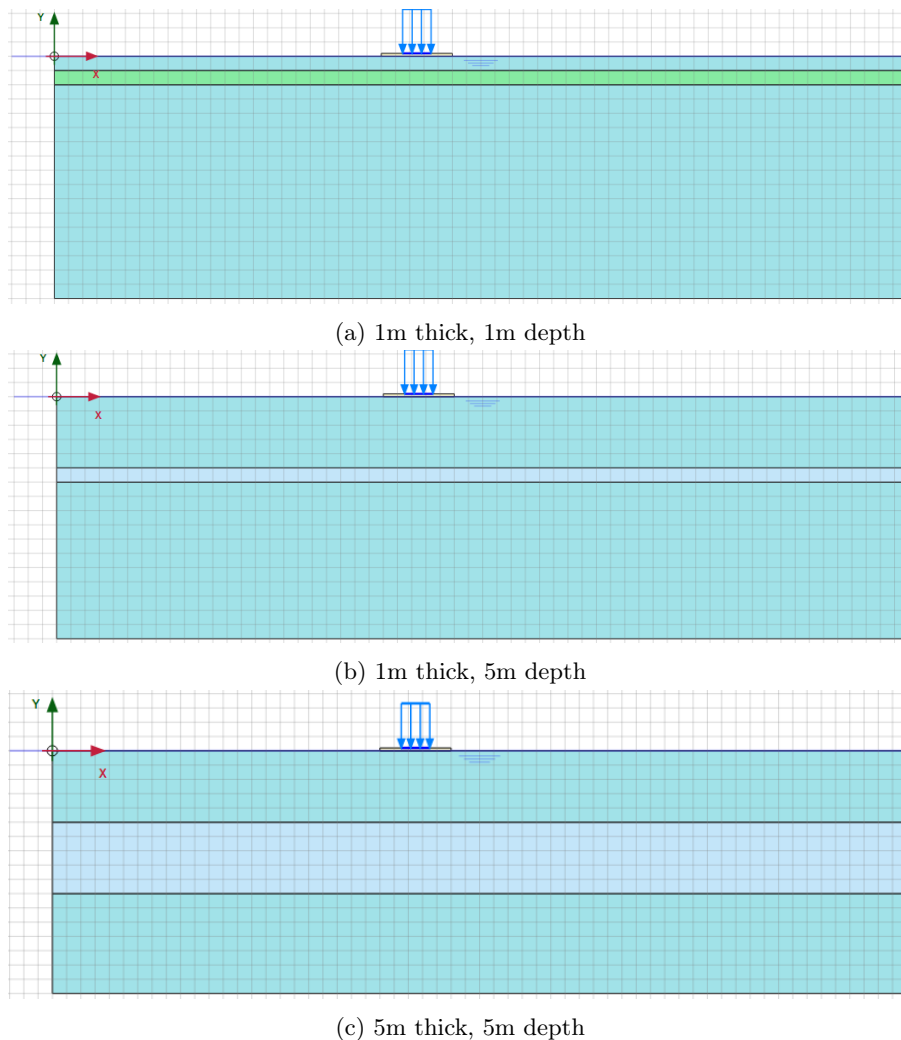


Figure 7.2: Variants used for the sensitivity analysis

7.6 Python code

The sensitivity analysis is performed by repeating the same deformation calculation in Plaxis while varying one parameter each time. This process is automated with python. The code uses a predetermined plaxis model, with a set geometry, structures, mesh, loading phases etc. and only changes 1 parameter of the middle layer as shown in Figure 7.2. After changing the parameter the calculation of the new situation is performed and the resulting deformation of a specific node is documented after each loading stage. These deformations are then used to perform the sensitivity analysis. The code as well as the input files included in Appendix A.2

7.7 Results

The results of the sensitivity analysis indicate the range of the possible deformation of a specific variant. For every variant the influence of each variable on this range is shown in a influence factor graph Figure 7.3-7.7. The deformation ranges of each variant is displayed in 7.5.

		1	2	3	4	5	6	7	8	9
Clay Weak Sandy	min	-6.11	-14.26	-4.40	-0.96	-5.09	-0.77	-11.75	-13.31	-1.35
	max	-2.18	-4.31	-0.81	-0.66	-1.60	-0.32	-1.55	-1.85	-0.45
Clay Very Sandy	min	-13.00	-11.29	-3.16	-1.66	-3.55	-0.62	-7.88	-7.56	-1.38
	max	-4.49	-3.44	-0.77	-0.90	-1.43	-0.36	-1.75	-1.95	-0.52
Clay Clean	min	-5.36	-10.60	-2.28	-1.07	-4.21	-0.69	-2.64	-3.91	-0.67
	max	-2.12	-1.24	-0.30	-0.63	-0.83	-0.28	-1.07	-1.07	-0.35
Clay Organic	min	-4.29	-7.68	-2.26	-0.99	-2.86	-0.56	-5.00	-6.01	-1.17
	max	-2.53	-3.34	-0.61	-0.70	-1.47	-0.33	-1.19	-1.44	-0.41
Peat	min	-35.21	0.00	-12.06	-3.15	-20.47	-2.23	-12.36	-21.70	-2.70
	max	-3.18	0.00	-0.88	-1.06	-2.13	0.00	-2.56	-2.74	-0.78

Table 7.5: Deformation with maximum and minimum parameters

The different load and geometry variants analyzed in this research are shown in Figure 7.2

Depth, thickness, load, consolidation time	Variant number
1m deep, 1m thick, 460 kPa, 2 hour	1
1m deep, 1m thick, 460 kPa, 6 hour	2
1m deep, 1m thick, 200 kPa, 2 hour	3
5m deep, 1m thick, 460 kPa, 2 hour	4
5m deep, 1m thick, 460 kPa, 6 hour	5
5m deep, 1m thick, 200 kPa, 2 hour	6
5m deep, 5m thick, 460 kPa, 2 hour	7
5m deep, 5m thick, 460 kPa, 6 hour	8
5m deep, 5m thick, 200 kPa, 2 hour	9

Table 7.6: Sensitivity analysis variants

The influence factor is assessed for the different soil types, as discussed in Table 7.2 separately. This is done to give an indication as to which parameters used in the prediction model can cause the greatest variation in the results. These parameters are then later analyzed further to investigate the impact of a more precise determination of these parameters could have on the accuracy of the predicted deformation results.

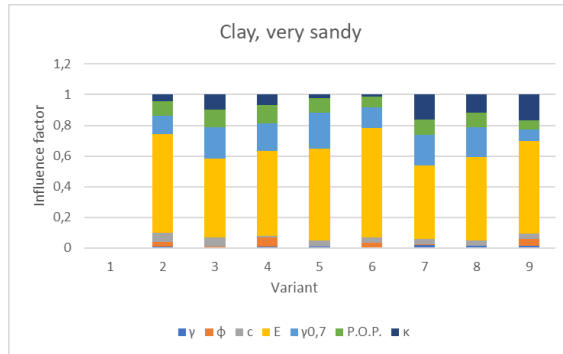


Figure 7.4: Influence factor Clay, very sandy

Weak sandy clay For the weak sandy clay, the stiffness parameters have the largest impact on the uncertainty of the model of each variant. The second most influential parameter is the P.O.P.. The permeability coefficient influence is larger for the variants with 2 hour consolidation time then the variants with 6 hour consolidation time.

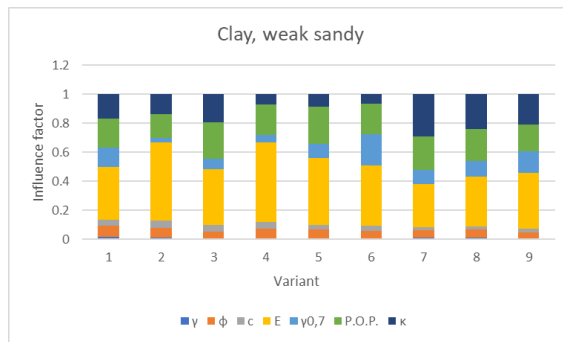


Figure 7.3: Influence factor Clay, weak sandy

Very sandy clay Once again the stiffness parameters have the largest influence of of the uncertainty of the model. When compared to weak sandy clay the p.o.p. is less influential on the result. The permeability coefficient also has less influence on the deformation range. The first variant could not be assessed due to a mistake in the input parameters during calculation.

Clean clay For clean clay the permeability coefficient becomes more influential for each variant. The stiffness parameters , p.o.p. and permeability coefficient account vor nearly all significant variance for clean clay.

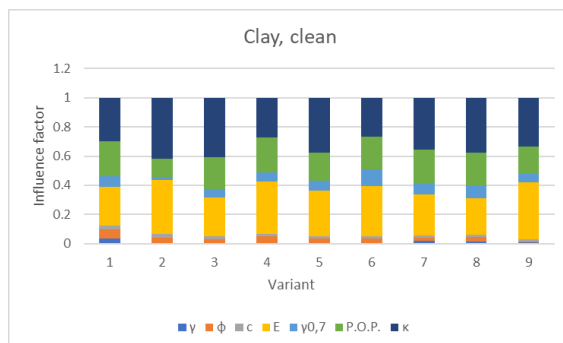


Figure 7.5: Influence factor Clay, clean

Clay, organic

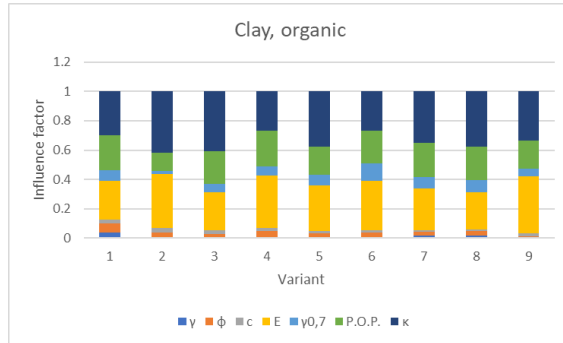


Figure 7.6: Influence factor Clay, organic

Peat The results for variants 1, 2 and 7 contained failures and could thus not be analyzed. From the remaining variants however it becomes evident that the P.O.P. and the permeability parameter have the greatest influence on the uncertainty of the model. The stiffness parameters are not as influential for the peat layer as for the other layers

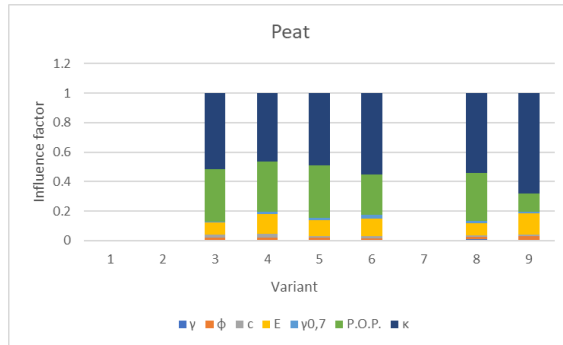


Figure 7.7: Influence factor Peat

7.8 Analysis

The parameters that generally have the most influence on the on the deformation range of the prediction model are the stiffness parameters, the permeability parameters and the P.O.P.. The stiffness parameters are most dominant for the generally coarser soils while the permeability coefficient becomes more influential as the average particle in the soil layer becomes smaller. The more in depth analysis of the results is provided in Chapter 8 as that chapter goes deeper into the influence of consolidation and layer thickness

The stiffness parameters are less influential for the peat layer due to the uncertainty range of this parameter. This range was determined based on the Sanglerat alpha factor as discussed in Section 7.5 which resulted in a small range for peat.

The high sensitivity of the model to the p.o.p. is expected to be a result of the large uncertainty range assumed in this research. The assumed range of 10kPa to 30kPa was used to see the impact it would have on the results. However, since these values were a broad estimate and not substantiated by research, the choice is made to limit the investigation of the soil parameter improvements in the following chapter to the stiffness and permeability parameters

8 | Soil parameter improvements

The uncertainty ranges of the most influential prediction model parameters as discussed previously, the permeability coefficient and stiffness, are tested on the impact this range has on the predicted deformation.

As discussed in section Section 7.5 the stiffness parameter as assessed in the sensitivity analysis is the combination of the E_{oed}^{ref} , E_{50}^{ref} and E_{ur}^{ref} and its range is defined in this project by the α factor as proposed by Sanglerat (1972). E_{50}^{ref} and E_{ur}^{ref} are determined as a factor of E_{oed}^{ref} dependent on the soil type as described by Table 4.1. The range of the permeability coefficient κ is determined from literature.

To determine the impact a more accurate assumption of these parameters would have on the predicted deformation the uncertainty range is divided in different percentiles. These represent specific values of the assessed parameters within the uncertainty range. The aim is to provide an indication of the effect extra soil investigation could have on the deformation prediction. For simplicity, the analysis is performed based on two assumptions. 1. The uncertainty range of the parameter follows a normal distribution and 2. extra soil investigation would return a deterministic value which could be used in the prediction model.

Based on these assumptions a new input file is created for to run with the Python script described in Section 7.6. The input is shown in Appendix A.2. The deformation prediction is performed for various percentiles of the parameter uncertainty range. Namely the 5, 25, 50, 75 and 95 percentiles. These percentiles are determined based on the previously determined 5% and 95% values.

8.1 Results

The results of the uncertainty range analysis are depicted here. These results show the deformation result of each variant and soil type for the uncertainty range of the stiffness and permeability parameters. Table 8.1 displays the ratio between the predicted deformation when the 5-percentile and the 95-percentile value of the uncertainty range of the parameters are used in the prediction model. This ratio stands for the maximum decrease in the predicted deformation possible when extra soil investigation was performed. These ratio's are used instead of the difference in deformation so it is applicable to more situations then the ones used in this project. The **Red** values indicate the cases where extra investigation might be beneficial while the **Green** values are cases where extra investigation will not be necessary. The colors fade between these to extremes.

			Clay, ws		Clay, vs		Clay, clean		Clay, organic		Peat	
			E	k	E	k	E	k	E	k	E	k
1m deep	1m thick	2hour	0.49	0.57	0.49	0.71	0.67	0.32	0.53	0.41	0.90	0.14
		6hour	0.49	0.81	0.49	0.93	0.60	0.24	0.53	0.53	0.85	0.11
5m deep	1m thick	2hour	0.59	0.69	0.63	0.89	0.73	0.39	0.66	0.66	0.95	0.16
		6hour	0.59	0.88	0.63	0.98	0.66	0.31	0.66	0.77	0.91	0.15
	5m thick	2hour	0.61	0.31	0.52	0.59	0.80	0.60	0.62	0.51	1.01	0.27
		6hour	0.56	0.41	0.52	0.71	0.77	0.42	0.57	0.52	0.99	0.17

Table 8.1: 95 % interval improvement ratio

Table 8.2 displays the ratio between the predicted deformation when the 5-percentile and the 50-percentile value of the uncertainty range of the parameters.

			Clay, ws		Clay, vs		Clay, clean		Clay, organic		Peat	
			E	k	E	k	E	k	E	k	E	k
1m deep	1m thick	2hour	0.65	1.00	0.63	1.01	0.77	0.45	0.67	0.79	0.95	0.42
		6hour	0.65	1.00	0.63	1.01	0.74	0.43	0.67	0.97	0.92	0.42
5m deep	1m thick	2hour	0.73	0.99	0.74	1.00	0.82	0.51	0.76	0.93	0.98	0.48
		6hour	0.72	0.99	0.74	0.99	0.78	0.50	0.76	1.00	0.95	0.50
	5m thick	2hour	0.75	0.75	0.66	0.95	0.87	0.63	0.74	0.68	1.01	0.40
		6hour	0.71	0.93	0.66	0.98	0.85	0.48	0.70	0.76	1.00	0.34

Table 8.2: 50 % interval improvement ratio

8.2 Analysis

It is important to note that the ratios depicted in Table 8.1 and Table 8.2 are by itself not an indication of whether extra soil investigation is advisable. If the improvement ratio is 0.5 for the 50% interval and the expected deformation of the specific layer is 3mm a more precise parameter determination would have a 50% chance to result in 1.5mm expected deformation. Thus a 1.5mm positive change. However if the original expected deformation for the layer is larger, for example 20mm even an improvement ratio of 0.7 will have a 50 % chance result in a 6mm decrease of deformation.

Based on the results it can be concluded that for clean clay, organic clay and peat it might be beneficial for the crane hardstand design to determine the permeability parameter more accurately, depending on the original expected deformation. For weak sandy and very sandy clay it might be beneficial to investigate the permeability if it were to be very low and thus the layer would not behave drained during the lifting stage. However, the odds of it being beneficial are quite low as for the 50% interval improvement it would not change the result for any variant tested in this thesis.

The benefit a more accurate determination of the stiffness would have a 50% chance to decrease the expected deformation ranging from 0.63 to 0.87 for each variant. Only for peat a more accurate stiffness parameters will not result in a significantly more beneficial deformation as these values for the 95% - interval improvement ratios range between 0.85 and 1.01.

8.2.1 Consolidation time influence

To analyze the influence of an increase in consolidation time the results of the 1m deep, 1m thick 2hour consolidation time variant is compared to the same layer with 6 hour consolidation time. Thus the only variable between the models is the consolidation phase time. These results are depicted in Figure 8.1.

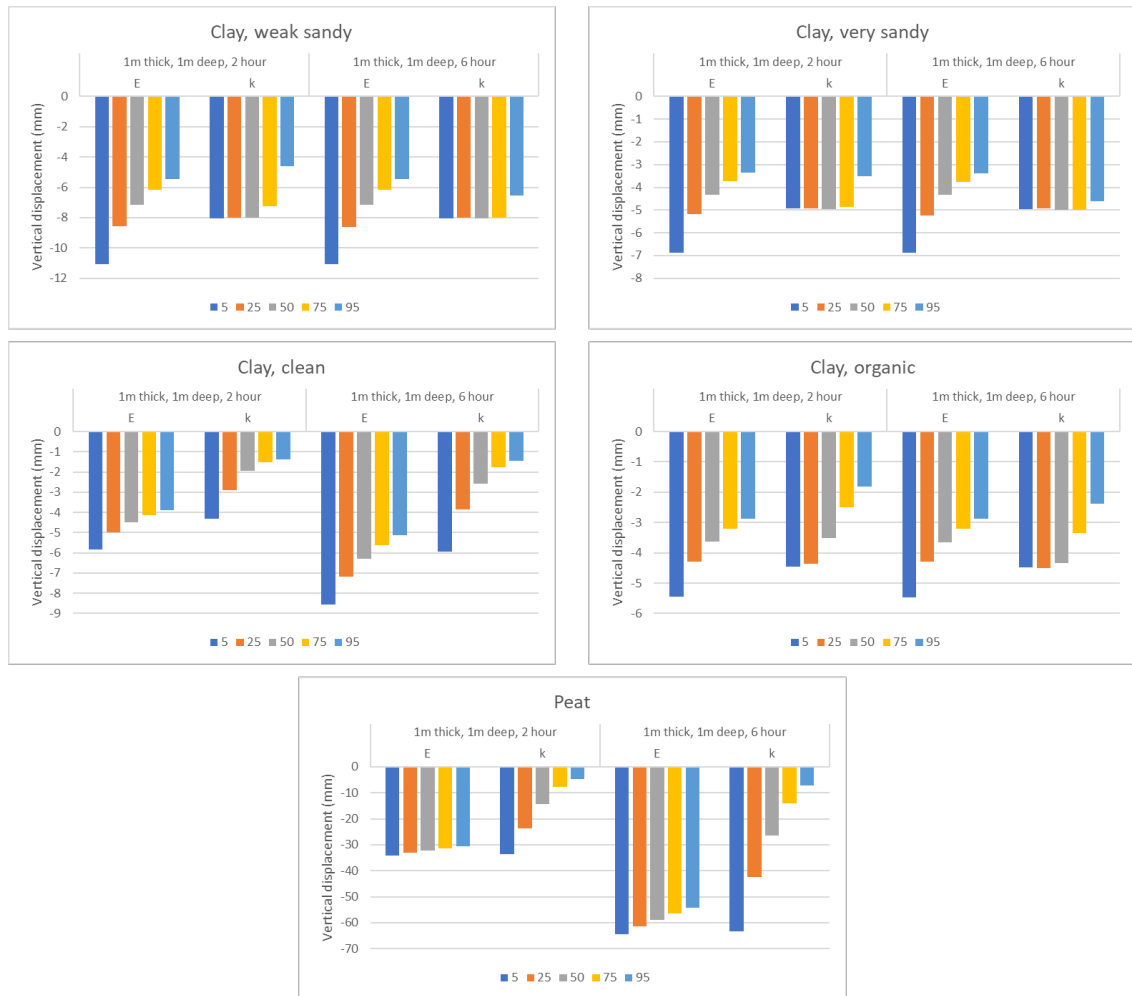


Figure 8.1: Consolidation phase time influence

The weak sandy and very sandy layers both have no decrease in deformation for a more advantageous (from a deformation standpoint) until the 75-percentile uncertainty interval of the permeability parameter. This indicates the layer to behave as a drained layer with those permeability values. The increase in consolidation time causes the layer to behave drained for a larger range of the permeability coefficient. The deformations for the stiffness interval are for weak sandy, very sandy and organic clay exactly the same for the 2 hour and 6 hour variant as the layer is fully drained after 2 hours already for the 5-th percentile permeability parameter used for those calculations.

The concept of consolidation has been briefly discussed in Section 3.3.1. Figure 8.2 shows the excess pore pressure in the clean clay layer as a result of the crane load before the calculation stage of the model was calculated. Figure 8.3 shows the pore pressure after a consolidation stage of 2 hours. The excess pore pressure has begun to dissipate from the layer and decreasing quicker closer to the sand layer. For the consolidation stage after 6 hours, Figure 8.4, it becomes clear that the larger time factor T caused by a larger consolidation time results in a higher degree of consolidation. A higher permeability coefficient would increase the consolidation rate resulting in a even larger influence of a longer consolidation time. However when the excess pore pressures have significantly decreased there will be no more significant deformation as a result of consolidation. The soil will behave as a drained soil and a longer consolidation time or higher permeability coefficient will not result in a larger vertical deformation. This is the case for the soils with high permeability in

Figure 8.1. A thicker layer will also take longer to consolidate, so a higher permeability coefficient as well as a longer consolidation phase will influence the deformation as a result of consolidation for a longer time period. In conclusion, the permeability coefficient will influence the deformation more, and is therefore more important to determine more accurately whenever a layer is thicker and the consolidation time is longer, as is backed up by the results of Table 8.1 and Table 8.2. This is true for all cases that do not behave fully drained.

The same trend holds up for the stiffness as a larger thickness and consolidation time lead to a larger deformation due to consolidation, the influence of the stiffness parameters will also increase.

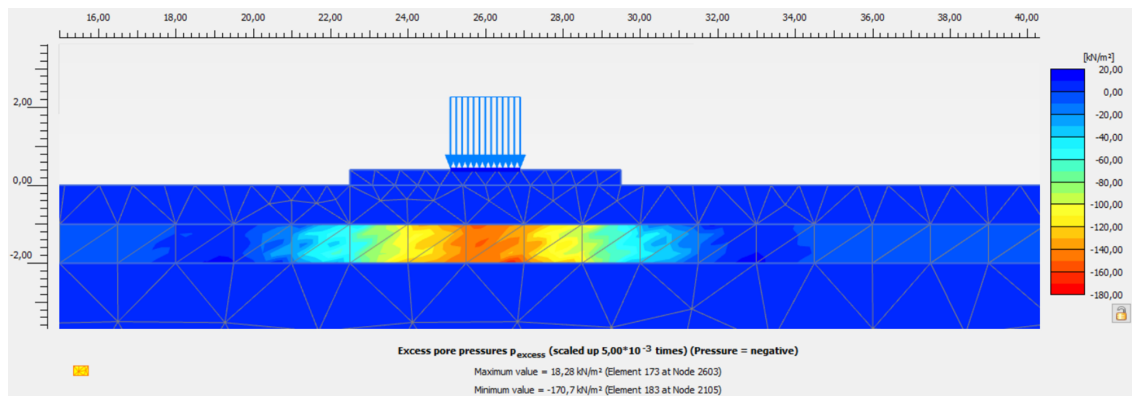


Figure 8.2: Clean clay pore pressure before consolidation stage

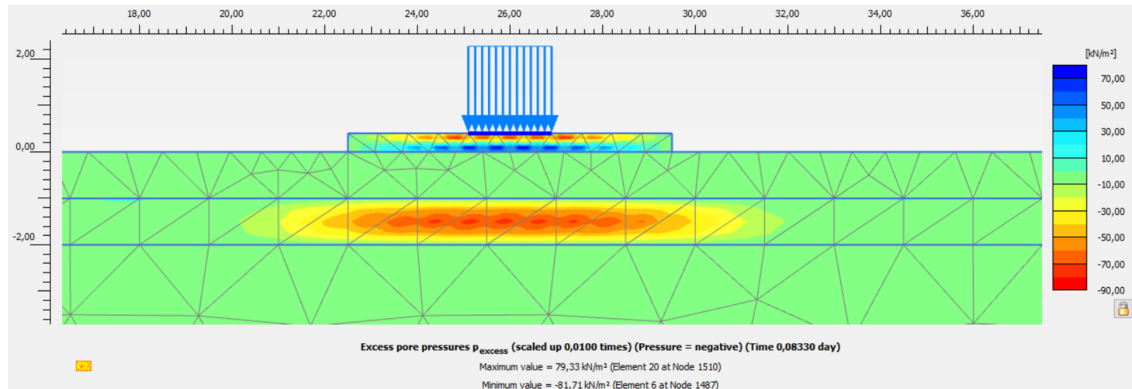


Figure 8.3: Clean clay pore pressure after 2hour consolidation stage

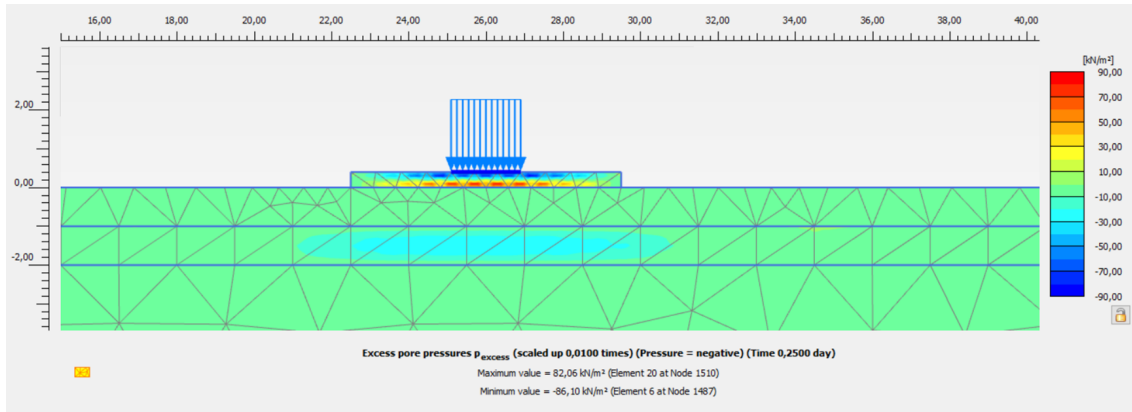


Figure 8.4: Clean clay pore pressure after 6hour consolidation stage

Figure 8.5 and Figure 8.6 indicate that a larger consolidation phase will indeed result in a larger deformation as long as the soil behaves (partially) undrained.

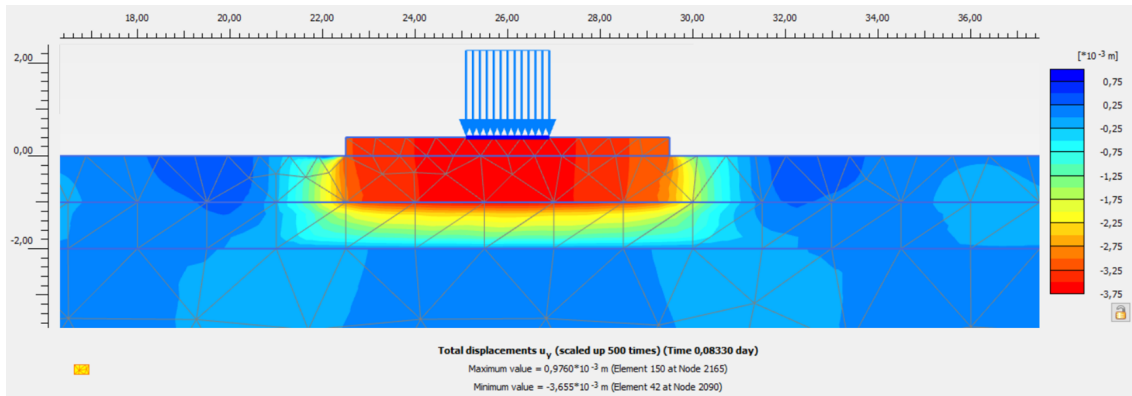


Figure 8.5: Clean clay deformation after 2hour consolidation phase

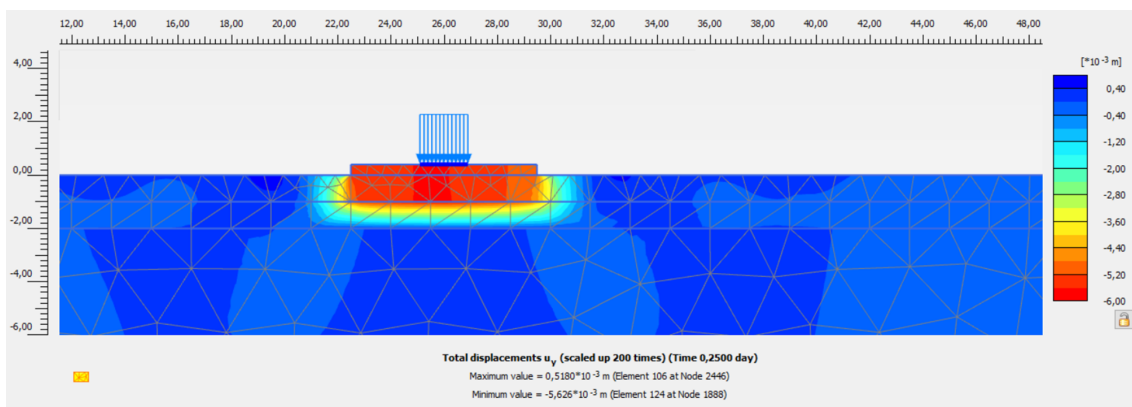


Figure 8.6: Clean clay deformation after 6hour consolidation phase

8.2.2 Layer thickness influence

To analyze the influence of layer thickness on the prediction results the variants of both thicknesses on 5m depth and 2 hour consolidation time

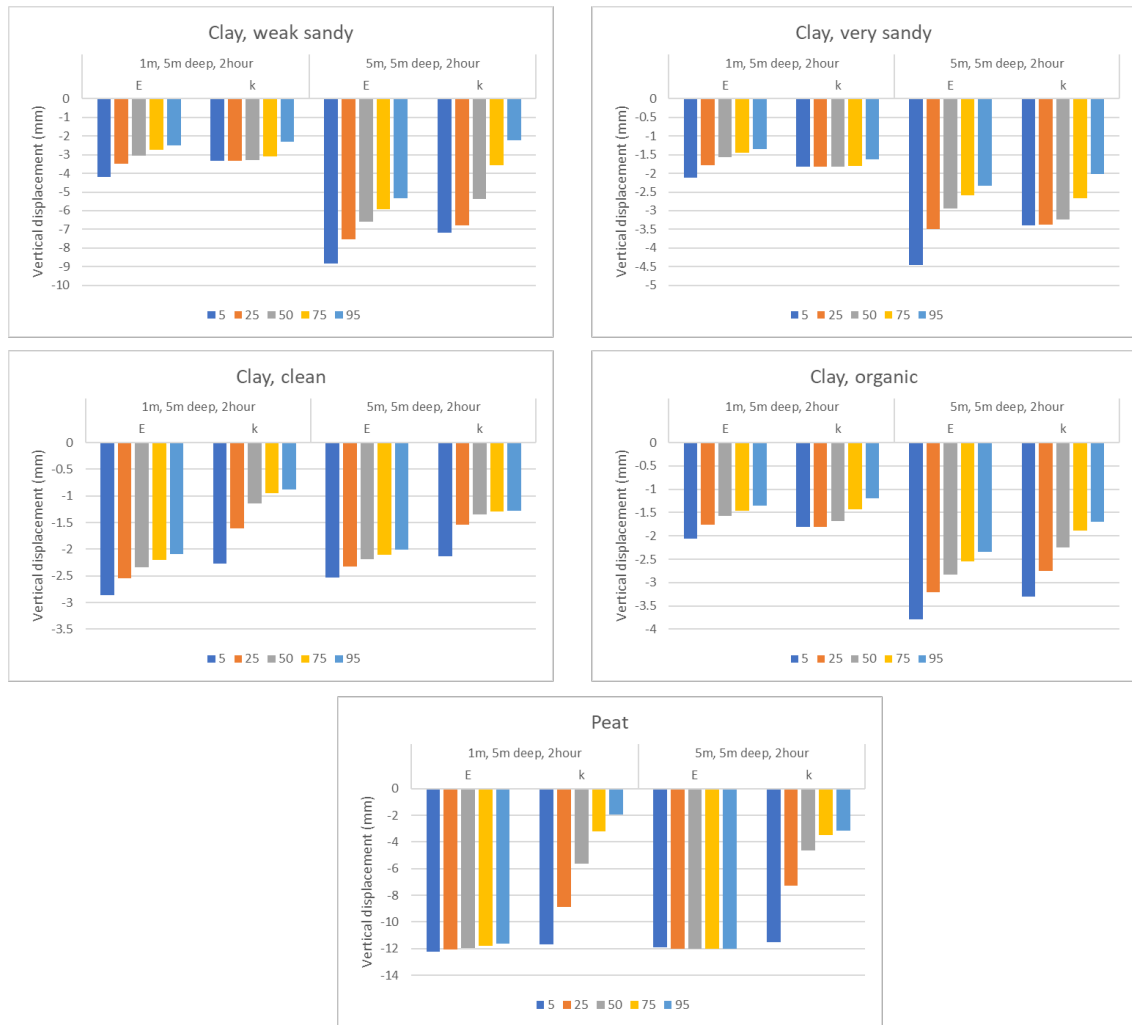


Figure 8.7: Layer thickness influence

Notable from these results is that for clean clay, the 5m thick layer is predicted to deform less than the 1m thick layer. This is a result of the smaller time factor T as a result of the longer drainage length displayed in Figure 3.3. This in combination with the smaller pressure change at the bottom of the layer due to the load spreading as discussed in section 3.1.2 results in a total smaller deformation for the thicker layer.

These findings can be backed up by the pore pressure distribution before and after the consolidation stage of the clean clay layer Figure 8.8 and Figure 8.9. The lower pore pressure at the bottom of the clay layer is a result of the smaller soil pressure as a result of the load spreading throughout the soil profile.

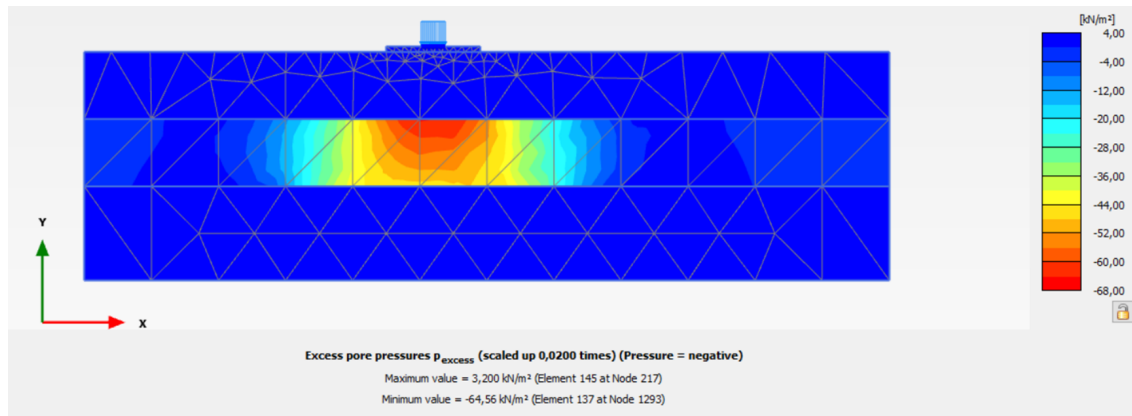


Figure 8.8: Pore pressure clean clay before consolidation stage

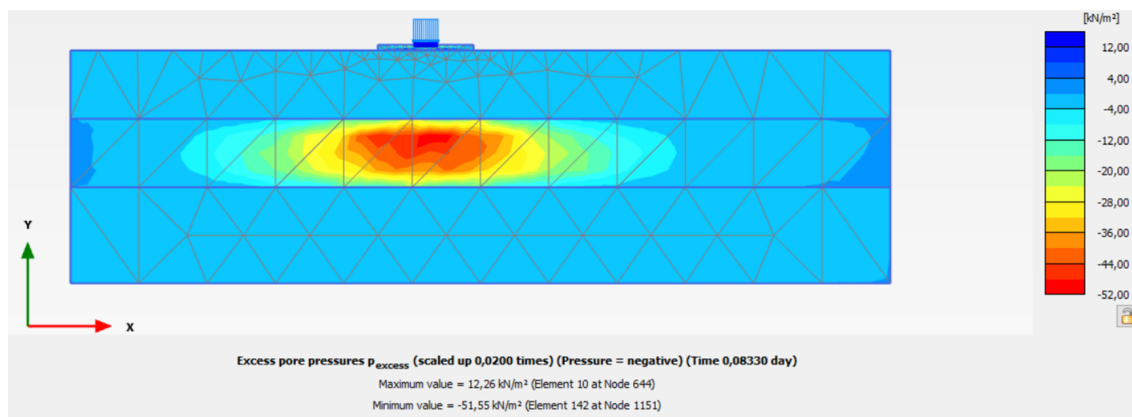


Figure 8.9: Pore pressure clean clay after 2 hour consolidation

9 | Discussion

This chapter discusses the results of each part of this thesis as well as the coherence between these parts.

This thesis originated as a result of a problem occurring during wind turbine lifting operations during the turbine build-up. Differential deformations of the soil caused by varying pressures applied on the crane-soil contact points lead to tipping of the crane. This problem can halt operations leading to costly delays.

This project aims to improve the current prediction method used to assess deformations of the crane hardstand, as a more accurate prediction will decrease the chance of unexpected differential settlement

As mentioned in Chapter 1 the thesis is divided in three separate parts:

1. Theory: A background study creating a complete picture concerning crane hardstands used for the lifting stage of a wind turbine installation. This in combination with the physical events occurring during loading should provide an overview of the wind turbine lifting operation. A literature study is furthermore used to investigate in what way the above ground physical events are expected to result in soil deformations.
2. Practice: The current prediction method is tested on how well it considers the deformation phenomena found in the literature study. As well as how this translates to the deformation occurring during real time lifting operations and full scale tests
3. Analysis: The current prediction method is compared to the results of the full scale monitoring and full scale tests. The current prediction model is also subjected to a sensitivity analysis to investigate which parameters are most influential on the model's result. The impact of extra soil investigation to better estimate the prediction model parameters is examined.

From the theory could be concluded that 4 expected phenomena would primarily influence the deformations of the crane hardstand during turbine lifting operations. Namely:

1. The un- and reloading nature of the crane operations could result in deformations in the form of: plastic strain accumulation, hysteresis, damping and energy dissipation.
2. Distribution of the load through the soil profile could influence the magnitude of the pressure change at a deformable soil layer at a certain depth
3. Primary compression strains upon virgin loading
4. Consolidation that occurs during the relatively 'short' time of a specific load case

The STOWA handbook on crane hardstands for installation of wind turbines provides an extensive explanation on crane hardstands. What preliminary geotechnical soil investigation is required, the design process and even the execution.

A closer look at the how the deformation prediction method as it is currently used however, indicates a few possibilities for a more accurate deformation prediction. Mainly the correlations used to determine model parameters from a CPT lead to a large range of uncertainty. Safety standards regulate that a 95% parameter certainty interval is required for the prediction calculations. Therefore, a large range of uncertainty results in an overestimation of the predicted deformations as a smaller uncertainty range with the same mean value will result in a more advantageous 95% certainty interval.

Aside from that, the soil layers with low permeability are modelled as undrained due to the 'short' duration of the load cases, and no time dependent behaviour is accounted for, which is deemed questionable.

The full scale monitoring provides an overview of the real time phenomena occurring during the lifting stage of the turbine installation. The re- and unloading of the load is observed but this is concluded not to lead to significant plastic deformations. Therefore, the choice is made not to investigate the cyclic loading further in this research.

For the monitoring cases considered in this project consolidation is not observed to have a significant impact on the deformation during a lifting stage. This is the case for these specific crane hardstand however, because with extensive pre- loading of half a year and a design of thick stratum layer extensive mitigation measures were already in place to minimize the consolidation part of the total deformation. However, over the entire duration of the crane operation the time dependent deformations were significant. Albeit not differential deformations.

The full scale tests however, indicate that significant deformations do occur over the short time period. For a crane hardstand with 3.5m of deform-able layers the 18mm of deformation over time accounted for 34% of the total deformation. Therefore the choice is made to include a consolidation phase in the further calculations performed in this research.

As became apparent by investigation of the current prediction method the parameter determination lead to large uncertainties in the Hardening Soil Small Strain prediction model used in PLAXIS. To suggest improvements on the current method and as an addition to the STOWA manual it is investigated what effect a more precise parameter determination might have on the deformation prediction. A sensitivity analysis is executed on specific variants as described in chapter Chapter 7 to indicate which parameters have the largest influence on the uncertainty of the model. The range of each model parameter is approximated based on the CPT-correlation used to determine the parameter in the current prediction method. The sensitivity analysis derived the stiffness component E (which is a combination of E_{oed}^{ref} , E_{50}^{ref} and E_{ur}^{ref}) and the permeability coefficient κ to have the largest influence on the uncertainty of the model.

To provide an indication which benefit a more accurate parameter determination as a result of more extensive soil investigation might have, the deformation is predicted for different percentiles of the parameters range of uncertainty. This is done based on two assumptions: 1. The uncertainty range of the parameter follows a normal distribution and 2. extra soil investigation would return a deterministic value which could be used in the prediction model. The maximum difference in deformation ratio extra soil investigation might have is depicted in Table 8.1. The impact ratio extra soil investigation is 50% likely to return is depicted in Table 8.2. These results are the ratio between the predicted deformation with and without more accurate parameter determination method. Whether extensive soil investigation will be beneficial depends on the improvement ratio in combination with the original predicted deformation. When the original deformation of a certain soil layer is large a less beneficial improvement ratio might already result in significant less deformation. While for a small initial deformation extra investigation will not be beneficial. Other factors such as whether the design is on the allowed deformation limit, if the same soil layer is present at more project locations will influence the benefit of extra soil investigation as well. This research is based on refinement of knowledge. The first phase is focused on gathering information on crane hardstands, the lifting phase of wind turbine installations and all possible deformation influences. Then the current deformation prediction method is analyzed and tested on the basis of full scale monitoring and test results. That phase is then analyzed to find shortcomings in the current method and make suggestions to improve the method. The resulting improvement interval ratios can be used in addition to the STOWA manual to create more accurate and beneficial crane hardstand designs to reduce the chance of differential settlement.

10 | Conclusions

The goal of this thesis was to answer the following research question.

What influences the deformation of a crane hardstand and how can this deformation be more accurately predicted to improve the design method?

This is done with the following structure. At first the hoisting process of the wind turbine installation is analyzed to understand how the process can result in soil deformations during lifting. Whether the soil profile is experiencing virgin or re-loading is indicated to have a large influence on the deformation. Aside from the loading conditions, the distribution of the load on the surface as well as throughout the soil profile together with time dependent behaviour (primarily consolidation) are also highlighted as estimated deformation influences.

The current predictions method is analyzed and tested on the bases of monitoring and full scale deformations tests. Possible shortcomings of the current method as proposed by M.P. Rooduijn (2019) are noted to be the absence of time dependent behaviour and the limited recommended soil investigation. The full scale monitoring analyses which deformation phenomena are visible during lifting activities. The re-unloading cycles are not resulting in significant plastic deformations and consolidation during a lifting stage. A small time dependent deformation of 1mm is observed during the boom letdown of WT4. Unforeseen events such as a higher occurring pressures than anticipated might result in larger deformations than estimated.

The full scale testing pointed out that displacements over time have a significant part in the total deformations. It does vary depending on the soil type and layer thickness. Testing location D1 had a soil profile consisting of primarily sand. For this location only 14% (2mm) of the total deformation of 12mm occurred over the 6 hour time period. While for location B3, consisting of a 3m thick weak clay/peat layer, 34% (18mm) out of a total 35mm deformation appeared during the 6 hour waiting period. From this it is concluded that time dependent behaviour can be a significant part of the total deformation depending on the soil profile. For this reason a consolidation phase is included in the rest of the research.

The sensitivity analysis indicates that the biggest uncertainties from the deformation predictions are caused by the ranges of the stiffness and permeability of the layers. The range as a result of parameter determination has a large impact of the deformation range. The effect a more accurate prediction might have on the expected deformation is researched at the soil parameter improvements.

Further analysis of the uncertainty range of the stiffness and permeability parameters provides an indication of the benefit more extensive soil investigation might provide for the deformation prediction. An overview is provided for the maximum predicted deformation decrease a more precise model parameter determination might result in, as well as the predicted deformation decrease extensive soil investigation has a 50% chance of realizing. For a peat layer a more accurate permeability parameter determination has a 50% chance to decrease the deformation prediction by 50-60% for each variant. The need for extra soil investigation should be weighed compared to the initial so

11 | Evaluation and recommendations

The findings of this thesis are meant as an addition to the STOWA manual to be used by a geo-technical engineer during the design phase of a crane-hardstand on soft soil. The results can be used as advise to the engineer with whether the deformation prediction model should include a consolidation phase. The thesis also provides an indication of the influence extra soil investigation to more accurately predict the stiffness and permeability of the soil might have on the predicted vertical deformation. This indication is presented tables that show the decrease in predicted deformation as a result of the 50- and 95 percentile interval improvement ratio for the uncertainty range of the stiffness and permeability parameters.

These are however, the results of the specific situation used in this research and should therefore be used as advise rather than to be 1 on 1 translated to the design at hand. Important to note is that the engineer should compare the ratio to the predicted deformation caused by a specific soil layers, because when the expected deformation is low a decrease of expected deformation of 50% might still be insignificant on the total expected deformation.

This research is applicable at the start of the design phase to determine the degree of mitigation measures needed for a design to stay under prescribed deformations of a specific project.

A big setback of the research came during the monitoring of the deformations of hoisting activities of the wind turbines. To document the outrigger pressures during hoisting a go pro camera was used pointed at the display located on the crane base. This crane base only displayed the outrigger pressures when running. However during most hoists the base was not required to be active and with fuel considerations these where shut off and not displaying the outrigger pressures. The gap in information during the monitoring made trying to fit the prediction model to reality useless. For this reason the monitoring is only used to recognize expected deformation phenomena.

Due to time considerations this research only investigates the soil model currently used in practice, Hardening Soil Small Strain, but does not research in what way other soil models might improve the deformation prediction accuracy. Therefor a recommendation for further research would be to analyze the influence on the prediction accuracy of for example the Soft Soil Creep model, as this model includes time dependent behaviour and is known to predict soft soil deformation accurately.

In the current prediction model only the normative crane pressure point (outrigger or crawler) is considered for the crane tilting assessment. This is because the influence between the pressure point will only decrease differential deformation. The normative pressure point (with the highest load) will influence the deformation under the other pressure points more than visa versa, causing the differential settlement to decrease. It would be interesting however, for further research to investigate how this thesis would translate to Plaxis 3D, and in what way Plaxis 3D might influence the deformation prediction accuracy.

References

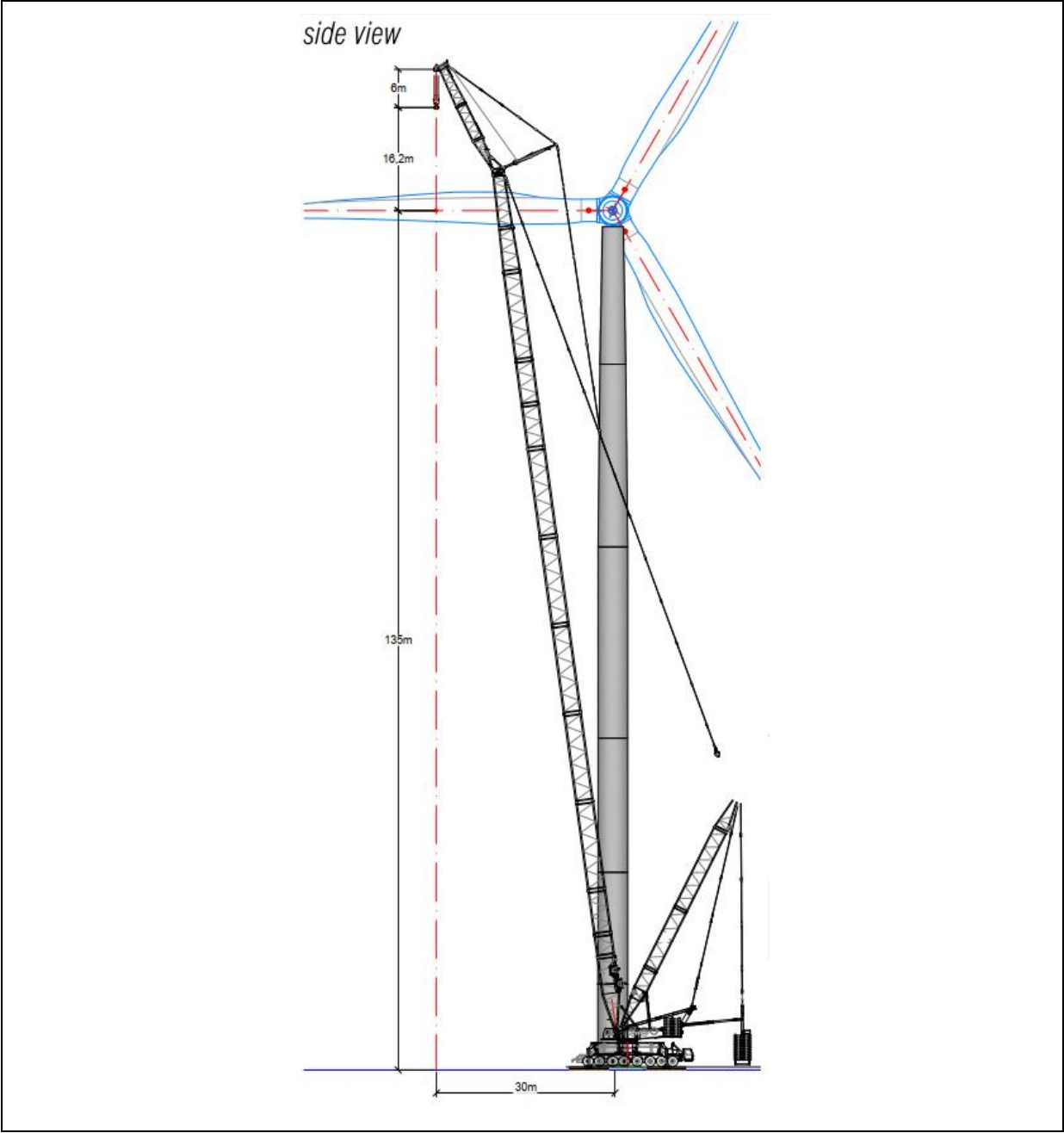
- Ahlvin, R., & Ulery, H. (1962). *Tabulated values for determining the complex pattern of stresses, strains and deflections beneath a uniform load on a homogeneous half space*. Highway Res. Rec.
- Bentley. (2023). Plaxis 2d scientific manual 2d.
- Boussinesq, J. (1883). *Application des potentials a l'etude de l'equilibre et due mouvement des solides elastiques*. Gaughier-Villars.
- Bowles, J. E. (1996). *Foundation analysis and design*. McGraw-Hill.
- Brinkgreve, R. (2022). Behaviour of soils and rocks: Modelling undrained behaviour. Delft University of Technology.
- Butterfield, R. (2011). An improved model of soil response to load, unload and re-load cycles in an oedometer. *SOILS AND FOUNDATIONS*, 51, 253-263.
- Cui, Y. J., Nguyen, X. P., Tang, A. M., & Li, X. L. (2013, 10). An insight into the unloading/reloading loops on the compression curve of natural stiff clays. *Applied Clay Science*, 83-84, 343-348. doi: 10.1016/j.clay.2013.08.003
- Das, B. M. (n.d.). *Shallow foundations bearing capacity and settlement third edition*.
- Das, B. M. (2017). *Shallow foundations bearing capacity and settlement third edition*. Taylor Francis Group, LLC.
- Geoservices, A. (2023). Cone penetration testing.
- Guo, L., Wang, J., Cai, Y., Liu, H., Gao, Y., & Sun, H. (2013, 7). Undrained deformation behavior of saturated soft clay under long-term cyclic loading. *Soil Dynamics and Earthquake Engineering*, 50, 28-37. doi: 10.1016/j.soildyn.2013.01.029
- HeavyLiftNews. (2021). Mammoet heavy duty pavements' director describes how enviro-mat cuts onshore wind assembly or maintenance time. Retrieved from <https://www.heavyliftnews.com/mammoet-heavy-duty-pavements-director-describes-how-enviro-mat-cuts-onshore-wind-assembly-or-maintenance-time/>
- Khoshghalb, A. (2013). On creep laboratory tests in soil mechanics. In L. Laloui & A. Ferrari (Eds.), *Multiphysical testing of soils and shales* (pp. 255–260). Berlin, Heidelberg: Springer Berlin Heidelberg.
- Lunne, T., Robertson, P., & J.J.M., P. (1997). *Cone-penetration testing in geotechnical engineering*. SPON Press, Taylor and Francis Group.
- M.P. Rooduijn, e. a. (2019). *Crane hardstands for installation of wind turbines*. Retrieved from www.stowa.nl
- Normcommissie"Geotechniek". (2017). *Nederlandse norm nen 9997-1+c2 (nl) geotechnisch ontwerp van constructies-deel 1: Algemene regels*.
- Robertson, P. K. (2009). Interpretation of cone penetration tests — a unified approach. *Canadian Geotechnical Journal*, 46(11), 1337-1355. Retrieved from <https://doi.org/10.1139/T09-065> doi: 10.1139/T09-065
- Sanglerat, G. (1972). The penetration and soil exploration. developonderzoment in geotechnical engineering. *Elsevier Scientific Publishing*.

- Sanin, M., & Wijewickreme, D. (2006). Cyclic shear response of channel-fill fraser river delta silt. *Soil Dynamics and Earthquake Engineering*, 26(9), 854-869. Retrieved from <https://www.sciencedirect.com/science/article/pii/S0267726105001843> doi: <https://doi.org/10.1016/j.soildyn.2005.12.006>
- Schmertmann, J. H., J.H., & Brown, P. (1978). Improved strain influence factor diagrams. *CUFAD, ASCE*, 104(8): 1131.
- StructX. (2023). Hydraulic conductivity ranges of various soil types. Retrieved from https://structx.com/Soil_Properties_007.html
- Suddepong, A., Chai, J., Shen, S., & Carter, J. (2015). Deformation behaviour of clay under repeated one-dimensional unloading-reloading. *Canadian Geotechnical Journal*, 52, 1035-1044. doi: 10.1139/cgj-2014-0216
- Tabsh, S. W., & Al-Shawa, A. R. (n.d.). Effect of spread footing flexibility on structural response. doi: 10.1061/ASCE1084-0680200510:2109
- Terzaghi, K., Peck, R. B., & Mesri, G. (1996). *Soil mechanics in engineering practice*. John Wiley & Sons.
- Terzaghi, R. P., K., & Mesri, G. (1995). Case history evaluation of the behavior of drilled shafts under axial and lateral loading.
- Timoshenko, S., & Goodier, J. (1951). *Theory of elasticity* (No. v. 1). McGraw-Hill.
- TNO. (2022). *Dinoloket ondergrondmodellen*. Retrieved from <https://www.dinoloket.nl/ondergrondmodellen>
- Toyota, H., & Takada, S. (2021). Soil element assessment of cyclic-load-induced settlement considering combination of vertical, horizontal, and shear stresses in cohesive soil. *Soils and Foundations*, 61(3), 752-764. Retrieved from <https://www.sciencedirect.com/science/article/pii/S0038080621000500> doi: <https://doi.org/10.1016/j.sandf.2021.02.007>
- Trautmann, C. H., & Kulhawy, F. H. (1987). A computer program for compression and uplift foundation analysis and design. *CUFAD*, 16.
- Vermeer, P., & Meier, C. (1998). Proceedings int. conf. on soil-structure interaction in urban civil engineering. , 177-199.
- Verruijt, A. (2016). *Theory and problems of poroelasticity*. Retrieved from <http://geo.verruijt.net>
- Westergaard, H. (1938). A problem of elasticity suggested by a problem in soil mechanics: Soft material reinforced by numerous strong horizontal sheets. *Contribution to the Mechanics of Solids, Stephen Timoshenko 60th Anniversary Volume*.
- Zhang, M., Sun, H., & Hou, M. (2020, 12). Pores evolution of soft clay under loading/unloading process. *Applied Sciences (Switzerland)*, 10, 1-13. doi: 10.3390/app10238468

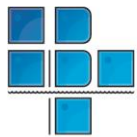
A | Appendices

A.1 Monitoring Plan and Results

Monitoring plan deformations MCHS WT2 and WT4



Client information

Client:**Contractor:**BT Geoconsult BV
INGENIEURSBUREAUBT Geoconsult BV (BTG)
Loire 204
2491 AM DEN HAAG
Phone: +31 (0)70-4159002

Document management

Document no.:	2019-1865/045 revision 1.a
Date:	May 12 th , 2022
Title:	Monitoring plan deformations MCHS WT2 and WT4
Project:	
Organisation:	BT Geoconsult BV.
Status:	Draft

Signature:

Author:	T.J.J. Krielaart
Authorisation:	ir. A.S. Ramkisoen

Revision:	Issued to:	Organisation:	Date:
-----------	------------	---------------	-------

Table of Contents

Client information	ii
Document management	ii
Table of Contents	iii
1 Introduction	1
2 Project information	2
2.1 Project information	2
2.2 Monitoring location.....	2
2.3 MCHS Design information	3
3 Soil stratification and geohydrology	5
3.1 Available geotechnical investigation	5
3.2 Surface level	5
3.3 Soil stratification.....	5
3.4 Geohydrology	6
4 Monitoring deformations	7
4.1 Monitoring points	7
4.2 Monitoring Protocol	9
4.3 Measurement accuracy	9
4.4 Allowable deformations.....	10
4.5 Documentation	10
4.6 Arrangements	10

1 Introduction

Vattenfall Wind Development is realizing a windfarm with 6 new wind turbines near Moerdijk and Lage-Zwaluwe. During installation of a wind turbine the subsoil on which the crane is founded may settle, causing the surface to subside locally (vertical deformation). When this subsiding does not occur uniformly over the total area underneath the crane, it is possible that the crane will start to tilt. For safety reasons the maximum allowable tilt of a crane is set to be 0.3° with a signal value of 0.2° . During installation each outrigger will be subjected to different loads causing the soil deformation underneath each one to be differential. In the design of the crane hardstand this requirement is taken into account. To ensure that the bearing capacity is sufficient and therefore decrease settlement Tensar geogrids were installed as the foundation of the crane. The design is validated with several design calculations carried out by the BoP contractor Heijmans. Furthermore in the crane there are built in systems which give warning signs when the maximum value or alarm value is exceeded.

Despite this and due to a long design period and lots of discussions during the design period Vattenfall decided to perform monitoring activities since the differential deformations can lead to complications. The actual behaviour of the crane outriggers during installation will be monitored as a measure to mitigate any unsafe situation on the basis of real-time monitoring data.

BT Geoconsult BV is one of the members of the committee that has issued the guidelines for crane hardstands in 2019/2020 in the Netherlands. There are several topics which need further research. Namely, the effect of the un-/reloading nature of the turbine installation has on the deformation. What part of the deformations is elastic and what part is plastic. Whether the relatively short period the crane is installed causes the compressible layers to solely behave undrained or whether drained behaviour impacts the deformation. How load spreading measures influence differential settlement

BT Geoconsult BV would like to make use of this opportunity to collect data in such a way that it can be further processed for research purposes as mentioned above. Results and conclusions from this research will give the engineering community more insight in the actual behaviour of the soil underneath the crane hardstands which is also beneficial for the developers of wind farms. A better understanding of the soil behaviour underneath crane hardstands will make future differential settlement predictions more accurate. This will decrease the chance of unexpected exceedance of the tilt limit that can lead to project delays, Therefore this plan of action is issued. This plan is based in the wind farm A16 at Klaverspoor.

2 Project information

2.1 Project information

The following project information is used for the design:

- [A] Drawing "Rigging Main crane" with reference 21HP_WT2 revision 3.0, dated May 4th 2022;
- [B] Report "Final design roads & crane hardstands" by with reference MEM-2217, dated 18 November 2021;
- [C] Report "Plaxisberekening draagvermogen WTG7", with reference MEM-2753, revision 5, dated November 4rd 2021;
- [D] Report "Onderbouwing C_u" by Heijmans, with reference MEM-2688 revision 3.0, dated 29 October 2021;
- [E] Document "Work method statement drainage MCHS during lifting"

Furthermore, information from verbal and digital communication with the client has been used.

2.2 Monitoring location

This monitoring plan is issued for 2 locations: WT2 and WT4. WT2 because it is the first turbine installed and WT4 because it has the most critical soil stratification (see Chapter 3) regarding settlements. The turbines will be installed by a LIEBHERR LG1750 crane which is supported by 4 outriggers. The crane layout is given in Figure 1.1 [A]. The outrigger is placed on top wooden or steel dragline mats to further spread the load over the soil surface.

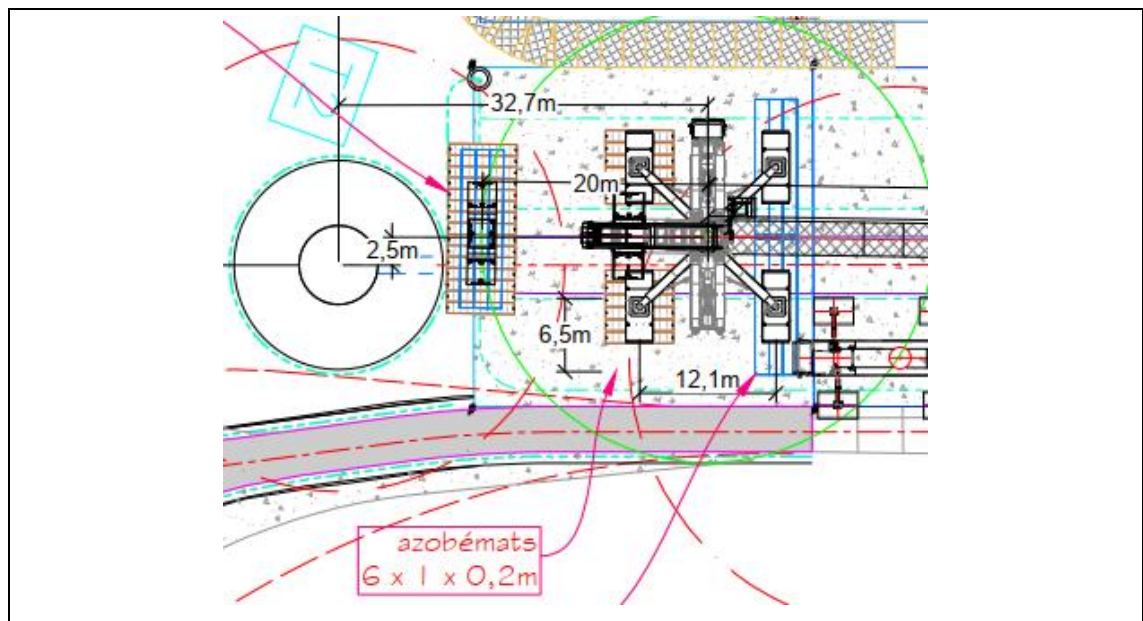


Figure 2.1 Dimensions and lay out crane. [A]

2.3 MCHS Design information

To meet the required bearing capacity of the platform stay within the requirements for differential settlement, the MCHS was built of a Tensar geogrid cell structure called stratum. On some location there was a top layer built up from mechanically stabilized layer (MSL) with horizontal geogrids, see Figure 2.1. The design is given in report [B] and additionally checked in [C]. Related to the design in report [D] substantiation of the soil parameter c_u is given after additional soil investigation and in [E] an important measure: draining before lifting is presented. A schematic depiction of how the load propagates through these layers is shown in Figure 2.1.

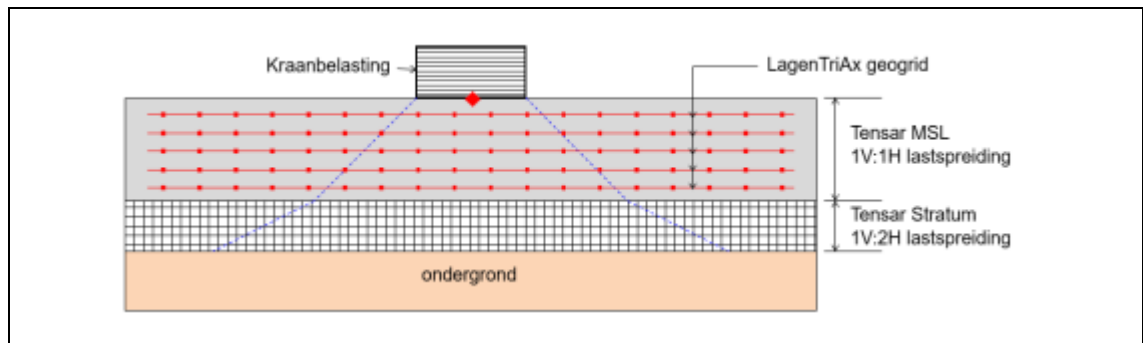


Figure 2.1 Load spreading through the MCHS stratum [B]

At the locations where the monitoring will take place WT2 and 4 the MCHS consists 2000 mm Tensar Stratum as shown in Figure 2.2 and 2.3.

Construction layout of main crane hardstand (MCHS)	Check on bearing capacity with crawler crane in position 2 (normative)
	<p>Undrained bearing capacity</p> <ul style="list-style-type: none"> • u.c of Λ_{GEO} of 1,004 < 1,00 meets requirement <p>Drained bearing capacity</p> <ul style="list-style-type: none"> • u.c of Λ_{GEO} of 0,288 < 1,00 meets requirement <p>Resistance to squeezing (lateral extrusion)</p> <ul style="list-style-type: none"> • u.c of Λ_{GEO} of 0,804 < 1,00 meets requirement <p>Resistance to horizontal sliding</p> <ul style="list-style-type: none"> • u.c of Λ_{GEO} of 0,462 < 1,00 meets requirement

Figure 2.2 MCHS stratum WT2 [B]

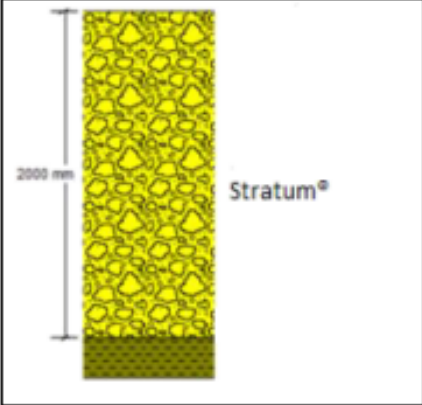
Construction layout of main crane hardstand (MCHS)	Check on bearing capacity with crawler crane in position 2 (normative)
	<p>Undrained bearing capacity</p> <ul style="list-style-type: none"> • u.c or Λ_{GEO} of 1,064 > 1,00* does not meet the requirement <p>Drained bearing capacity</p> <ul style="list-style-type: none"> • u.c of Λ_{GEO} of 0,358 < 1,00 meets requirement <p>Resistance to squeezing (lateral extrusion)</p> <ul style="list-style-type: none"> • u.c of Λ_{GEO} of 0,838 < 1,00 meets requirement <p>Resistance to horizontal sliding</p> <ul style="list-style-type: none"> • u.c of Λ_{GEO} of 0,462 < 1,00 meets requirement

Figure 2.3 MCHS stratum WT4 [B]

As mentioned in Figure 2.3 the requirement was not met in this report. The designer mentioned that these calculations have a conservative approach. Additional FEM based calculations were carried out as presented in [C] to demonstrate the safety of the MCHS.

3 Soil stratification and geohydrology

3.1 Available geotechnical investigation

An overview of the provided and used geotechnical investigation for WTG-3 and WTG-4 is shown in Table 3.1 and Table 3.2. The geotechnical investigation is included in [C].

Table 3.1: Overview of available geotechnical investigation WTG-3

Source [-]	Relevant investigation [-]	Distance to project location [m]	Depth [m NAP]
Document "WPA16, Klaverspoor – Onderbouwing Cu"	12 CPT's 2 boreholes	0 to 100	CPT's: - 30,0 Boreholes: - 21,0

Table 3.2: Overview of available geotechnical investigation WTG-4

Source [-]	Relevant investigation [-]	Distance to project location [m]	Depth [m NAP]
Document "WPA16, Klaverspoor – Onderbouwing Cu"	12 CPT's 2 boreholes	0 to 100	CPT's: - 22,0 Boreholes: - 21,0

3.2 Surface level

The surface levels at WT2 and WT4 are 1.21 m and 1.24 m respectively.

3.3 Soil stratification

From interpretation of the available geotechnical investigation a general soil stratification at the project location is determined. For the intermediate locations, an interpolation is made using surrounding soil investigation. The global soil stratification is shown in Table 3.3 and Table 3.4.

Table 3.3: Indicative soil stratification WT2

Grondlaag nr. [-]	Niveau grondlaag [-]	Grondsoort [-]
1	from NAP – 1,2 m (=Surface level) to NAP – 1,5 m à NAP – 2,1m	Top layer: Clay, slightly organic, silty
2	From NAP – 1,5 m à NAP – 2,1 m to NAP – 5,5 m à NAP – 6,1 m	Peat
3	From NAP – 5,5 m à NAP – 6,1 m to NAP – 10,0 m à NAP – 12,5 m	Sand, slightly silty
4	From NAP – 10,0 m à NAP – 12,5 m to NAP – 20,0 m à NAP – 22,0 m	Sand, layered clay
5	From NAP – NAP – 20,0 m à NAP – 22,0 m To maximum obtained depth (NAP – 29,0 m)	Clay, silty

Table 3.4 Indicative soil stratification WT4

Grondlaag nr. [-]	Niveau grondlaag [-]	Grondsoort [-]
1	from NAP - 1,2 m (= Surface level) to NAP - 2,0 m à NAP - 3,0 m	Top layer: Clay, slightly organic, silty
2	From NAP - 2,0 m à NAP - 3,0 m to NAP - 5,5 m à NAP - 6,0 m	Peat
3	From NAP - 5,8 m à NAP - 6,8 m to NAP - 12,0 m à NAP - 13,5 m	Sand, silty
4	From NAP - 12,0 m à NAP - 13,5 m to NAP - 18,0 m à NAP - 18,5 m	Clay, sandy
5	From NAP - 15,0 m à NAP - 16,5 m to NAP - 18,0 m à NAP - 18,5 m	Clay, sandy
6	From NAP - 18,0 m à NAP - 18,5 m To maximum obtained depth (NAP - 22 m)	Sand, slightly silty

3.4 Geohydrology

The geohydrological conditions at the project location were determined in [B] and depicted in Table 3.5.

Table 3.5 Geohydrological conditions project

Turbine	Summer level [NAP - m]	Winter [NAP - m]	GWL including bulge [NAP - m]
WTG-3	-1.8	-2.2	-1.7
WTG-4	-1.8	-2.2	-2.7

The head in the sand aquifer between NAP - 6.0 m and NAP - 16.0 m is determined according to [B] and set to NAP - 2.5 m.

Due to the large depth of the MCHS, part of the stratum is projected to be below ground level. To ensure strength during lifting, the ground water in the hardening package is drained with groundwater pumps as discussed in [E]. The drain water courses surrounding the MCHS locations ensure the drainage water does not cause problems for the water system.

4 Monitoring deformations

Due to the tight restrictions on tilting of the crane during operation it is important to have a good understanding of the deformation of the crane outriggers at different loading levels. To ensure safety during lifting operations and for research purposes the deformations of the crane outriggers are monitored during different phases of the lifting operations. It is important to register the deformation and the actual load at the same time. The deformation will be recorded by means of a Robotic Total Station. The measurements and the time representative load situation must be documented accurately.

Elaboration on the approach is presented in subchapter 4.5. Documentation.

4.1 Monitoring points

An overview of each outrigger with corresponding letter (A-D) is depicted in figure 4.1

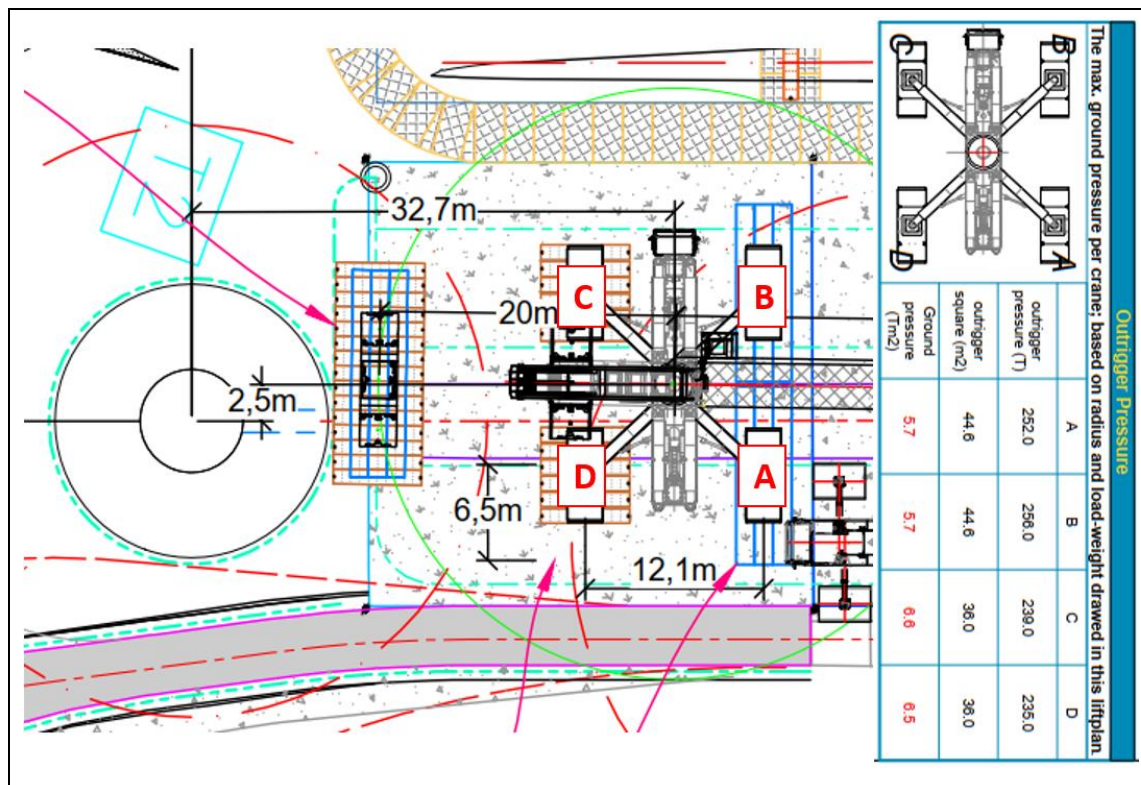


Figure 4.1 Dimensions and lay out crane WT2 with outrigger letters.

For the monitoring of the differential settlements 4 measurement points are considered, 1 in the middle of each outrigger. A depiction of the 4 measurement points for WT2 is given in Figure 4.2: Number 1, 2, 3 and 4.

Aside from the differential settlement measurements the corners of the wooden dragline mats underneath the most critical outrigger C are also measured (5, 6, 7 en 8) to give an indication of the spreading of the mats on the Tensar geogrid surface. Whenever time

implication is a factor (during a loading phase or rigging of the boom) the measurement points in the middle of the outriggers (1-4) have priority. They should be measured before points (5-8). For WTG-4 the same points are measured as indicated in Figure 4.3. The most critical outrigger is outrigger C so for that outrigger again the corners of the wooden dragline mats are measured with priority for points 1-4.

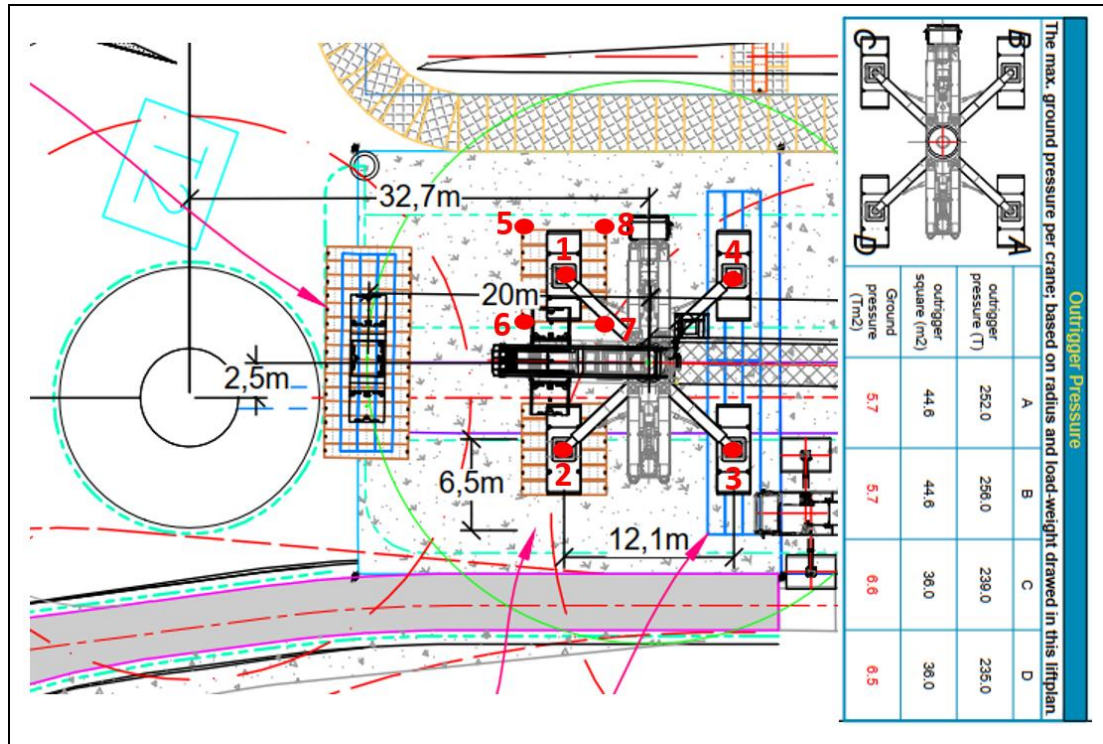


Figure 4.2 Measurement points for WT2

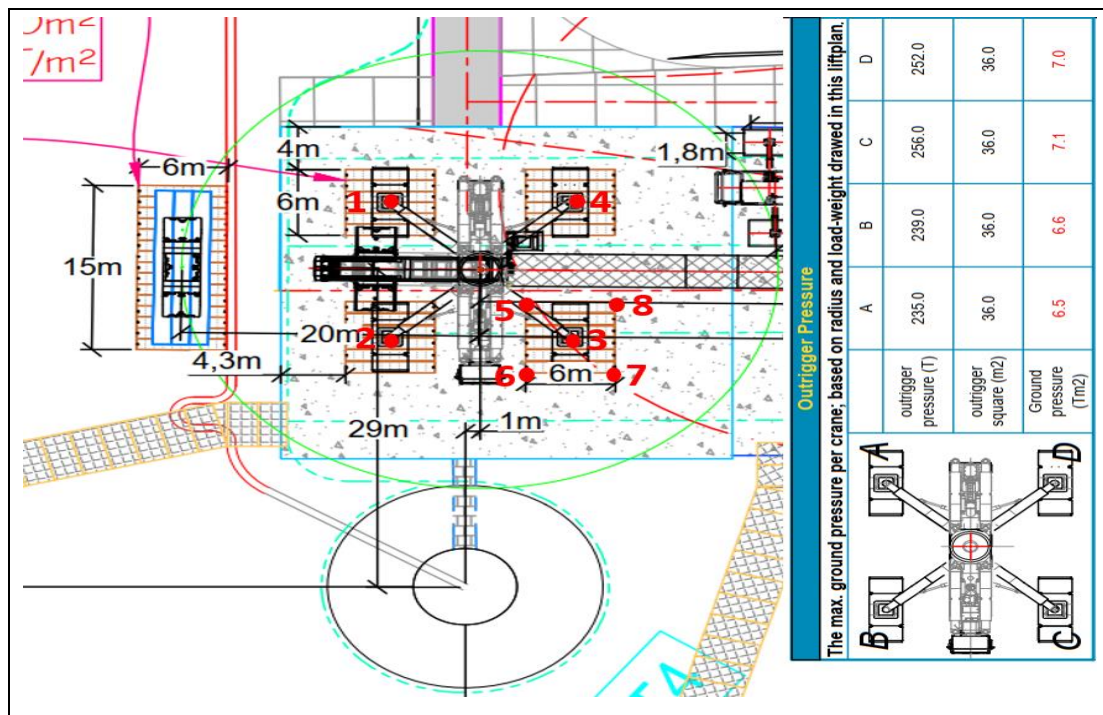


Figure 4.3 Measurement points for WT4

4.2 Monitoring Protocol

The most critical load situations are right after the boom erection (269 degrees), whenever the boom with highest load (tower installation) is directly over 1 outrigger(3) . It is important to get the measurements before, during and after the critical load states to get an understanding of both the elastic and plastic deformations. The moments of measurement are shown in Table 4.1. In case it is not possible to measure all moments then the focus will be on the highlighted measuring moments.

Table 4.1: Measurement moments during lifting operations

Measuring moment [-]	Description [-]
1	Baseline measurement before crane build up (on mats, no outrigger pressure)
2	Measurement after build up, excluding ballast
3	Measurement when full ballast is applied
4	Measurement right before boom rigging
5	Measurement at the most critical situation during the boom rigging
6	Measurement when the rigging is complete
7	Measurement during 360 test turn (when over 1 outrigger (example. B for WT2))
8	Measurements in-between loading phases for drained behaviour every 15 min
9	Measurement before the most critical tower element lift (Bottom)
10	Measurement during the most critical tower element lift (Bottom)
11	Measurement after the most critical tower element lift (Bottom)
12	Measurements in-between loading phases for drained behaviour every 15 min
13	Measurement before the nacelle or drivetrain lift
14	Measurement during the nacelle or drivetrain lift
15	Measurement after the nacelle or drive train lift
16	Measurements in-between loading phases for drained behaviour every 15 min
17	Measurement before boom laydown
18	Measurement during boom laydown, most critical moment
19	Final measurement after boom laydown

4.3 Measurement accuracy

The measurements should be done with equipment capable of measuring with an accuracy of +/- 0.5 mm. The accuracy should be demonstrated by performing a double baseline measurement.

4.4 Allowable deformations

The distance between each outrigger and the resulting maximum allowable settlement is depicted in table 4.3.

Outriggers	C.t.c. distance	Signal value settlement 0.2°	Max. allowable differential settlement 0.3°
[-]	[m]	[mm]	[mm]
A-D	12.10	42	63
A-C	17.25	60	90
A-B	12.30	43	64
B-C	12.10	42	63
B-D	17.25	60	90
C-D	12.30	43	64

4.5 Documentation

For the monitoring it is especially important to know the exact load situation at the time of the measurements. The loads are displayed on a screen in the operation chamber of the crane. A camera is aimed at this screen from within the operation chamber while filming a timelapse. The start time of the timelapse is documented carefully. At the same time a timelapse camera is setup aiming at the crane filming the lifting operations over time. The starting time of this timelapse should also be documented carefully.

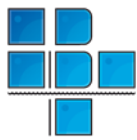
After every measuring moment the following needs to be documented:

- Location with the letters and numbers of the measuring points (Robotic Total Station)
- Date and time of the measurements (Robotic Total Station)
- Results of the x, y and z-coordinates (Robotic Total Station)
- Load situation at the time of the measurements (Timelapse camera)
- Lifting position crane (GoPro camera);

If everything is documented correctly it becomes possible to combine every measurement over time with the corresponding lifting phase and loads.

4.6 Arrangements

To ensure proper documentation of the results agreements have to be made between the researchers and the constructors. The surveyor has to be notified on the measuring moments where time is important (During lifting operations). During this time measuring points 1-4 have priority over points 5-8 and need to be measured as continuously as possible. Furthermore an agreement has to be made with the crane machinist to get permission to film within the crane cabin to document the load cases. The differential settlements have to be assessed real time to give an indication of the tilting angle.



Project: Wind Farm

Title: Summary monitoring results during lifting operation WT2 and WT4

Document no.: 2022-1865/46 version 1.a

Date: July 14th 2022

Organisation: BT Geoconsult B.V.

Status: provisional

Issued to:

Signature:

Author: T.J.J. Krielaart

Authorisation:

Appendices

I Monitoring results WTG2;

II Monitoring results WTG4.

Multiple wind turbine projects in West Brabant are being realised to increase the renewable energy production of this area. This specific project, Windfarm A16 concerns six of these turbines realized by . Whenever an excess load is exerted on a soil surface the soil starts to deform. Whenever the change in load and therefore the deformation is larger underneath 1 side of the crane the crane starts to tilt. For safety reasons the maximum allowable tilt of a crane is set at 0.3° with a signal value of 0.2°. During lifting the tilt is carefully monitored in the crane cabin. To minimize the deformation / tilt, crane hardstands are designed for each specific location turbine. The hardstands considered during this monitoring are WT2 and WT4. After soil investigations these locations were deemed most susceptible to deformations. The hardstands are designed with a 2 meter Tensar Stratum layer to increase the bearing capacity as further discussed in the monitoring plan: 2022-1865/46 monitoring plan. During operations the water level was kept below the hardstands by pumps to ensure sufficient bearing capacity. The least critical outriggers were supported on wooden dragline mats and the most critical by larger steel mats, to increase the load spreading. Figure 1 gives an overview of how the outriggers are attached to the surface.

Eventhough the MCHS's are not expected to exceed the maximum allowable differential settlement limits, monitoring is done to check the effectiveness of the mitigation measures as well as to gather data which will be used in further research to help further understand the soil behaviour as a result of the high temporal loads characteristic to on-shore turbine installations.



Figure 1: Load spreading mitigation measures

Monitoring protocol

The monitoring protocol is described in detail in the monitoring plan 2022-1865/46. The deformation of each outrigger will be monitored during specific phases of the installation process. A timelapse camera is installed documenting the position of the crane and a go pro camera is attached to the crane to document the outrigger pressure at a specific time. An example of this is shown in Figure 2. With this extra information the deformations can be explained by the real time pressures occurring.



Figure 2: Pictures of the crane position as well as the outrigger pressures corresponding to measuring moment 15 of the boom rigging of WT4

Monitoring results

The monitoring was applied at two locations within the project. Namely at WT2 and at WT4. The soil profile as well as the MCHS structure of these locations are described in the monitoring plan. For extra load spreading and therefor to decrease deformation metal mats instead of wooden draglines were applied underneath the most critical outriggers (The outriggers from measurement point 1 and 2 from figure 3).

The measurement points monitored for WT2 are shown in Figure 3. Because it was not possible to locate the total station used for the monitoring at a location from where all 4 outriggers would be visible at WT4. It was opted for a location where only 3 outriggers would be monitored. The measuring points at WT4 would differ from the monitoring plan and they are depicted in Figure 4.

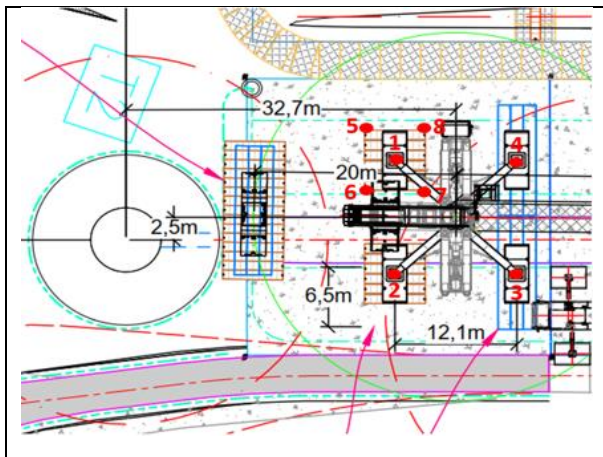


Figure 3: Measuring points WT2

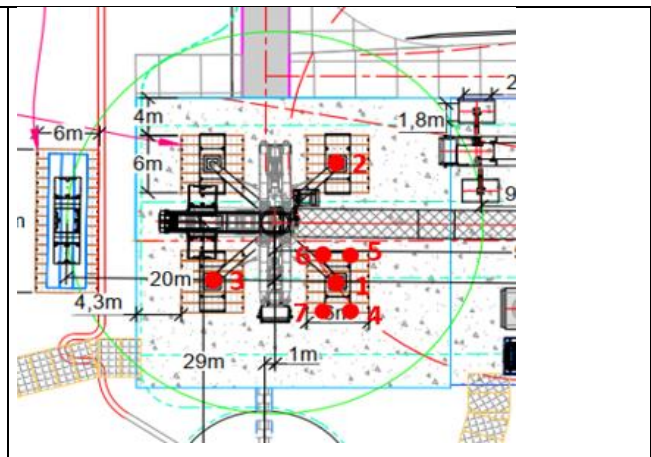


Figure 4: Measuring points WT4

The raw monitoring data is included in the appendices of this memo. To make the results easier to interpret they are presented in Figure 5-6 for WT2 and Figure 7-11 for WT4. These graphs plot the settlement (in mm) starting from a baseline measurement (0 settlement) for each measured outrigger over time. The time and description of the different measuring moments for each monitoring stage together with the outrigger pressures at this time are depicted in Table 1-2 for WT2 and Table 3-7 for WT4. The position of the crane during the measuring moments is established with a time-lapse camera. These results are also included in the appendices.

It is considered a safe operation when the tilt of the crane is not exceeding the signal value of 0.2° or the limit value of 0.3° . The signal value can be interpreted to a differential settlement of 42 mm based on a centre to centre outlined distance of the outriggers of 12.1 m, or 60 mm based on the diagonal centre to centre distance of 17.3 m of the outriggers. As can be seen from the graphs these values were not exceeded and no such incidents were reported by the crane operator.

Assessments WT2:

Between the two monitoring stages done at WT2 the mirror's used to determine the deformation by the total station were moved. Therefore, the total deformations could not be compared between the boom rigging and the lifting of tower mid-3.

- Boom Rigging:

The largest differential settlement occurs at measuring moment 2 between outrigger 1 and 4 and is 8mm. This is only 19% of the allowable differential settlement before the signal value of 42mm.

Remarks Boom rigging: The pictures of the outrigger pressures during the boom rigging stage were too vague to determine the outrigger pressures during this phase. Therefore they could not be included in the results

- Lifting tower Mid 3:

The largest differential settlement occurs at measuring moment 2 between outrigger 1 and 4

and is 11mm. This is 26% of the allowable differential settlement before the signal value of 42mm.

Remarks lifting tower Mid 3: During measuring moment 8 the superlift was blocking the line of sight between the total station and measuring point 2. It is therefor not depicted in the results.

Assessments WT4:

- Boom rigging

The largest differential settlement occurs at measuring moment 2 between outrigger 1 and 3 and is 8mm. This is 19% of the allowable differential settlement before the signal value of 42mm.

Remark boom rigging: Before the first measurement the crane was already under tension because the superlift was attached over the entire weekend. Because of this the 'zero measurement was taken at measuring moment 23, when the pressures on all outriggers were equal and the only load was the deadweight of the crane. All the deformations are determined from this moment as 0

- Lifting bottom tower

The largest differential settlement occurs at measuring moment 2 between outrigger 2 and 3 and is 13mm. This is 22% of the allowable differential settlement before the signal value of 60mm.

Remark Bottom tower: Because the auxiliary crane blocked the line of sight to measuring point 2 the mirror was moved. This movement is adjusted for in the results by equalling the deformation of point 2 after the last phase to the deformation of point 1 as these should be approximately the same.

- Lifting the drivetrain and Hub

The largest differential settlement occurs at measuring moment 2 between outrigger 1 and 3 and is 6mm. This is 14% of the allowable differential settlement before the signal value of 42mm.

Remark drivetrain and hub: Because the drivetrain and hub were not expected to result in large deformations the undercarriage of the crane would not be running. Therefor it was not possible to monitor the outrigger pressures

- Lowering of the boom

The largest differential settlement occurs at measuring moment 2 between outrigger 1 and 3 and is 7 mm. This is 12% of the allowable differential settlement before the signal value of 60mm.

- Total process

The largest differential settlement during the entire instalment of WT4 is 13 mm.

Results WT2

Measuring day 1: Boom Rigging

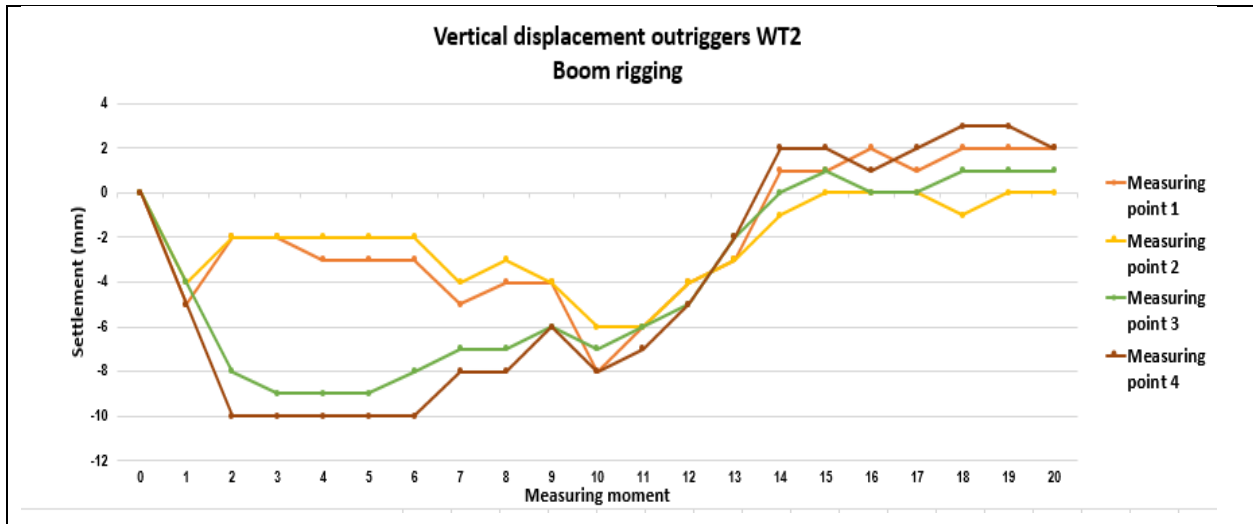


Figure 5: Monitoring results boom rigging WT2

Table 1: Measuring moments boom rigging WT2

Measuring moment [-]	Description [-]	Time [-]
0	Zero measurement before boom rigging	8:30:00
1	Start boom rigging	8:40:00
2	Boom rigging 2m high superlift is floating	8:44:50
3	Boom rigging 10m high superlift is floating	8:47:40
4	Boom rigging 20m high	8:49:40
5	Boom rigging 30m high	8:51:50
6	Boom rigging 40m high	8:53:50
7	Boom rigging 50m high superlift is touched down	8:55:50
8	Boom rigging 70m high superlift is picked back up	8:57:50
9	Boom rigging 80m high superlift is touched down	9:00:00
10	Boom is lifted back down a little and superlift is lifted again	9:03:00
11	Boom is lifted back to 80 m and superlift is touched back down	9:06:00
12	Boom rigging 90 m and the effect of the superlift is gradually decreased	9:10:00
13	Boom rigging 100m	9:13:00
14	Boom rigging ready	9:16:00
15	Ballast weight above point 1 during turning	9:25:00
16	Ballast weight between point 1 and 4	9:26:00
17	End turning weight between 1 and 4	9:28:00
18	Weight above point 4	9:40:00
19	Weight between point 1 and 3	9:41:00
20	Last measurement, weight between 1 and 2	9:43:00

Measuring day 2: Lifting of Tower Mid 3

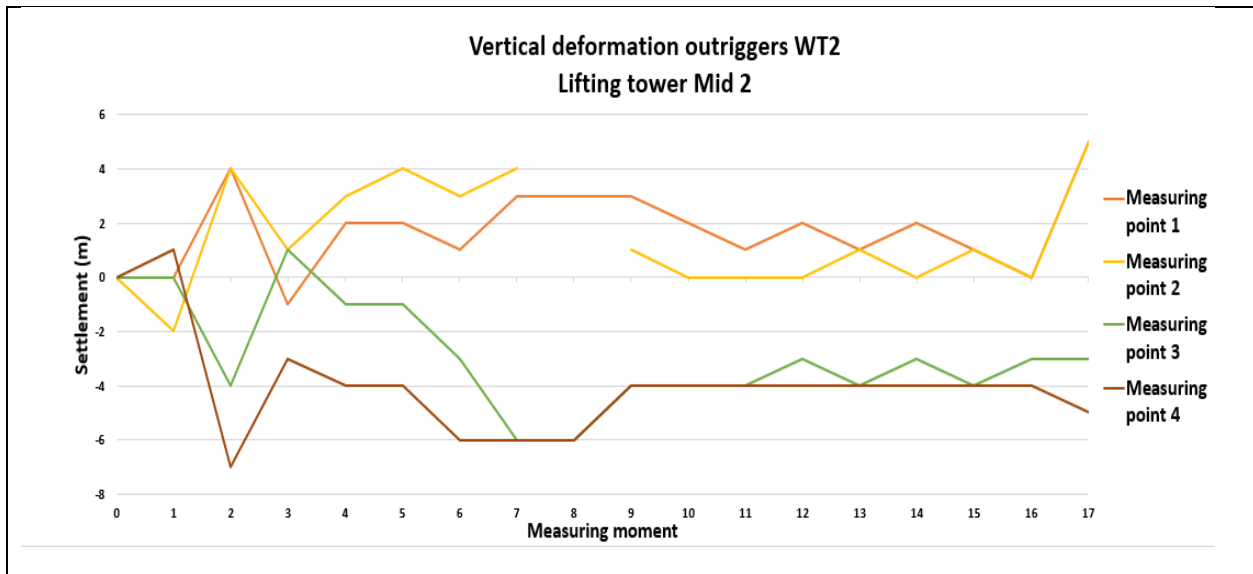


Figure 6: Monitoring results lifting of tower mid 3 WT2

Table 2: Measuring moments lifting of tower mid 3 WT2

Nr	Description	Time	Outrigger pressure			
			1	2	3	4
0	Zero measurement	07:16	225	235	148	154
1	Only own weight of crane and superlift	07:34	223	251	154	142
2	Superlift between 3 and 4, no extra load	07:43	158	141	223	252
3	Superlift above 1, no extra load	08:49	251	208	127	186
4	Start with tension on the tower	09:26	222	206	181	205
5	The tower is lifted	09:36	218	208	186	206
6	The load is fully above 3	09:38	227	207	178	208
7	Aux crane is not under tension	09:39	241	209	168	208
8	Aux crane is loose	09:41	190	205	238	228
9	Tower above 3	09:47	186	204	245	230
10	Tower between 3 and 2	09:48	186	199	245	236
11	Tower above 2	09:49	185	220	247	221
12	Tower above 2	09:50	192	237	237	208
13	Tower between 1 and 2	09:51	213	241	213	205
14	Tower next to the foundation between 1 and 2	09:52	212	244	214	201
15	Tower right above foundation	09:54	221	244	207	201
16	Tower is partially carried by the foundation	10:02	227	246	202	201
17	Tower is fully loose	10:22	163	164	186	198

Results WT4

Measuring day 1: Boom rigging WT4

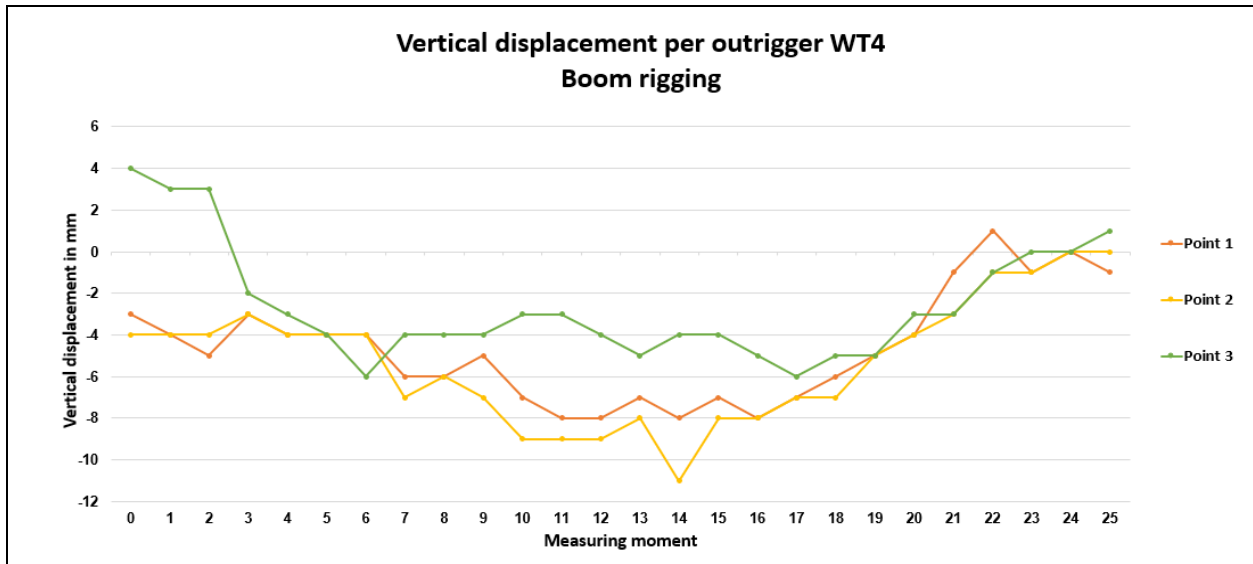


Figure 7: Monitoring results boom rigging WT4

Table 3: Measuring moments boom rigging WT4

Nr.	Description	Time	Outrigger pressure			
			1	2	3	4
0	Zero measurement	08:08:00	236	249	195	189
1	First measurement	08:10:00	236	249	195	189
2	Second measurement	08:16:30	236	249	198	190
3	Start lift without lifting block	08:25:20	228	240	270	260
4	2m lift without lifting block	08:26:50	246	257	270	261
5	2m lift Superlift is lifted	08:29:20	244	255	277	266
6	Back down superlift is still lifted	08:33:00	243	255	279	268
7	2m high lifting block is under tension	08:42:00	272	283	261	254
8	5m high lifting block is under tension	08:43:20	272	283	261	254
9	15m high lifting block is under tension	08:45:00	273	284	260	254
10	20m high lifting block is lifted in the air	08:47:00	294	306	243	238
11	30m high	08:49:00	295	307	242	238
12	40m high	08:50:00	294	306	242	238
13	60m high	08:53:40	291	304	244	240
14	lifted back down to 50m	08:57:00	292	304	244	240
15	60m high	09:04:00	283	299	251	245
16	80m high	09:06:40	273	290	260	254
17	90m high superlift is back down	09:09:30	252	268	275	267
18	100m high	09:11:30	252	270	256	253
19	110m high	09:14:30	222	239	249	245
20	120m high	09:16:20	203	221	229	225

21	130m high	09:18:00	170	187	220	218
22	140m high	09:19:30	153	167	196	194
23	End hoist superlift is loose	09:25:40	161	174	169	167
24	Ballast between 1 and 3	09:28:40	161	172	168	169
25	Final position	09:31:30	159	171	164	169

Measuring Day 1: Bottom Tower

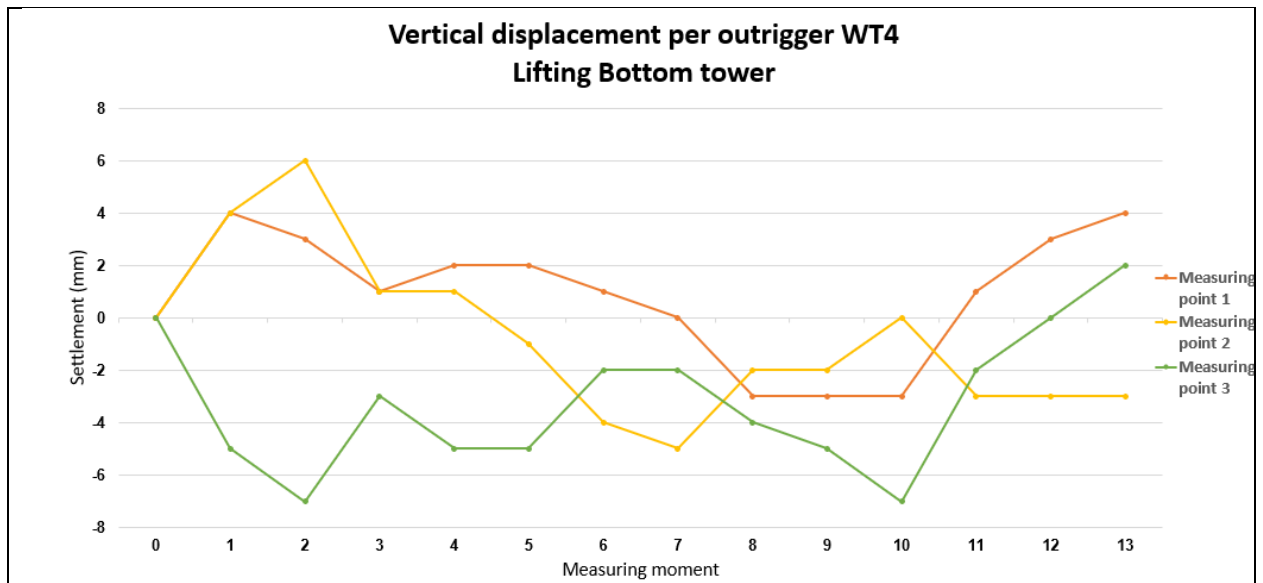


Figure 8: Monitoring results lifting bottom tower WT4

Table 3: Measuring moments lifting bottom tower WT4

nr	Description	Time	Outrigger pressure			
			1	2	3	4
0	Zero measurement during boom rigging	15:01:10	236	249	195	189
1	Measurement before lifting	15:34:00	133	152	200	184
2	Superlift is above 3 before attaching tower	16:08:40	151	124	259	217
3	Start lifting bottom	16:20:30	187	207	206	214
4	Weight of the bottom is for 50% on main crane (horizontal)	16:22:00	188	209	204	213
5	Bottom tower is vertical	16:33:00	183	202	222	230
6	Auxiliary crane is loose, weight is fully supported by the crane above point 2	16:34:30	196	266	174	229
7	Tower above point 2	16:36:40	206	274	167	221
8	Tower above point 1	16:37:50	248	236	194	185
9	Tower above the foundation (between 1 and 3)	16:40:00	243	191	240	188
10	Tower 1 meter above the ground level	16:43:00	150	180	251	182
11	Tower is down superlift is still in the air	16:51:20	182	227	185	223
12	Tension is of the cables, ground is fully carrying bottom	16:53:30	135	233	128	221
13	Final measurement superlift still in the air	17:19:00	135	233	126	221

Measuring day 2: Lifting of the drivetrain and the hub

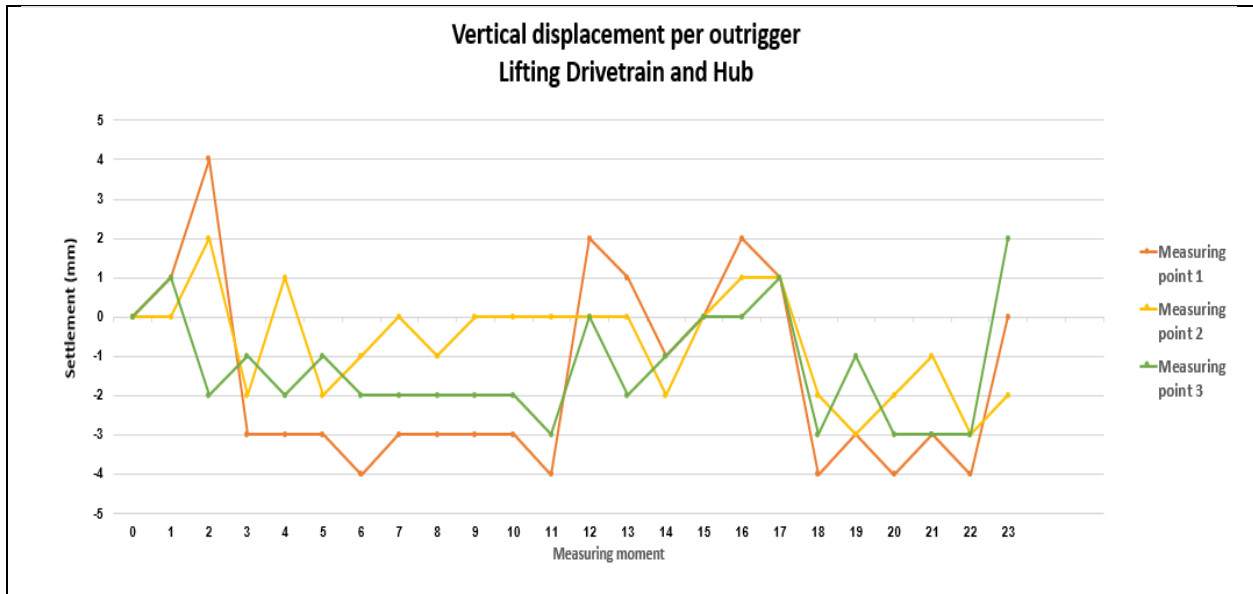


Figure 9: Monitoring results lifting drivetrain and hub WT4

Table 4: Measuring moments lifting drivetrain and hub WT4

Nr.	Description	Time
0	Zero measurement superlift is lifted	06:43:40
1	Installment of the installment cables	06:51:20
2	Crane is above drivetrain, superlift is down	06:56:50
3	Drivetrain and superlift are lifted	06:26:00
4	Drivetrain put back down superlift still lifted	07:30:10
5	Drivetrain is lifted again	07:32:30
6	Drivetrain is above point 1, 15m	07:39:00
7	Drivetrain is above point 1, 50m	07:45:30
8	Drivetrain is above point 1, top of the turbine	07:50:50
9	Drivetrain is straight above the turbine	07:55:30
10	Drivetrain still above the turbine	08:04:40
11	Drivetrain is being installed still under tension	08:12:40
12	Drivetrain is loose, crane is between point 1 and 2	09:29:30
13	Repositioning of the hub	09:48:30
14	Full weight of the hub is on the crane	09:49:40
15	Hub is touched back down for preparations	09:58:00
16	Part of the nacelle roof is lifted	10:04:00
17	Crane is above hub	10:46:30
18	Hub is lifted from the ground	11:17:50
19	Hub is lifted 20 m high	11:20:00
20	Hub is lifted 80 m high right next to the turbine	11:24:50
21	Hub is at the height of the nacelle	11:28:20
22	Hub is being installed	11:47:00
23	Kables are no longer under tension, hub is installed	12:11:00

Measuring day 3: Lowering of the boom

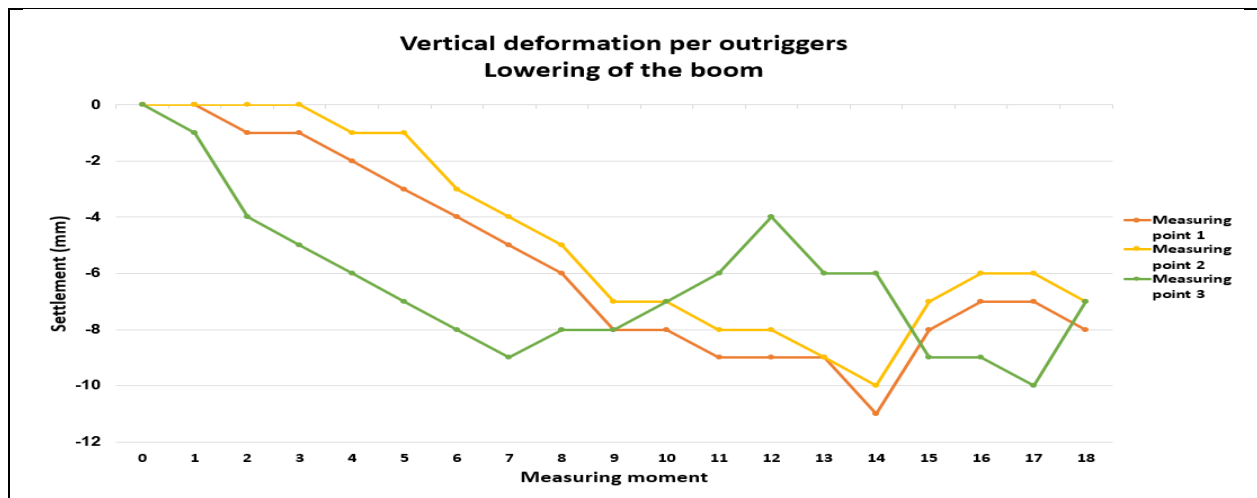


Figure 10: Monitoring results lowering of the boom WT4

Table 5: Measuring moments lowering of the boom WT4

Nr.	Description	Time	Outrigger pressure			
			1	2	3	4
0	Zero measurement	19:57:50	0	0	0	0
1	Superlift is attached	20:24:20	0	0	0	0
2	Superlift is lifted and crane has gone down 10m	20:28:00	138	151	219	205
3	Crane has gone down 20m	20:29:20	160	170	221	207
4	Crane has gone down 30m	20:30:30	174	188	243	230
5	Crane has gone down 40m	20:32:00	191	203	247	234
6	Crane has gone down 50m	20:33:40	206	220	261	247
7	Crane has gone down 60m	20:35:40	223	238	269	257
8	Crane has gone down 70m	20:37:20	241	255	269	257
9	Crane has gone down 80m, superlift is lifted from the ground	20:38:45	258	273	267	255
10	Crane has gone down 90m	20:40:30	269	285	264	251
11	Crane has gone down 100m	20:42:30	279	296	254	243
12	Crane has gone down 110m	20:43:40	285	302	248	238
13	Lifting block is just above the ground	20:45:20	291	308	243	234
14	Lifting block is touched down	20:52:40	295	313	238	229
15	Crane is hanging right above the hanging standard	20:53:40	280	301	249	238
16	Crane is resting upon wooden draglines	20:59:50	246	265	269	259
17	Crane is lifted again for 1 meter above wooden draglines	21:02:30	249	262	282	269
18	Full weight is down	21:06:10	251	269	234	220

Measuring day 1-3: Total installation process

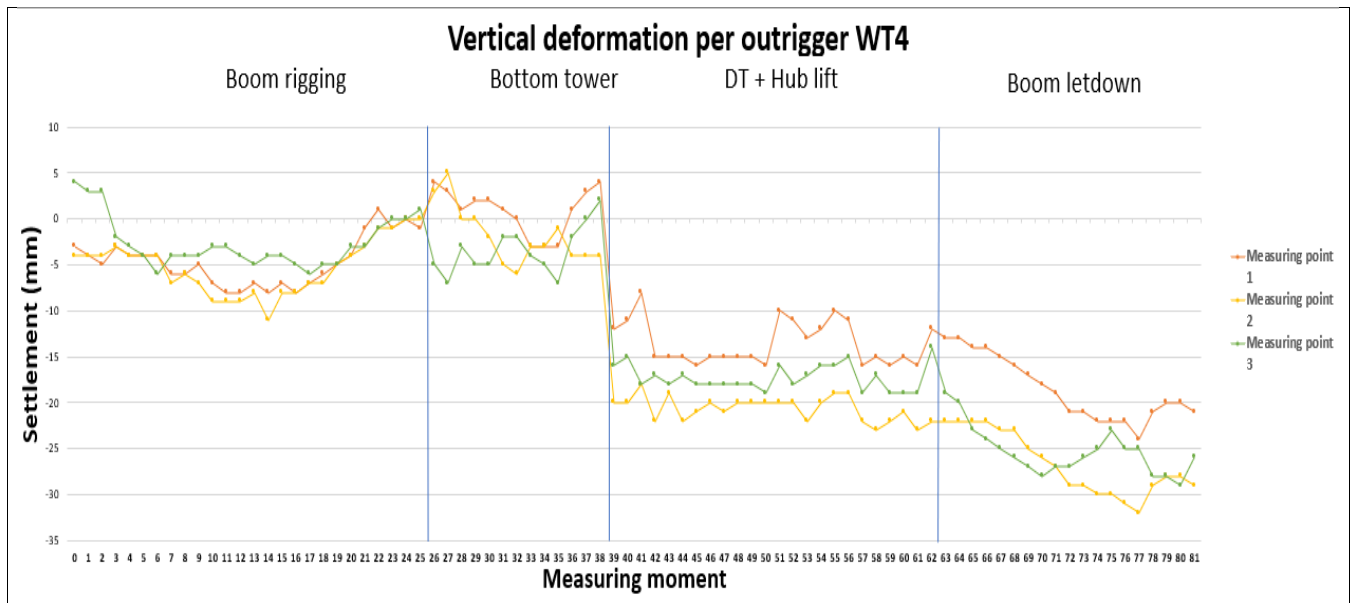


Figure 11: Monitoring results of the installation of WT4

Nr.	Description	Real time	1	2	3	4
0	Zero measurement	08:08:00	236	249	195	189
1	First measurement	08:10:00	236	249	195	189
2	Second measurement	08:16:30	236	249	198	190
3	Start lift without lifting block	08:25:20	228	240	270	260
4	2m lift without lifting block	08:26:50	246	257	270	261
5	2m lift Superlift is lifted	08:29:20	244	255	277	266
6	Back down superlift is still lifted	08:33:00	243	255	279	268
7	2m high lifting block is under tension	08:42:00	272	283	261	254
8	5m high lifting block is under tension	08:43:20	272	283	261	254
9	15m high lifting block is under tension	08:45:00	273	284	260	254
10	20m high lifting block is lifted in the air	08:47:00	294	306	243	238
11	30m high	08:49:00	295	307	242	238
12	40m high	08:50:00	294	306	242	238
13	60m high	08:53:40	291	304	244	240
14	lifted back down to 50m	08:57:00	292	304	244	240
15	60m high	09:04:00	283	299	251	245
16	80m high	09:06:40	273	290	260	254
17	90m high superlift is back down	09:09:30	252	268	275	267
18	100m high	09:11:30	252	270	256	253
19	110m high	09:14:30	222	239	249	245
20	120m high	09:16:20	203	221	229	225
21	130m high	09:18:00	170	187	220	218
22	140m high	09:19:30	153	167	196	194
23	End hoist superlift is loose	09:25:40	161	174	169	167
24	Ballast between 1 and 3	09:28:40	161	172	168	169
25	Final position all outrigger pressures are equal (baseline measurement)	09:31:30	159	171	16	169
26	Measurement before lifting	15:34:00	133	152	200	184
27	Superlift is above 3 before attaching tower	16:08:40	151	124	259	217
28	Start lifting bottom	16:20:30	187	207	206	214
29	Weight of the bottom is for 50% on main crane (horizontal)	16:22:00	188	209	204	213
30	Bottom tower is vertical	16:33:00	183	202	222	230
31	Auxiliary crane is loose, weight is fully supported by the crane above point 2	16:34:30	196	266	174	229
32	Tower above point 2	16:36:40	206	274	167	221
33	Tower above point 1	16:37:50	248	236	194	185
34	Tower above the foundation (between 1 and 3)	16:40:00	243	191	240	188
35	Tower 1 meter above the ground level	16:43:00	150	180	251	182
36	Tower is down superlift is still in the air	16:51:20	182	227	185	223
37	Tension is of the cables, ground is fully carrying bottom	16:53:30	135	233	128	221
38	Final measurement superlift still in the air	17:19:00	135	233	126	221
39	Zero measurement superlift is lifted	08:08:00	0	0	0	0

40	Installment of the installment cables	08:10:00	0	0	0	0
41	Crane is above drivetrain, superlift is down	08:16:30	0	0	0	0
42	Drivetrain and superlift are lifted	08:25:20	0	0	0	0
43	Drivetrain put back down superlift still lifted	08:26:50	0	0	0	0
44	Drivetrain is lifted again	08:29:20	0	0	0	0
45	Drivetrain is above point 1, 15m	08:33:00	0	0	0	0
46	Drivetrain is above point 1, 50m	08:42:00	0	0	0	0
47	Drivetrain is above point 1, top of the turbine	08:43:20	0	0	0	0
48	Drivetrain is straight above the turbine	08:45:00	0	0	0	0
49	Drivetrain still above the turbine	08:47:00	0	0	0	0
50	Drivetrain is being installed still under tension	08:49:00	0	0	0	0
51	Drivetrain is loose, crane is between point 1 and 2	08:50:00	0	0	0	0
52	Repositioning of the hub	08:53:40	0	0	0	0
53	Full weight of the hub is on the crane	08:57:00	0	0	0	0
54	Hub is touched back down for preparations	09:04:00	0	0	0	0
55	Part of the nacelle roof is lifted	09:06:40	0	0	0	0
56	Crane is above hub	09:09:30	0	0	0	0
57	Hub is lifted from the ground	09:11:30	0	0	0	0
58	Hub is lifted 20 m high	09:14:30	0	0	0	0
59	Hub is lifted 80 m high right next to the turbine	09:16:20	0	0	0	0
60	Hub is at the height of the nacelle	09:18:00	0	0	0	0
61	Hub is being installed	09:19:30	0	0	0	0
62	Kables are no longer under tension, hub is installed	09:25:40	0	0	0	0
63	Zero measurement	19:57:50	0	0	0	0
64	Superlift is attached	20:24:20	0	0	0	0
65	Crane has gone down 10m	20:28:00	138	151	219	205
66	Crane has gone down 20m	20:29:20	160	170	221	207
67	Crane has gone down 30m	20:30:30	174	188	243	230
68	Crane has gone down 40m	20:32:00	191	203	247	234
69	Crane has gone down 50m	20:33:40	206	220	261	247
70	Crane has gone down 60m	20:35:40	223	238	269	257
71	Crane has gone down 70m	20:37:20	241	255	269	257
72	Crane has gone down 80m , superlift is lifted from the ground	20:38:45	258	273	267	255
73	Crane has gone down 90m	20:40:30	269	285	264	251
74	Crane has gone down 100m	20:42:30	279	296	254	243
75	Crane has gone down 110m	20:43:40	285	302	248	238
76	Lifting block is just above the ground	20:45:20	291	308	243	234
77	Lifting block is touched down	20:52:40	295	313	238	229
78	Crane is hanging right above the hanging standard	20:53:40	280	301	249	238
79	Crane is resting upon wooden draglines	20:59:50	246	265	269	259
80	Crane is lifted again for 1 meter above wooden draglines	21:02:30	249	262	282	269
81	Full weight is down	21:06:10	251	269	234	220

Conclusion

Based on the measured settlements the following conclusion is drawn. All measured differential settlements were within the tolerances and did not exceed the signal values corresponding to 0.2° tilt position of the crane. Therefore, the limit value was also not reached. The maximum differential settlement that was measured is 13 mm which is lower than the applicable signal value of 42 mm. Based on these results it is confirmed with measurements that the crane hardstands fulfil the requirements.

A.2 Python code and sensitivity analysis input

Parameter Name	Volumiek ge		Hoek van inv Cohesie		Conusfactor a [-]	Stijfheidsparameters	
	γ_{unsat} [kN/m ³]	γ_{unsat} [kN/m ³]	ϕ' [o]	c [kPa]		Eoed'ref [kPa]	E'50ref [kPa]
1 Total min	18,00	18,00	22,50	60,00	2,00	5840,00	11680,00
2 Clay, weak Sandy	18,00	18,00	22,50	60,00	3,00	8760,00	17520,00
3 $\gamma_{\text{unsat_min}}$	21,43	21,43	22,50	60,00	3,00	8760,00	17520,00
4 ϕ_{max}	18,00	18,00	29,91	60,00	3,00	8760,00	17520,00
5 c_{max}	18,00	18,00	22,50	93,75	3,00	8760,00	17520,00
6 E_min	18,00	18,00	22,50	60,00	2,00	5840,00	11680,00
7 E_max	18,00	18,00	22,50	60,00	5,00	14600,00	29200,00
8 $g_{0,7_min}$	18,00	18,00	22,50	60,00	3,00	8760,00	17520,00
9 $g_{0,7_max}$	18,00	18,00	22,50	60,00	3,00	8760,00	17520,00
10 OCR_max	18,00	18,00	22,50	60,00	3,00	8760,00	17520,00
11 k_{max}	18,00	18,00	22,50	60,00	3,00	8760,00	17520,00
12 Total max	21,43	21,43	29,91	93,75	5,00	14600,00	29200,00
13 Total min	18,00	18,00	27,50	40,00	1,00	7371,50	7371,50
14 Clay, very sandy	18,00	18,00	27,50	40,00	2,00	14743,00	14743,00
15 $\gamma_{\text{unsat_min}}$	21,43	21,43	27,50	40,00	2,00	14743,00	14743,00
16 ϕ_{min}	18,00	18,00	35,87	40,00	2,00	14743,00	14743,00
17 c_{min}	18,00	18,00	27,50	62,50	2,00	14743,00	14743,00
18 E_min	18,00	18,00	27,50	40,00	1,00	7371,50	7371,50
19 E_max	18,00	18,00	27,50	40,00	3,00	22114,50	22114,50
20 $g_{0,7_min}$	18,00	18,00	27,50	40,00	2,00	14743,00	14743,00
21 $g_{0,7_max}$	18,00	18,00	27,50	40,00	2,00	14743,00	14743,00
22 OCR_max	18,00	18,00	27,50	40,00	2,00	14743,00	14743,00
23 k_{max}	18,00	18,00	27,50	40,00	2,00	14743,00	14743,00
24 Totaal max	21,43	21,43	35,87	62,50	3,00	22114,50	22114,50
25 Totaal min	17,00	17,00	17,50	45,65	4,50	5538,67	11077,33
26 Klei, schoon	17,00	17,00	17,50	45,65	4,50	12462,00	24924,00
27 $\gamma_{\text{unsat_min}}$	20,24	20,24	17,50	45,65	4,50	12462,00	24924,00
28 ϕ_{min}	17,00	17,00	23,65	45,65	4,50	12462,00	24924,00
29 c_{min}	17,00	17,00	17,50	71,33	4,50	12462,00	24924,00
30 E_min	17,00	17,00	17,50	45,65	4,50	5538,67	11077,33
31 E_max	17,00	17,00	17,50	45,65	4,50	16616,00	33232,00
32 $g_{0,7_min}$	17,00	17,00	17,50	45,65	4,50	12462,00	24924,00
33 $g_{0,7_max}$	17,00	17,00	17,50	45,65	4,50	12462,00	24924,00
34 OCR_max	17,00	17,00	17,50	45,65	4,50	12462,00	24924,00
35 k_{max}	17,00	17,00	17,50	45,65	4,50	12462,00	24924,00
36 Totaal max	20,24	20,24	23,65	71,33	4,50	16616,00	33232,00
37 Totaal min	15,00	15,00	15,00	30,00	2,00	3415,50	6831,00
38 Klei, humeus	15,00	15,00	15,00	30,00	2,00	4554,00	9108,00
39 $\gamma_{\text{unsat_min}}$	17,86	17,86	15,00	30,00	2,00	4554,00	9108,00
40 ϕ_{min}	15,00	15,00	20,41	30,00	2,00	4554,00	9108,00
41 c_{min}	15,00	15,00	15,00	46,88	2,00	4554,00	9108,00
42 E_min	15,00	15,00	15,00	30,00	2,00	3415,50	6831,00
43 E_max	15,00	15,00	15,00	30,00	2,00	9108,00	18216,00
44 $g_{0,7_min}$	15,00	15,00	15,00	30,00	2,00	4554,00	9108,00
45 $g_{0,7_max}$	15,00	15,00	15,00	30,00	2,00	4554,00	9108,00
46 OCR_max	15,00	15,00	15,00	30,00	2,00	4554,00	9108,00
47 k_{max}	15,00	15,00	15,00	30,00	2,00	4554,00	9108,00
48 Totaal max	17,86	17,86	20,41	46,88	2,00	9108,00	18216,00
49 Totaal min	12,00	12,00	15,00	40,00	1,00	674,00	1348,00
50 Veen	12,00	12,00	15,00	40,00	1,00	674,00	1348,00
51 $\gamma_{\text{unsat_min}}$	14,29	14,29	15,00	40,00	1,00	674,00	1348,00
52 ϕ_{min}	12,00	12,00	20,41	40,00	1,00	674,00	1348,00
53 c_{min}	12,00	12,00	15,00	62,50	1,00	674,00	1348,00
54 E_min	12,00	12,00	15,00	40,00	1,00	674,00	1348,00
55 E_max	12,00	12,00	15,00	40,00	1,00	1011,00	2022,00
56 $g_{0,7_min}$	12,00	12,00	15,00	40,00	1,00	674,00	1348,00
57 $g_{0,7_max}$	12,00	12,00	15,00	40,00	1,00	674,00	1348,00
58 OCR_max	12,00	12,00	15,00	40,00	1,00	674,00	1348,00
59 k_{max}	12,00	12,00	15,00	40,00	1,00	674,00	1348,00
60 Totaal max	14,29	14,29	20,41	62,50	1,00	1011,00	2022,00

Parameter Name	Eurref [kPa]	Macht m [-]	Initial shear strain GO_ref [kPa]	Shear strain g_0,7 [-]	OCR OCR [-]	POP POP [kN]	KO KO [-]	k k [m/day]
Total min	58400,00	0,90	97333,33	0,00	1,00	10,00	0,62	4,75E-01
Clay, weak Sandy	87600,00	0,90	146000,00	0,00	1,00	10,00	0,62	4,75E-01
y_unsat_min	87600,00	0,90	146000,00	0,00	1,00	10,00	0,62	4,75E-01
phi_max	87600,00	0,90	146000,00	0,00	1,00	10,00	0,50	4,75E-01
c_max	87600,00	0,90	146000,00	0,00	1,00	10,00	0,62	4,75E-01
E_min	58400,00	0,90	97333,33	0,00	1,00	10,00	0,62	4,75E-01
E_max	146000,00	0,90	243333,33	0,00	1,00	10,00	0,62	4,75E-01
g0,7_min	87600,00	0,90	146000,00	0,00	1,00	10,00	0,62	4,75E-01
g0,7_max	87600,00	0,90	146000,00	0,00	1,00	10,00	0,62	4,75E-01
OCR_max	87600,00	0,90	146000,00	0,00	1,00	30,00	0,62	4,75E-01
k_max	87600,00	0,90	146000,00	0,00	1,00	10,00	0,62	4,75E-04
Total max	146000,00	0,90	243333,33	0,00	1,00	30,00	0,50	4,75E-04
Total min	36857,50	0,90	61429,17	0,00	1,00	10,00	0,54	4,75E-01
Clay, very sandy	73715,00	0,90	122858,33	0,00	1,00	10,00	0,54	4,75E-01
y_unsat_min	73715,00	0,90	122858,33	0,00	1,00	10,00	0,54	4,75E-01
phi_min	73715,00	0,90	122858,33	0,00	1,00	10,00	0,41	4,75E-01
c_min	73715,00	0,90	122858,33	0,00	1,00	10,00	0,54	4,75E-01
E_min	36857,50	0,90	61429,17	0,00	1,00	10,00	0,54	4,75E-01
E_max	110572,50	0,90	184287,50	0,00	1,00	10,00	0,54	4,75E-01
g0,7_min	73715,00	0,90	122858,33	0,00	1,00	10,00	0,54	4,75E-01
g0,7_max	73715,00	0,90	122858,33	0,00	1,00	10,00	0,54	4,75E-01
OCR_max	73715,00	0,90	122858,33	0,00	1,00	30,00	0,54	4,75E-01
k_max	73715,00	0,90	122858,33	0,00	1,00	10,00	0,54	4,75E-04
Totaal max	110572,50	0,90	184287,50	0,00	1,00	30,00	0,41	4,75E-04
Totaal min	55386,67	0,90	92311,11	0,00	1,00	10,00	0,70	4,06E-04
Klei, schoon	124620,00	0,90	207700,00	0,00	1,00	10,00	0,70	4,06E-04
y_unsat_min	124620,00	0,90	207700,00	0,00	1,00	10,00	0,70	4,06E-04
phi_min	124620,00	0,90	207700,00	0,00	1,00	10,00	0,60	4,06E-04
c_min	124620,00	0,90	207700,00	0,00	1,00	10,00	0,70	4,06E-04
E_min	55386,67	0,90	92311,11	0,00	1,00	10,00	0,70	4,06E-04
E_max	166160,00	0,90	276933,33	0,00	1,00	10,00	0,70	4,06E-04
g0,7_min	124620,00	0,90	207700,00	0,00	1,00	10,00	0,70	4,06E-04
g0,7_max	124620,00	0,90	207700,00	0,00	1,00	10,00	0,70	4,06E-04
OCR_max	124620,00	0,90	207700,00	0,00	1,00	30,00	0,70	4,06E-04
k_max	124620,00	0,90	207700,00	0,00	1,00	10,00	0,70	8,64E-07
Totaal max	166160,00	0,90	276933,33	0,00	1,00	30,00	0,60	8,64E-07
Totaal min	40986,00	1,00	68310,00	0,00	1,00	10,00	0,74	8,64E-03
Klei, humeus	54648,00	1,00	91080,00	0,00	1,00	10,00	0,74	8,64E-03
y_unsat_min	54648,00	1,00	91080,00	0,00	1,00	10,00	0,74	8,64E-03
phi_min	54648,00	1,00	91080,00	0,00	1,00	10,00	0,65	8,64E-03
c_min	54648,00	1,00	91080,00	0,00	1,00	10,00	0,74	8,64E-03
E_min	40986,00	1,00	68310,00	0,00	1,00	10,00	0,74	8,64E-03
E_max	109296,00	1,00	182160,00	0,00	1,00	10,00	0,74	8,64E-03
g0,7_min	54648,00	1,00	91080,00	0,00	1,00	10,00	0,74	8,64E-03
g0,7_max	54648,00	1,00	91080,00	0,00	1,00	10,00	0,74	8,64E-03
OCR_max	54648,00	1,00	91080,00	0,00	1,00	30,00	0,74	8,64E-03
k_max	54648,00	1,00	91080,00	0,00	1,00	10,00	0,74	4,32E-05
Totaal max	109296,00	1,00	182160,00	0,00	1,00	30,00	0,65	4,32E-05
Totaal min	8088,00	0,90	13480,00	0,00	1,00	10,00	0,74	8,64E-03
Veen	8088,00	0,90	13480,00	0,00	1,00	10,00	0,74	8,64E-03
y_unsat_min	8088,00	0,90	13480,00	0,00	1,00	10,00	0,74	8,64E-03
phi_min	8088,00	0,90	13480,00	0,00	1,00	10,00	0,65	8,64E-03
c_min	8088,00	0,90	13480,00	0,00	1,00	10,00	0,74	8,64E-03
E_min	8088,00	0,90	13480,00	0,00	1,00	10,00	0,74	8,64E-03
E_max	12132,00	0,90	20220,00	0,00	1,00	10,00	0,74	8,64E-03
g0,7_min	8088,00	0,90	13480,00	0,00	1,00	10,00	0,74	8,64E-03
g0,7_max	8088,00	0,90	13480,00	0,00	1,00	10,00	0,74	8,64E-03
OCR_max	8088,00	0,90	13480,00	0,00	1,00	30,00	0,74	8,64E-03
k_max	8088,00	0,90	13480,00	0,00	1,00	10,00	0,74	4,32E-05
Totaal max	12132,00	0,90	20220,00	0,00	1,00	30,00	0,65	4,32E-05

		yunsat	ysat	phi	c	EOed'ref	E'50ref	Eurref	m	G0ref	g0,7	OCR	POP	K0	k
		[kN/m3]	[kN/m3]	[o]	[kPa]	[kPa]	[kPa]	[kPa]	[-]	[kPa]	[-]				
Clay, weak sandy	E25	18	18	22,5	60	8030	16060	80300	0,9	133833,3	0,000186988	1	10	0,617317	0,4752
	E50	18	18	22,5	60	10220	20440	102200	0,9	170333,3	0,000146919	1	10	0,617317	0,4752
	E75	18	18	22,5	60	12410	24820	124100	0,9	206833,3	0,000120992	1	10	0,617317	4,75E-01
	K25	18	18	22,5	60	8760	17520	87600	0,9	146000	0,000171406	1	10	0,617317	0,084468272
	K50	18	18	22,5	60	8760	17520	87600	0,9	146000	0,000171406	1	10	0,617317	0,015020819
	K75	18	18	22,5	60	8760	17520	87600	0,9	146000	0,000171406	1	10	0,617317	0,002671121
	E25	18	18	22,5	60	11057,25	11057,25	55286,25	0,9	92143,75	0,000271589	1	10	0,617317	0,4752
Clay, very sandy	E50	18	18	22,5	60	14743	14743	73715	0,9	122858,3	0,000203692	1	10	0,617317	0,4752
	E75	18	18	22,5	60	18428,75	18428,75	92143,75	0,9	153572,9	0,000162953	1	10	0,617317	0,4752
	K25	18	18	27,5	40	14743	14743	73715	0,9	122858,3	0,000178134	1	10	0,538251	0,084468272
	K50	18	18	27,5	40	14743	14743	73715	0,9	122858,3	0,000178134	1	10	0,538251	0,015020819
	K75	18	18	27,5	40	14743	14743	73715	0,9	122858,3	0,000178134	1	10	0,538251	0,002671121
	E25	17	17	17,5	45,65	8308	16616	83080	0,9	138466,7	0,000148084	1	10	0,699294	0,00040608
	E50	17	17	17,5	45,65	11077,33	22154,67	110773,3	0,9	184622,2	0,000111063	1	10	0,699294	0,00040608
Clay, clean	E75	17	17	17,5	45,65	13846,67	27693,33	138466,7	0,9	230777,8	8,88502E-05	1	10	0,699294	0,00040608
	K25	17	17	17,5	45,65	12462	24924	124620	0,9	207700	9,87224E-05	1	10	0,699294	8,73024E-05
	K50	17	17	17,5	45,65	12462	24924	124620	0,9	207700	9,87224E-05	1	10	0,699294	1,87727E-05
	K75	17	17	17,5	45,65	12462	24924	124620	0,9	207700	9,87224E-05	1	10	0,699294	0,00000406
	E25	15	15	15	30	4838,625	9677,25	58063,5	1	96772,5	0,000166501	1	10	0,741181	0,00864
	E50	15	15	15	30	6261,75	12523,5	75141	1	125235	0,00012866	1	10	0,741181	0,00864
	E75	15	15	15	30	7684,875	15369,75	92218,5	1	153697,5	0,000104834	1	10	0,741181	0,00864
Clay, organic	K25	15	15	15	30	4554	9108	54648	1	91080	0,000176907	1	10	0,741181	0,002298866
	K50	15	15	15	30	4554	9108	54648	1	91080	0,000176907	1	10	0,741181	0,000611665
	K75	15	15	15	30	4554	9108	54648	1	91080	0,000176907	1	10	0,741181	0,000162747
	E25	12	12	15	30	758,25	1516,5	9099	0,9	13480	7,99E-04	1	10	0,741181	8,64E-03
	E50	12	12	15	30	842,5	1685	10110	0,9	13480	0,000798621	1	10	0,741181	8,64E-03
	E75	12	12	15	30	926,75	1853,5	11121	0,9	13480	0,000798621	1	10	0,741181	8,64E-03
	K25	12	12	15	30	674	1348	8088	0,9	13480	0,001195307	1	10	0,741181	2,30E-03
Peat	K50	12	12	15	30	674	1348	8088	0,9	13480	0,001195307	1	10	0,741181	6,12E-04
	K75	12	12	15	30	674	1348	8088	0,9	13480	0,001195307	1	10	0,741181	1,63E-04

```

from plxscripting.easy import *
import time
import pandas as pd
import numpy as np
from pandas import read_csv
import os

password = 'FAG3Rwn!=x4?zVh?'

s_i, g_i = new_server('localhost', 10000, password=password)

s_i.open(r'E:\1m_5mdiep_greaterload\1m_5mdiep_greaterload.p2dx")

param = read_csv(r'E:\1m_5mdiep_greaterload\1m_5mdiep_greaterload.csv', skiprows = 2,
index_col=0, sep = ';')
Soil_params = []
Deformation1 = np.zeros(len(param))
Deformation2 = np.zeros(len(param))

for i, row in enumerate(param.index):
    s_i.open(r'E:\1m_5mdiep_greaterload\1m_5mdiep_greaterload.p2dx')
    Soil_params.append(["MaterialName", param.iloc[i,0]),
                        ("SoilModel", 4),
                        ("POP", param.iloc[i,18]),
                        ("OCR", param.iloc[i,17]),
                        ("gammaUnsat", param.iloc[i,1]),
                        ("gammaSat", param.iloc[i,2]),
                        ("cref", param.iloc[i,6]),
                        ("E50ref", param.iloc[i,11]),
                        ("Eoedref", param.iloc[i,10]),
                        ("Euref", param.iloc[i,12]),
                        ("gamma07", param.iloc[i,16]),
                        ("G0ref", param.iloc[i,15]),
                        ("phi", param.iloc[i,4]),
                        ("Rinter", param.iloc[i,14]),
                        ('DrainageType', 'Undrained(A)'),
                        ("powerm", param.iloc[i,13]),
                        ("KONC", param.iloc[i,22]),
                        ("perm_primary_horizontal_axis", param.iloc[i,23]),
                        ("perm_vertical_axis", param.iloc[i,23])])

```

```

try:
    g_i.setmaterial(g_i.Soillayer_2.Soil, g_i.soilmat(*Soil_params[i]))

    g_i.gotostages()
    phase0_s = g_i.Phases[1]
    phase1 = g_i.Phases[2]

    output_port = g_i.selectmeshpoints()
    s_o, g_o = new_server('localhost', output_port, password=password)
    g_o.addcurvepoint("node", (26, -0.25))

    g_o.update()
    s_o.close()

    g_i.calculate()
    g_i.save(r"E:\1m_5mdiep_greaterload\string{}.p2dx".format(i))
    output_port = g_i.view(phase0_s)
    s_o, g_o = new_server('localhost', output_port, password=password)

    curvepoint_o = g_o.CurvePoints.Nodes[-1]
    value_o = g_o.getsingleresult(phase0_s, g_o.ResultTypes.Soil.Uy, curvepoint_o)
    value_1 = g_o.getsingleresult(phase1, g_o.ResultTypes.Soil.Uy, curvepoint_o)
    Deformation1[i] = value_o
    Deformation2[i] = value_1
    print(Deformation1)
    print(Deformation2)
except:
    break

param['Deformation'] = Deformation1
param['Consolidation'] = Deformation2
print(param)
param.to_csv(r'E:\1m_5mdiep_greaterload\Deformationresult.csv', sep = ';')

```

The screenshot shows the 'Max Crane Load [Phase_1]' settings. The parameters are organized into three sections:

Name	Value
General	
ID	Max Crane Load [Phase_1]
Start from phase	Initial phase
Calculation type	Plastic
Loading type	Staged construction
ΔM_{stage}	1,000
ΔM_{weight}	1,000
Pore pressure calculation type	Phreatic
Thermal calculation type	Ignore temperature
Time interval	0,000 day
First step	1
Last step	129
Design approach	(None)
Special option	0
Deformation control parameters	
Ignore undr. behaviour (A _v)	<input type="checkbox"/>
Reset displacements to zero	<input checked="" type="checkbox"/>
Reset small strain	<input checked="" type="checkbox"/>
Reset state variables	<input type="checkbox"/>
Reset time	<input type="checkbox"/>
Updated mesh	<input type="checkbox"/>
Updated water pressure	<input type="checkbox"/>
Ignore suction	<input checked="" type="checkbox"/>
Cavitation cut-off	<input type="checkbox"/>
Cavitation stress	100,0 kN/m ²
Numerical control parameters	
Max cores to use	256
Max number of steps store	1
Use compression for result	<input type="checkbox"/>
Use default iter parameters	<input type="checkbox"/>
Max steps	4000
Tolerated error	0,01000
Max unloading steps	5
Max load fraction per step	0,5000
Over-relaxation factor	1,200

Figure A.1: Calculation stage 2 settings

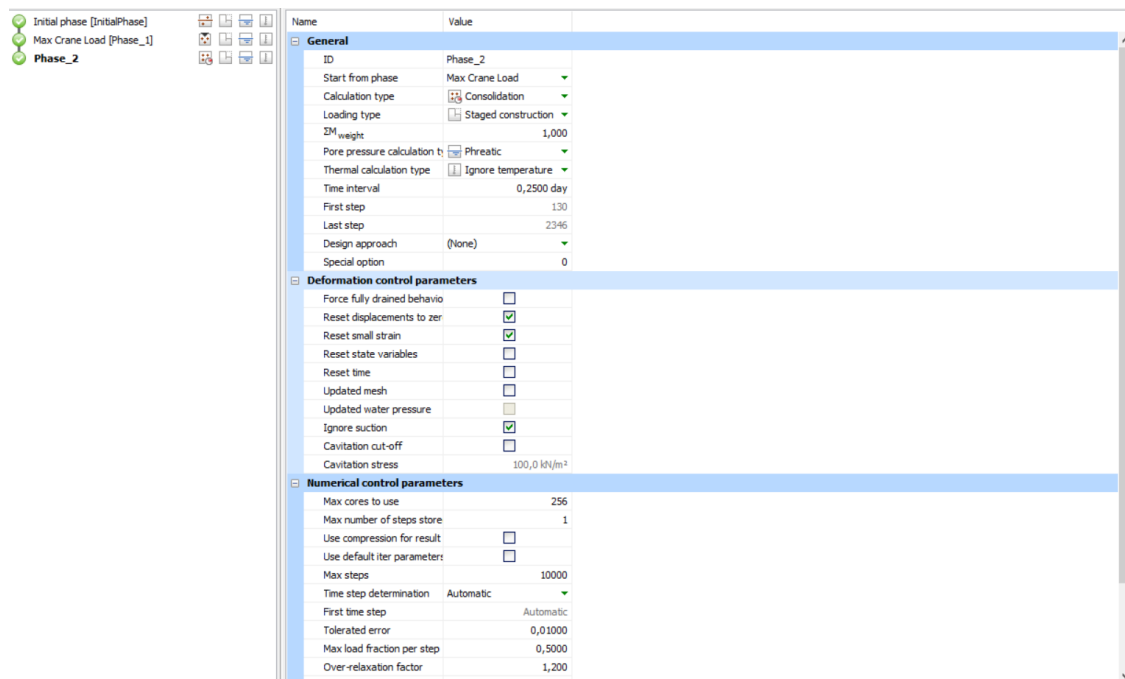


Figure A.2: Calculation stage 3 settings

A.3 Uncertainty range results

	1		2		3		4		5		6		7		8		9	
	E	k	E	k	E	k	E	k	E	k	E	k	E	k	E	k	E	k
5	-11.07	-8.04	-11.08	-8.05	-3.63	-2.72	-4.21	-3.32	-4.23	-3.33	-0.60	-0.50	-8.84	-7.19	-9.58	-7.44	-1.18	-0.93
25	-8.57	-8.02	-8.60	-8.03	-2.88	-2.72	-3.50	-3.32	-3.50	-3.33	-0.52	-0.50	-7.53	-6.78	-7.86	-7.42	-0.98	-0.93
50	-7.14	-8.01	-7.15	-8.05	-2.45	-2.71	-3.05	-3.30	-3.06	-3.30	-0.47	-0.50	-6.61	-5.38	-6.76	-6.90	-0.86	-0.92
75	-6.16	-7.26	-6.18	-8.01	-2.15	-2.48	-2.74	-3.11	-2.74	-3.27	-0.44	-0.50	-5.91	-3.58	-5.98	-4.92	-0.77	-0.78
95	-5.46	-4.62	-5.47	-6.55	-1.94	-1.66	-2.49	-2.30	-2.50	-2.94	-0.42	-0.48	-5.35	-2.22	-5.40	-3.04	-0.71	-0.59

Table A.1: Clay, weak sandy

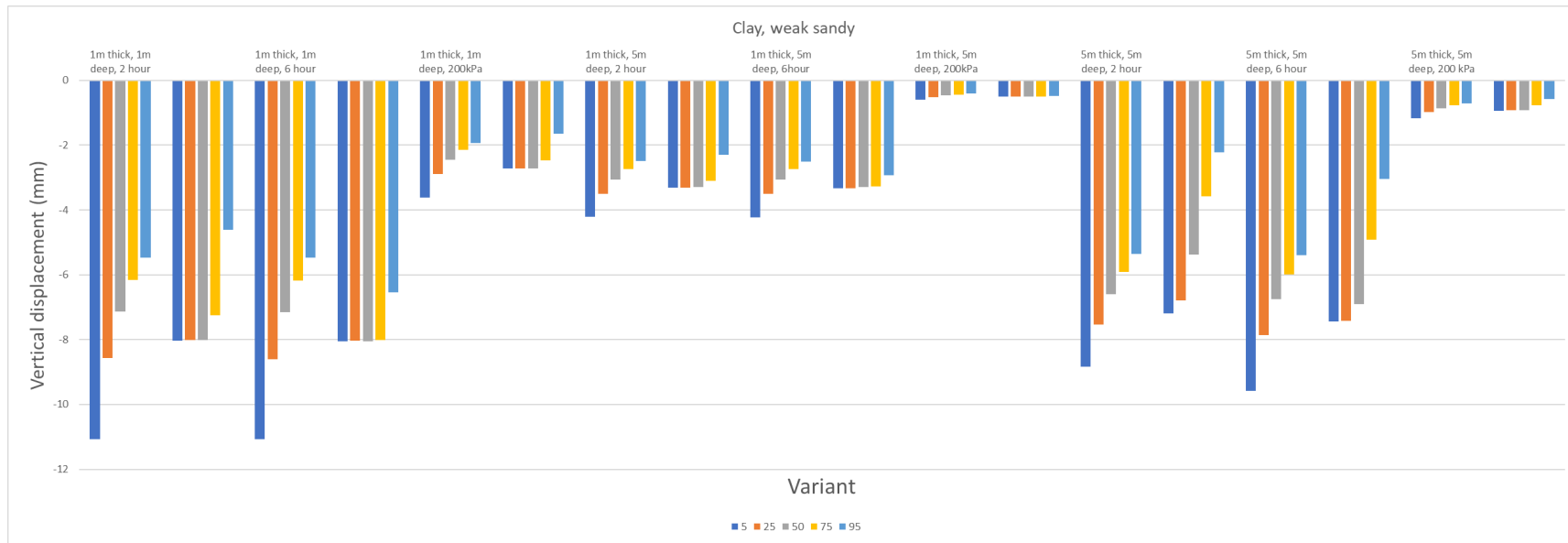


Figure A.3: Clay, weak sandy improvements

	1		2		3		4		5		6		7		8		9	
	E	k	E	k	E	k	E	k	E	k	E	k	E	k	E	k	E	k
5	-6.88	-4.94	-6.88	-4.95	-1.48	-1.41	-2.12	-1.82	-2.14	-1.82	-0.53	-0.43	-4.46	-3.40	-4.47	-3.41	-1.20	-0.85
25	-5.19	-4.93	-5.23	-4.94	-1.19	-1.40	-1.78	-1.82	-1.77	-1.82	-0.45	-0.43	-3.49	-3.38	-3.49	-3.38	-0.93	-0.85
50	-4.32	-4.97	-4.33	-4.98	-1.02	-1.40	-1.57	-1.82	-1.57	-1.81	-0.41	-0.43	-2.94	-3.24	-2.93	-3.34	-0.78	-0.85
75	-3.75	-4.86	-3.76	-4.98	-0.91	-1.38	-1.45	-1.81	-1.44	-1.81	-0.38	-0.43	-2.59	-2.66	-2.58	-3.13	-0.69	-0.77
95	-3.36	-3.51	-3.37	-4.62	-0.84	-1.12	-1.34	-1.62	-1.35	-1.79	-0.36	-0.43	-2.33	-2.01	-2.33	-2.40	-0.63	-0.61

Table A.2: Clay, very sandy

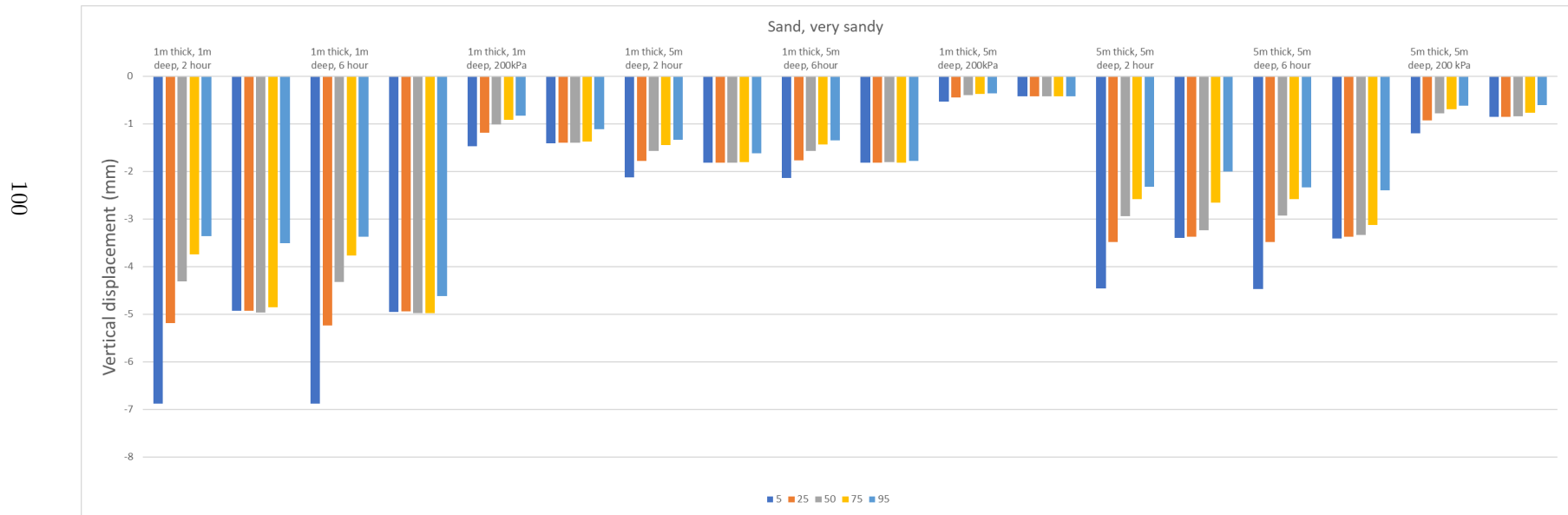


Figure A.4: Clay, very sandy improvements

	1		2		3		4		5		6		7		8		9	
	E	k	E	k	E	k	E	k	E	k	E	k	E	k	E	k	E	k
5	-5.83	-4.31	-8.54	-5.94	-2.14	-1.64	-2.87	-2.26	-3.90	-2.89	-0.60	-0.48	-2.53	-2.14	-3.65	-3.02	-0.66	-0.54
25	-5.00	-2.88	-7.17	-3.86	-1.87	-1.06	-2.55	-1.61	-3.38	-2.08	-0.54	-0.40	-2.33	-1.54	-3.33	-1.91	-0.60	-0.44
50	-4.50	-1.94	-6.29	-2.57	-1.70	-0.66	-2.34	-1.15	-3.03	-1.46	-0.49	-0.33	-2.19	-1.34	-3.11	-1.45	-0.55	-0.40
75	-4.14	-1.51	-5.63	-1.78	-1.58	-0.47	-2.20	-0.94	-2.77	-1.06	-0.47	-0.30	-2.10	-1.30	-2.95	-1.31	-0.52	-0.38
95	-3.89	-1.38	-5.13	-1.45	-1.50	-0.41	-2.09	-0.88	-2.57	-0.91	-0.44	-0.28	-2.01	-1.28	-2.82	-1.28	-0.50	-0.38

Table A.3: Clay, clean

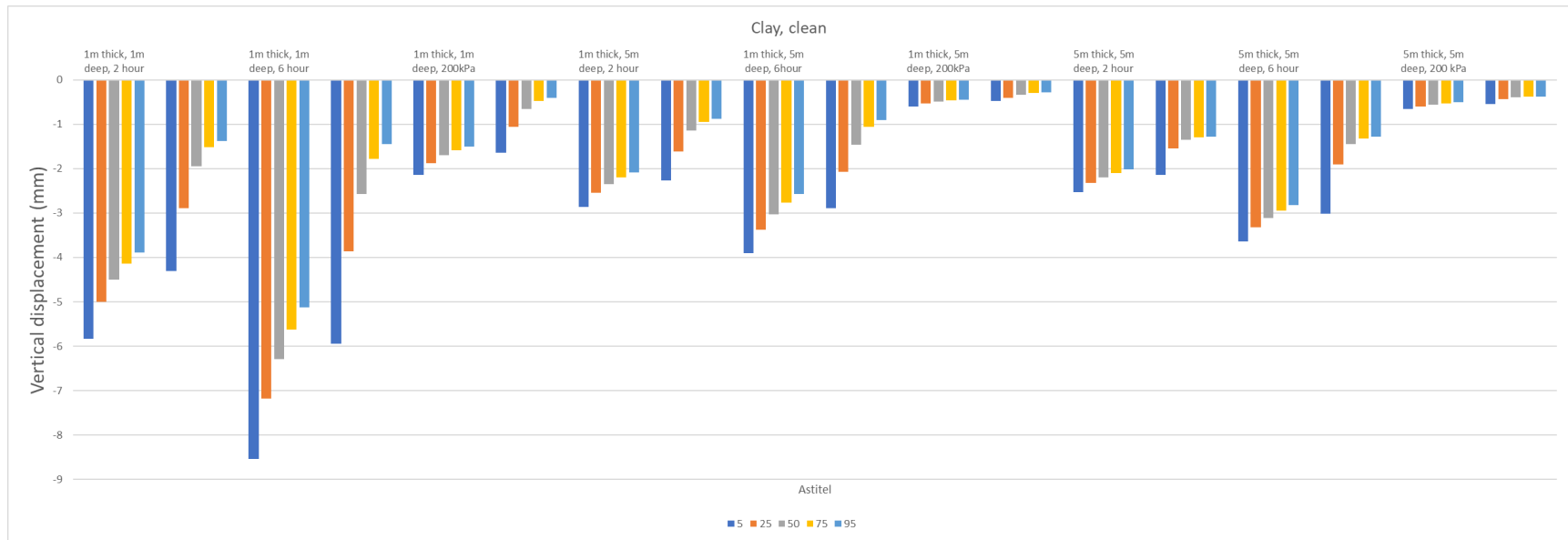


Figure A.5: Clay, clean

	1		2		3		4		5		6		7		8		9	
	E	k	E	k	E	k	E	k	E	k	E	k	E	k	E	k	E	k
5	-5.44	-4.46	-5.46	-4.48	-1.49	-1.25	-2.07	-1.81	-2.07	-1.81	-0.52	-0.46	-3.80	-3.31	-4.16	-3.51	-1.11	-0.95
25	-4.29	-4.37	-4.30	-4.50	-1.20	-1.23	-1.76	-1.80	-1.77	-1.81	-0.45	-0.46	-3.21	-2.75	-3.39	-3.27	-0.91	-0.83
50	-3.63	-3.50	-3.64	-4.34	-1.03	-1.09	-1.58	-1.69	-1.57	-1.80	-0.41	-0.46	-2.82	-2.24	-2.93	-2.66	-0.79	-0.68
75	-3.20	-2.51	-3.20	-3.35	-0.92	-0.85	-1.46	-1.44	-1.45	-1.65	-0.38	-0.43	-2.55	-1.89	-2.61	-2.17	-0.70	-0.57
95	-2.88	-1.81	-2.89	-2.39	-0.84	-0.64	-1.36	-1.20	-1.36	-1.39	-0.36	-0.38	-2.35	-1.69	-2.38	-1.84	-0.64	-0.51

Table A.4: Clay, organic

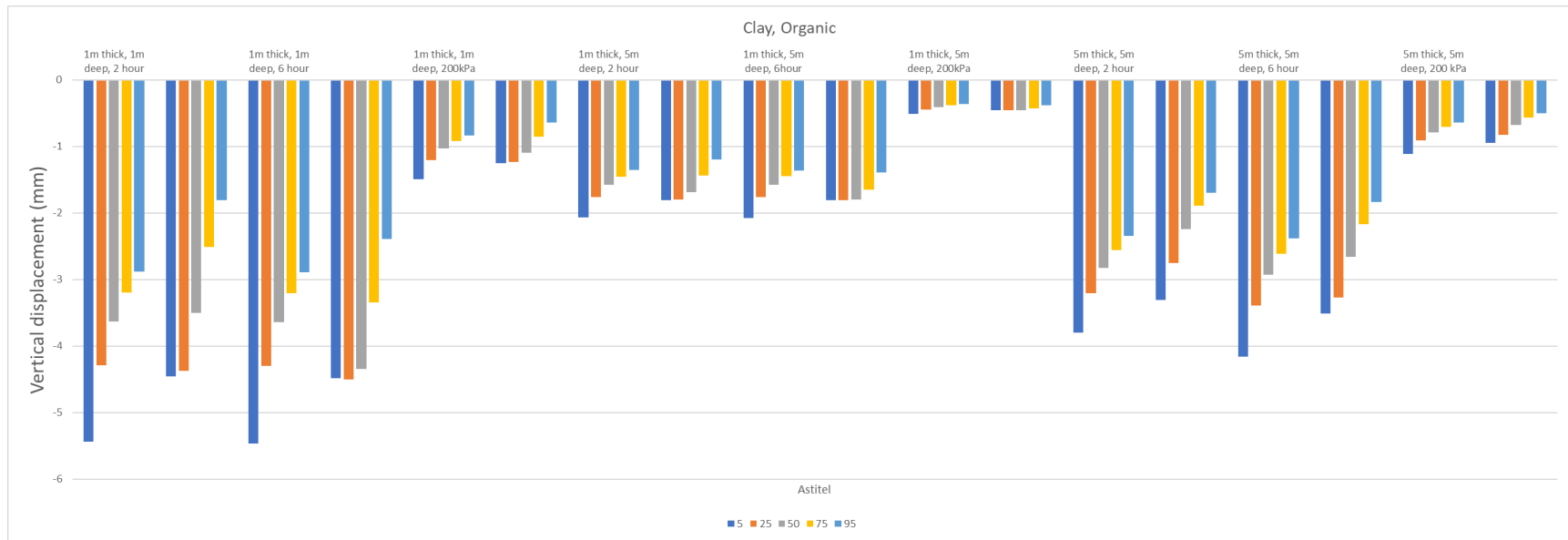


Figure A.6: Clay, organic improvements

	1		2		3		4		5		6		7		8		9	
	E	k	E	k	E	k	E	k	E	k	E	k	E	k	E	k	E	k
5	-34.12	-33.64	-64.35	-63.38	-12.02	-11.52	-12.22	-11.67	-20.34	-19.10	-2.21	-2.03	-11.93	-11.53	-21.53	-20.38	-2.69	-2.66
25	-33.14	-23.73	-61.53	-42.43	-11.81	-8.02	-12.09	-8.86	-19.87	-14.27	-2.24	-1.68	-12.02	-7.27	-21.58	-12.28	-2.71	-1.88
50	-32.24	-14.24	-58.89	-26.37	-11.63	-4.63	-11.95	-5.60	-19.39	-9.62	-2.27	-1.24	-12.03	-4.63	-21.51	-6.96	-2.72	-1.32
75	-31.42	-7.62	-56.56	-14.02	-11.41	-2.37	-11.80	-3.20	-18.92	-5.46	-2.29	-0.84	-12.04	-3.51	-21.38	-4.36	-2.73	-1.03
95	-30.69	-4.66	-54.39	-7.07	-11.25	-1.29	-11.66	-1.92	-18.44	-2.95	-2.30	-0.57	-12.01	-3.13	-21.27	-3.39	-2.73	-0.93

Table A.5: Peat

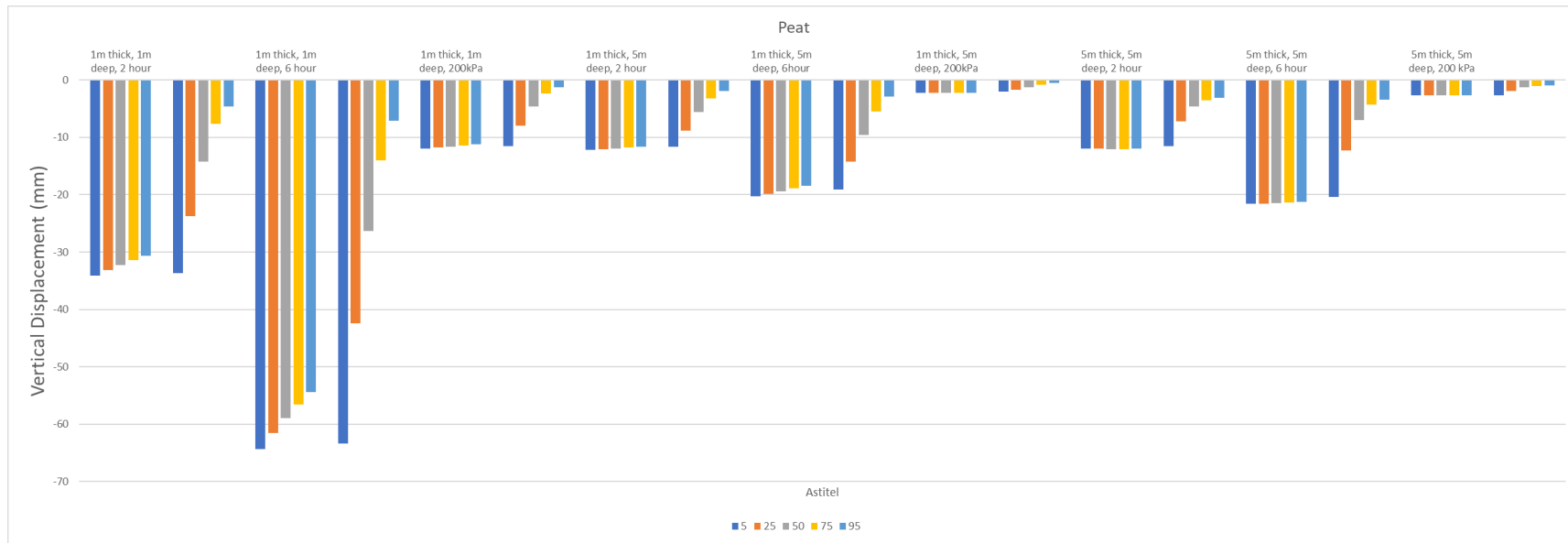


Figure A.7: Peat improvements